Design and implementation of a modular,
customizable and multi-modality compatible
actuator with position feedback

C. (Charalambos) Rossides

MSc Report

Committee:
Prof.dr.ir. S. Stramigioli
Ir. F.S. Farimani
Dr.ir. D.M. Brouwer
Dr. S. Manohar

UNIVERSITY OF TWENTE.

MIRA CTIT
BIOMEDICAL TECHNOLOGY
AND TECHNICAL MEDICINE

Design and Implementation of a Modular, Customizable, Multi-Modality Compatible Actuator with Position Feedback

Charalambos Rossides

Monday 22$^{\text{nd}}$ August, 2016

List of Figures

List of Tables

Preface

This project sums up all the effort, the passion and the devotion that have characterised me during the past two years in my pursuit for specialisation in the fields of systems and control. It has been quite a journey indeed and the truth is that many people deserve my gratitude.

To begin, I would like to thank my supervisors. To Ir. Foad Sojoodi Farimani, thank you for your daily supervision and the endless patience. To Dr. Ir. Dannis M. Brouwer, thank you for your interest in the progress of my project and your priceless advice. I would like to thank Prof. Dr. Ir. Stefano Stramigioli for the eye opening courses on Robotics during my studies at the University of Twente. The inspiration gained during those courses have re-ignited my passion about robotics and control. Finally, I would like to thank Prof. Srirang Manohar for accepting the invitation to be a member of my assessment committee, even on such a short notice.

To Vincent Groenhuis, thank you for the invaluable help and the experienced point of view regarding pneumatics and prototyping.

It would be an omission not to express my acknowledgement to the Robotics And Mechatronics department and the University of Twente for the availability on expensive equipment, tools and materials.

Greetings to Ing. Gerben te Riet o/g Scholten, whose insight and advice regarding 3D-printing, laser-cutting and prototyping in general have been exceptionally helpful. I would also like to thank my colleagues Ruud Spoor and Evyatar Bukai whose advice and support helped me to complete this project.

Special thanks to my soul-mate Stella Manoli. Thank you for supporting me throughout these two years, for your help and your endless smile.

To my parents, thank you for your lifetime support. Thank you for being there no matter what, thank you for your care and for financing my life and education all those years.

Finally, I would like to thank my closest friends and classmates for without their company, support and encouragement the whole task of studying abroad for two years would be unachievable.

Charalambos Rossides
Enschede, Monday 22nd August, 2016

Abstract

During this project, a multi-modality compatible (MRI & CT) actuator is designed and prototyped. Possible applications include the actuation of robotic/tele-manipulated systems for minimally invasive image guided interventions (e.g. an MRI compatible system for steering a rigid needle for lung cancer biopsy). In a MR environment, this pneumatic stepper motor is powered by compressed air travelling through a long hose of at least $5m$. Thus a pneumatic tube model is derived in order to relate the output pressure with the diameter, the length and the input pressure of plastic pneumatic tubes. The competence of the model is evaluated by experimentation. The dynamics imposed by this model may be decoupled from the actuator using a pneumatically actuated pneumatic valve, acting as a relay, which was also designed and prototyped during this project. Along with the actuator and the valve, a multi-modality compatible fibre-optic position sensor is designed and prototyped as a module to be attached on the actuator. Indirect, code based CAD design methods have been put into practice. The designer of such a system to defines the desired performance parameters and the CAD models are produced in an automated way.

Summary

During the last decades, minimally Invasive Interventions (MII) are becoming the preferred tissue sampling technique due to a range of reasons. MII, require small incisions and reduced infringement to the patient's body. This leads to quick recovery times and minimal scarring. Appropriate Imaging Modalities (IM) such as Magnetic Resonance Imaging (MRI) and Computed Tomography (CT) are used by doctors according to their preference in order to identify regions of interest where they consequently use tele-manipulated devices to intervene. Naturally, appropriate instrumentation is necessary in order to assist doctors to perform such kinds of operations. These devices must comply with the extraordinarily strict health and safety standards as well as satisfy requirements such as accuracy, precision and safety.

According to Stoianovici (2005), if a device is suitable to use in MRI scanners, then with few additional requirements it is possible to include the remaining modalities. Thereafter, in the 1990s, research groups around the world set on to develop MRI compatible robots, since MRI compatibility implies multi-modality compatibility as well. Factors such as the enormous magnetic fields involved, the confined space and the applicable regulations, significantly restrict the design space of such systems. According to Gassert et al. (2006), "The main challenge during the design of such a system is the choice of an adequate actuator and drive system. As in a traditional design, this choice depends largely on the task, required output power, maximum force, speed, and acceleration, as well as apparent inertia of the components to be actuated." This thesis project addresses this particular problem. A multi modality compatible (MMC), parametrically designed actuator is designed and prototyped following code based CAD modelling techniques. This kind of design is aiming towards easy and cheap adaptation and use on different mechanical structures, spanning a large range in terms of physical dimensions, output power, speed and accuracy.

MRI scanners use an enormous magnetic fields (in the range of one to few Tesla) in order to create high contrast images of soft tissue. Therefore, the produced image is distorted, unless the space around the scanner is unpolluted from any kind of magnetic radiation. This is partially achieved by enclosing the scanner in a Faraday cage. The working principle of the MRI scanner is so confining that makes traditional mechatronic devices unsuitable to use in MR environments. Firstly, permanent magnets are not allowed in the MRI scanner's FoV, since the static magnetic field would attract them towards the bore. Conductive materials are not allowed either, since the pulsating magnetic field of the scanner induces electric currents, creating electrical interference and overheating (Stoianovici, 2005). Any electric current is paired with a magnetic field around it, which potentially affects the signal received by the scanner.

After a thorough investigation of the MRI compatible materials, it is decided that MotoP should be a non-metallic, non-magnetic, pneumatic, stepping motor. According to the problem definition, the designed actuator should be used in a broad range of applications, comprising different kind of mechanisms with versatile performance requirements. Thus, it should be modular (designed as a mechanism to be mounted on other mechanical structures) and customizable (must be dimensionalised properly to meet a given set of performance requirements). For safety reasons, it must be possible for the surgeon to stop the procedure at any time and move the mechanism by hand. Therefore, the designed actuator should not lock at any point and it must be back-drivable. Since, this requirement induces uncertainty in the position of the actuator, a position sensor is also designed and prototyped in order to allow for accurate position estimation (see Figure 2).

The medical nature of the application field of the actuator drives most of the design choices that are made. It is of paramount importance for it to be inherently safe. To this end the design
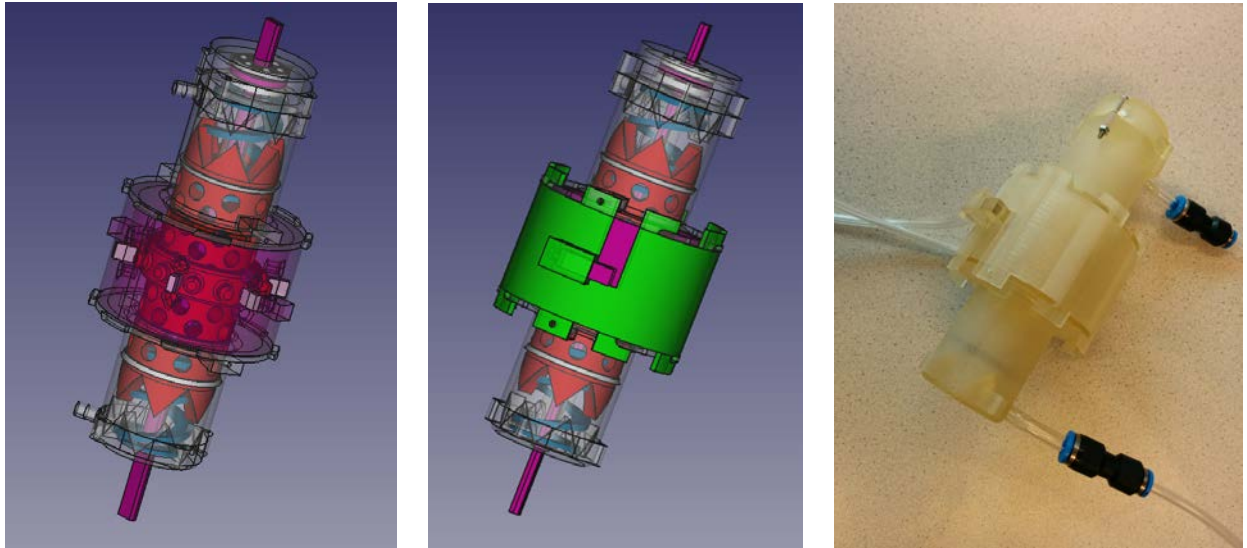
Figure 1: MotoP 2.01 overview
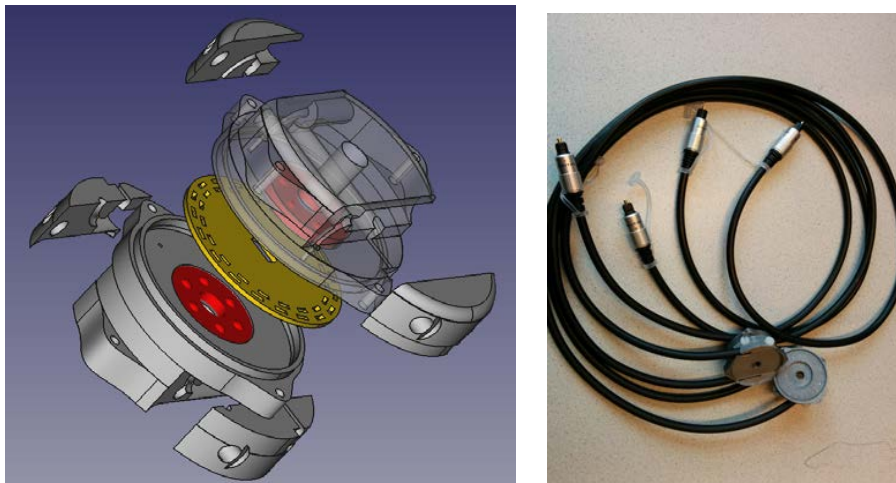
Figure 2: Encoder overview

(a) Rotation teeth misalignment is necessary

(b) Deadlock hazard
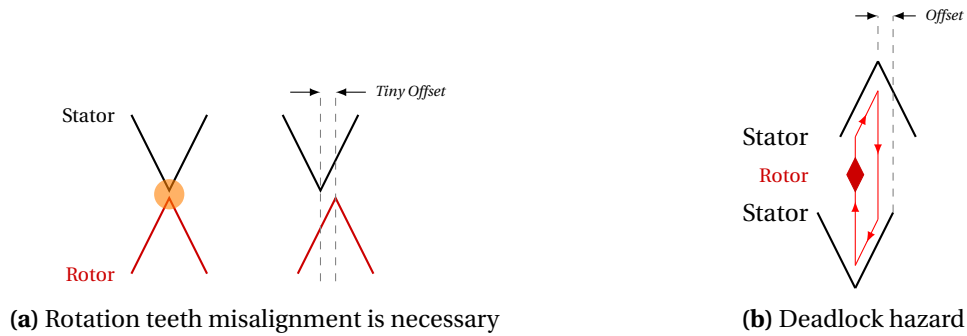
Figure 3: New principle

should be such that the actuator never clogs. At any point in time, at any point within the actuation period, it is possible to move the device by applying certain inputs, regardless what the previous state had been. Symmetry is intensively pursued when it comes to the shape, the involved forces or any other aspect. This introduces uniform mass distribution and uniform wear of materials resulting in increased performance. Freedom of customisability plays an important role as well. The design is such, that it alleviates inherent constraints and allows for customisability according to a set of performance requirements. Having these aspects in mind, during the conceptual design phase, it is attempted to derive the optimal shape of the actuator. The rotor design (see Figure 1) introduces the so much craved for symmetry, not only upon the rotor itself, but on the whole design as well. Latent in the design of the opposing chambers driving the rotor, is a negative feedback mechanism. When a given chamber is pressurised, the rotor moves towards the opposing chamber which was pressurised earlier. It now de-pressurises through its driving valve towards the environment, thus resisting the motion. This mechanism, reduces in principle the percussion force when the rotor reaches its extreme positions. The rotor design provides force symmetry at each stroke as well. The exerted force is always on the axial direction, which means that vibrations are constrained to the shaft axis. Most importantly though, it maximises the area usage of the bore as well as the area used for rotation teeth.

The new design comprises opposing rotation teeth on both the stator and the rotor. It is proven that in order to respect the bi-directionality requirement, the teeth must be symmetric and aligned. This introduces a deadlock hazard, as shown in Figure 3b. A module called the direction selector alleviates this deadlock and provides a mechanism to chose the direction of rotation. It is practically a rim which holds an extra teeth rack (shift teeth), responsible for the tiny offset required at each stroke. While the rotor moves from one extreme to the other, a pin attached on it comes in contact with the shift teeth on the direction selector, forcing it to rotate by a tiny offset and misalign the rotation teeth rack of the rotor w.r.t. the rotation teeth rack of the stator. The principle is depicted in Figure 4. In order to introduce back-drivability with adjustable stiffness according to the requirements, the back drivability rubbers are introduced (see Figure 1 left). The shift teeth are split and rectangular rubbers are placed in between, which may be engraved by laser-cutting, tuning their stiffness on demand. This design choice allows for a stepwise back-drivable mode, making sure that any manipulator driven by this actuator is kept in place when the back-drivable mode is activated. Finally, when the actuator is in back-drivable mode, the rotor should be kept in the neutral position (middle), such that the rotor pins are kept between the shift teeth. Two opposing springs are used as a retraction mechanism to serve this purpose.
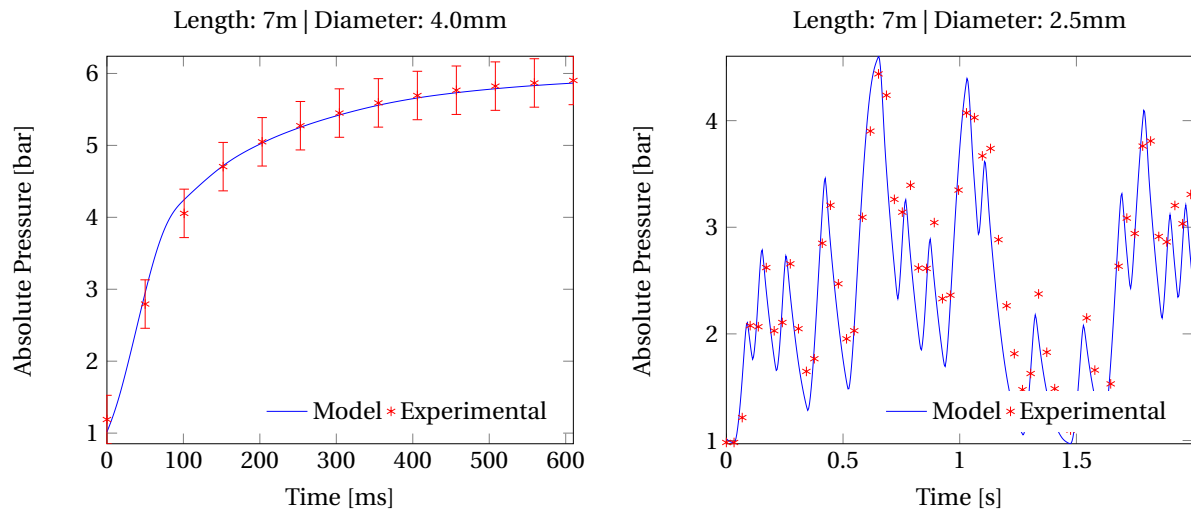
Figure 5: Pneumatic hose model
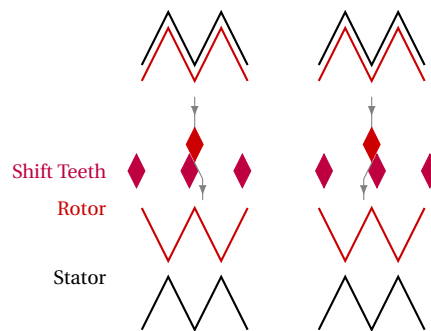
Figure 4: Direction selector principle. Left: Anti-Clockwise rotation (towards the right side). Right: Clockwise rotation (towards the left side)

It is common practice to drive this kind of actuators from outside the MRI room, along approximately $5m$ long air tubes. In order to aid in the process of selecting tubes of optimal dimensions depending on the application, a macroscopic model of the air hose is derived. It encompasses characteristics of the hose such as its length, diameter and material properties, as well as the supply pressure. Next, the model is validated by experimentation. The mean fitting error over all step response experiments is $\bar{E} = 0.0305825$ while the mean fitting error measured on a random input signal is $\bar{E} = 0.1402298$. Examples of the model fitting are shown in Figure 5.

The hose introduces some delay in the system and reduces its bandwidth. In order to make the whole system independent of the air hose dynamics, a multi-modality compatible pneumatically actuated pneumatic valve is designed (ValveP shown in Figure 6). It is triggered by a signal of minimal pressure, releasing highly pressurised air towards the actuator, performing like an amplifier. Therefore, it can be placed inside the MRI room, close to the imager (approximately $1m$ away). This configuration allows for a highly frequent control signal to trigger the valve from long distance with high pressure and high speed, which yields increased power.

Depending on the particularities of each design, either an Objet Eden 250 with Fullcure 720 resin, or an Ultimaker 2 with ABS plastic have been used for prototyping. The development of MotoP was conducted in iterations, with the 5th one being the last due to time constraints.

Attempting to characterise MotoP 2.015, it was not possible to swipe through different working pressures, because two of the shift teeth failed and the actuator was not functional any more. Excess leakage yielded significantly reduced pressure in the bores. Due to this reason,
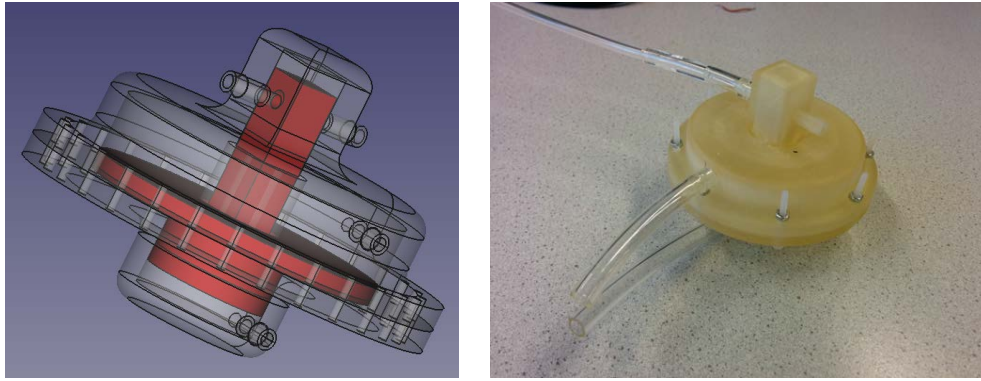
Figure 6: ValveP overview

the actuator was not functional until the retraction springs were removed. Although MotoP 2.015 was designed to deliver $1Nm$ of torque at $0.5barG$ (size $134.2mm\ x\ \oslash 77mm$) it delivers roughly three times less torque than its predecessor (Zhi's actuator), the shift teeth failed due to the material's (Fullcure 720 resin) poor mechanical properties. The dynamic behaviour of the actuator is non-linear. Apparently, the rotor's mass stores momentum while it travels from one extreme position to another. This, introduces dynamics to the system. The static torque was greater than $269.5mNm$, and the maximum dynamic torque is $64.68mNm$ at frequency $w = 1.05rad/s$ actuated through a zero length hose. Its performance diverges from the theoretical values due to the excess air leakage. In theory, it should be possible to outperform Zhi's actuator in terms of delivered torque with a MotoP 2 comparable in size when the leakage issue is solved.

As far as MotoP is concerned, more work has to be done before it is ready to be used on a mechanical structure. Better sealing is needed in order to achieve the desired pressure in the barrels and therefore the desired forces. Even if this is the case though, the currently used material is so fragile, that the shift teeth will fail instantly. Two actions have to be taken in order to avoid this. Firstly, the mass of the rotor must be reduced, decreasing the stored momentum and thus the implied forces. Secondly, a material with better mechanical properties must be used. Finally, proper retraction springs must be used according to the necessary retraction forces in each case. A concept for the next iteration (MotoP 2.016) is finally proposed that allows for better sealing and reduced mass. ValveP on the other hand is functionally competent. Still, the material properties do not allow for a robust prototype. Therefore, the design may be structurally changed in order to improve its strength. The sealing issue is existing in the valve as well. Finally, the encoder is working properly. Further steps should include choosing proper fibre optic cables with low attenuation and integrating those for distances of about $5m$.

Contents

1 Introduction

During the last decades, minimally Invasive Interventions (MII) are becoming the preferred tissue sampling technique due to a range of reasons. MII, require small incisions and reduced infringement to the patient's body. This leads to quick recovery times and minimal scarring.

Naturally, appropriate instrumentation is necessary in order to assist doctors to perform such kinds of operations. Evidently, a combination of factors such as safety, sterilisability, accuracy, precision, make the task of designing such tools extremely challenging.

However, even with high precision available, when the target towards which the end effector must be steered is not accurately known, the device would be ineffective. Thereafter, appropriate Imaging Modalities (IM) such as Magnetic Resonance Imaging (MRI), Computed Tomography (CT), X-Ray, Ultra Sound (US) and Positron Emission Tomography (PET), are used by doctors according to their preference in order to identify regions of interest where they consequently use tele-manipulated devices to intervene. Notably, often more than one IM have to be used in order to conclude to a diagnosis.

Thereupon emerges the challenge! The need to develop medical tools that may be used concurrently with the imaging device. These devices must not only comply with the extraordinarily strict health and safety standards, but they must also provide added value to patients and doctors. They should outperform previously available tools in terms of effectiveness, ease of use, dexterity. Notably, the prevailing factor that determines the commercial success of such systems, would be their cost effectiveness.

1.1   Problem Statement

Particular difficulties in developing instruments suitable for use in multiple IMs are delineated in section 3.1. In the 1990s, research groups around the world set on to develop MRI compatible devices, since as described in the above mentioned section, if a device is suitable to use in MRI scanners, then with few additional requirements it is possible to include the remaining modalities. This task proved to be particularly difficult since a series of factors such as the enormous magnetic fields involved, the confined space and the applicable regulations, significantly restrict the design space of such systems.

Evidently, the design of MRI compatible manipulators is principally driven by the actuation principle/system to be used. According to Gassert et al. (2006), "The main challenge during the design of such a system is the choice of an adequate actuator and drive system. As in a traditional design, this choice depends largely on the task, required output power, maximum force, speed, and acceleration, as well as apparent inertia of the components to be actuated." As a result, the development cost of the system is significantly increased, hindering the economic feasibility of the final commercial product.

This thesis project addresses this particular problem, it aims to provide an actuator suitable to drive devices inside a range of different imagers such as MRI and CT scanners. To this end, a multi modality compatible (MMC), parametrically designed actuator is developed and prototyped. The mathematical model is used in code based CAD modelling in order to produce the final designs given a minimal set of performance specifications. This kind of design is aiming towards easy and cheap adaptation and use on different mechanical structures, spanning a large range in terms of physical dimensions, output power, speed and accuracy. Additional features of position sensing are incorporated in order to facilitate high accuracy closed loop control and safe interaction with human subjects respectively.

2 Overview

Before proceeding with the design of a new actuator, it is important to examine what the challenges are, what has already been attempted, what works and what does not. In this chapter, the macroscopic picture of the problem is firstly drawn in section 2.1. Then, an initial, basic design space exploration is attempted, confining the actuation principle to pneumatics in section 2.2. Finally, the present state of the art is outlined in section 2.3, preparing the ground for the design of the new actuator 3.6).

2.1   MR Environments and Compatibility

Magnetic Resonance Imaging (MRI) is one of the best techniques currently available in hospitals, used for accurate diagnosis. It comprises superior soft tissue contrast, compared to conventional X-ray, ultrasound and computed tomography (CT) imaging (Fisher et al., 2014). However, the lack of tools compatible to the MR Environments, often force the radiologists and clinicians to detect a lesion in MRI and perform the biopsy sampling using a different modality, particularly when the lesion is clearly visible only in the MRI. This obviously induces a range of different issues, i.e. it is often impossible to re-locate the lesion, the need of multiple scans, patient discomfort, increased cost. Radiologist Dr. Jeroen Veldman says: "We need to do the intervention on the device that detects the lesion", which eventually boils down to the need of developing MR compatible tools.

MRI scanners use an enormous static magnetic field (in the range of one to few Tesla) in order to align nuclei within the human body (Huettel et al., 2009). Secondary resonating magnetic fields are generated next, in order to disturb these aligned nuclei and "measure" their response. Thereafter, rises the need for preserving the space around the scanner unpolluted from any kind of magnetic radiation. This is achieved by enclosing the scanner in a Faraday cage, which in practice is an electromagnetically shielded room.

The above mentioned working principle of the MRI scanner is so confining that makes traditional mechatronic devices unsuitable to use in MR environments. Firstly, permanent magnets (ferromagnetic materials) are not allowed in the MRI scanner's FoV, since the static magnetic field would attract them towards the bore. Conductive materials (eg. metallic elements) are not allowed either, since the pulsating magnetic field of the scanner induces electric currents, creating electrical interference and overheating (Stoianovici, 2005).

Moreover, it is important not to tamper with the quality of the electromagnetic field of the scanner. Any electric current is paired with a magnetic field around it, which potentially affects the signal received by the scanner and misinterpreted in the resulting image. Thereafter, elements that may affect the electromagnetic field of their surroundings (e.g. wires with running electricity, magnetic or metallic parts) should be avoided, or at least used such that their effect is minimised.

But of course, not all non-compatible materials affect the scanner in the same way. Naturally, the need for an MRI-Compatibility definition has emerged, and unfortunately, a range of unclear definitions have gradually been used, introducing confusion and difficulty to follow. In his paper, Stoianovici (2005) firstly summarises a range of test guidelines by GE for their Sigma SP scanner. [1] This has been a landmark document regarding MR Safety and MR compatible materials for quite some time after its publication. Unfortunately, it is no longer available, since GE has withdrawn it from their system. Nevertheless, it is worth to mention some ideas described by GE and summarised by Stoianovici (2005).

---

[1] General Electric Healthcare; MR Safety and Compatibility: Test Guidelines for Sigma SP

$\Delta\chi := |\chi_o - \chi_m|$	Description	Example Materials
Group 1: $\Delta\chi = 3ppm$	No detectable image artifacts when inside tissue	nylon, silicon, nitride ceramics, teflon, polysulfone, carbon fiber composites, vespel, plexiglass, zirconia ceramics, wood, copper
Group 2: $\Delta\chi = 10ppm$	Noticeable, but often insignificant, image artifacts	alumina, ceramics, silicon, quartz, lead, zinc
Group 3: $\Delta\chi = 200ppm$	Easily noticed artefacts, but often acceptable for particular applications	titanium, molybdenum, tungsten, graphite, tantalum, elgiloy, esbrid ceramics, zirconium, aluminum

Table 2.1: `Zone 1` materials categorised in groups according to their magnetic susceptibility according to GE

According to GE, a device shall be considered MRI safe if:

    – It presents no additional risk for the patient and operator

and MRI Compatible if and only if:

    – Its use in the MRI environment does not adversely impact the image quality
    – It performs its intended function when used in the MRI environment in a safe and effective manner.

Undoubtedly, this definition is rather vague and inaccurate, however it has been used by GE who later-on in the same document, defines four zones of MRI compatibility, labelled from 1 to 4, with the highest level of compatibility being `Zone 1`. Although the four zones are not thoroughly examined here due to the document's depreciated nature, it suffices to say the following: According to GE, a device would be compatible with `Zone 1` if it is MRI compatible and it could remain in the imaging volume and in contact with the patient throughout the procedure and MRI scanning.

GE then proceeds to the classification of several materials according to their MRI compatibility. `Zone 1` materials are classified with respect to the difference of their magnetic susceptibility (χ_m) and the magnetic susceptibility of human tissue[2] ($\chi_o = 29.05ppm$), according to Table 2.1

Stoianovici (2005) proceeds and generalises the MR compatibility definition, including MRI and X-Ray scanners as follows:

Multi-imager Compatibility Definition
Multi Modality Compatible (MMC) instruments should not:

- interfere with the normal functionality of the imager

- create artefacts or image distortion

- impede the visualization of the anatomical target

Stoianovici explicitly states that "ultrasonic imagers do not impose additional requirements" and proposes to use the property of radiolucency (X-rays transparency) for X-Ray imagers, as the equivalent of magnetic susceptibility.

---

[2]For atmospheric air $\chi_{air} = 0.36ppm$

A definition for MRI safety/compatibility similar to the GE version has also been given in 2001 by ASTM International (2001), which states that a device is considered MR-safe if:

- it presents no risk to the patient or other individuals
- but it still may adversely affect diagnostic information

MR-compatible if:

- it is MR-safe
- it does not significantly adversely affect diagnostic information
- its operation is not adversely affected by MR scanners

Unavoidably, the multiple definitions have been confusing and used incorrectly over the years (Sajima et al., 2012), which led to a new definition in 2005, again by ASTM International (2005). This updated definition, introduces a new term ("MR-Unsafe"), while replacing the confusing "MR-Compatible" with "MR-Conditional" as follows:

MR Compatibility Definition[3]
An item is considered to be
MR-Safe if:

- it poses no known hazards in the MR environment

MR-Conditional if:

- it poses no known hazards in the MR environment with specified conditions of use

MR-Unsafe if:

- it is known to pose hazards in all MRI environments

Therefore, using "MR-Safe" items in the MR environment does not guarantee the intact of MR image quality and its diagnostic information (Chen et al., 2014b). Since the artefacts or disturbances induced by the use of an item may vary in a continuous range from little to high, the item can not be characterised as completely compatible or completely incompatible. Nonetheless, the grade of compatibility is explicitly defined by the conditions of a range of evaluation experiments and their results.

Such experiments may vary in conditions such as static magnetic field strength, spatial gradient, time varying magnetic fields, radio frequency (RF) fields, and specific absorption rate. The examined result factors include possible induced displacement force and torque, RF heating, safety issues such as thermal injury, neuro-stimulation, acoustic noise, interaction among devices, and the safe functioning of the item in combination to the safe operation of the MR system. MR-Safety on the other hand is not validated by experiments but by providing a scientifically based rationale (Magnetic Resonance Safety Testing Services, 2016).

It is therefore apparent that in order to design an inherently MR-Safe actuator which is also MR-Conditional under the strictest conditions, the wisest choice is to chose solely Group 1 materials. This conclusion will also drive the choice of actuation principle in the proceeding section.

2.2   Actuation Principles

The above mentioned mixture of constraints make the task of designing an actuation system for operation in MR environment a difficult challenge. Researchers have come up with a range of different solutions, sometimes straightly facing the problem and sometimes working around

---

[3]From this point on, this definition is going to be used. When "MR-compatible" is mentioned, this phrase will signify a concept rather than a definition.

Actuation Method	Advantages	Limitations	Mechanical Bandwidth	Backdrivability
Mechanical Transmission	• Using MR-compatible materials enables placement and actuation close to or within the imaging region • Can be combined with any other actuator to increase MR compatibility or to work within limited space • Cables have low inertia and can be guided through the mechanical structure	• Lack of flexibility: requires a fixed supporting structure • Redirection mechanisms increase complexity and add friction • Design must account for placement of penetration panel if the master actuator is located outside of the MR room	< 100 Hz	Low to high, depending on gears and reduction ratio
Pneumatic	• Simple and flexible installation • High power/weight ratio • Pressure supply may already be available; compressor can be located outside of the MR room • Using MR-compatible materials enables placement close to or within the imaging region	• Compressibility (limited bandwidth) and delay • Precise position control is difficult • Limited range • Complex infrastructure if compressor is required • Noisy	< 10 Hz	Limited by joint friction
Hydraulic	• Flexible installation • High power/weight ratio • Hydraulic pump or master actuator (in case of hydrostatic transmission) can be located outside of the MR room • Using MR-compatible materials enables placement close to or within the imaging region • Can be used for force feedback	• Stribeck friction (nonlinear) • Limited range • Complex infrastructure • Oil leakage • High inertia	< 20 Hz	Low (limited by Stribeck friction)
Electric / Electromagnetic	• Can be placed where actuation takes place (direct drive) if safety and compatibility allow for it • Can be combined with a mechanical, pneumatic or hydrostatic transmission to increase distance to imaging region • Allow compact design • High precision and unlimited range (depending on actuator)	• Devices must be placed at a minimum distance from the imaging region and require extensive compatibility testing • Safety and compatibility may vary with position • Performances may vary with placement and orientation	< 50 Hz	High (except for ultrasonic motor)

Table 2.2: Comparison of Actuation Methods. Courtesy Gassert et al. (2006)

it. Summing up all that work, Gassert et al. (2006) outlined the possible actuation methods for devices operating in MR environments. They decomposed them in three categories:

1. Intrinsically MR-compatible
An actuator in this category contains none of the hazardous materials mentioned in the previous section. Specifically, ferromagnetic or electrically conducting materials are prohibited. Moreover, electric energy is not carried into the MR room. Finally, nonferromagnetic conducting materials may be used in particular cases, depending on their placement. Mechanical, hydrostatic or pneumatic actuators are some examples of this category.

2. Electric actuators
In this category, the actuation is carried out over electric fields that are generated inside the MR room using electricity which enters into the room by electrically conductive cables. In order to minimise the disturbance generated by the electric field, low currents and consequently high voltages are used. Also, appropriate shielding and power and signal filtering is applied. Piezoelectric/ultrasonic, electroactive and ion conducting polymers, electrorheological fluid brakes and electrostatic actuators fall into this category. In contrast with the third category, actuators in this group do not contain ferromagnetic components or permanent magnets.

3. Electromagnetic actuators
This is the most incompatible category. These actuators usually contain ferromagnetic components (or permanent magnets), e.g conventional electric DC motors. A different approach is to use the static magnetic field of the MR scanner to create currents by induction which drive the electric actuator in the classic way (Lorentz actuators / magnetomechanical vibrotactile devices). Actuators of this category must be anchored at a safe distance from the scanner, be well shielded, and transmit force and motion over a transmission mechanism made out of compatible materials.

Gassert et al. (2006) collected their findings in a table, which is apposed here (Table 2.2) for convenience. According to Fisher et al. (2014), ultrasonic motors appear to be the most common actuation method in MRI robotics. However, it seems to be unavoidable to keep the actuator $0.3 - 1\,m$ from the imager's isocenter (usually enclosed in a Faraday cage), in order to minimize EM interference due to the electric currents and the conducting materials in the motor. Regardless, the EM leakage can never be completely alleviated. Naturally, it has so far become apparent that electric and electromagnetic actuators come with increased concerns regarding safety and compatibility. They can only be put into use under particular circumstances of which one is principally alarming: Their safety state clearly depends on their positioning. This makes it exceptionally difficult, if not impossible to design an all purpose, modular actuator, suitable to be used as a Commercial Off The Shelf (COTS) product for any robot operating in MR environments. Thereafter, this actuation method is rejected in the context of this thesis.

Next, the hydraulics are examined as a possible alternative. They comprise some very attractive characteristics. Their high power/weight ratio, and the possibility of using hydrostatic transmission by incorporating a master and a slave cylinder are indeed two strong points. However, the eventuality of oil leakage is unacceptable in a surgical environment. Thereafter, using hydraulic principles, would again impose the requirement of placing the actuator far from the patient, making the system compatible only under some strict positioning conditions. This is also to be avoided as far as this project is concerned.

Finally, the combination of pneumatically actuated mechanisms and mechanical transmissions wherever needed, seems to fit the golden rule for a range of reasons. According to Uzuka et al. (2009), pneumatic actuators have unique features such as a simple structure, light weight and low cost, characteristics that are highly desired. Also, pressurised air is readily available in hospitals, making the installation easier and much cheaper. Moreover, there is no need for pneumatic transmission lines to be closed, since any excess air may be damped in the surrounding environment. Not only air is harmless to the patient, but it is also invisible to the scanners. Finally, it is possible to place the necessary control electronics and electrical components outside the scanner room, which eliminates the MR constraints to the necessary electrical and electronic components and has already bean successfully demonstrated to be feasible in different MRI devices (Fisher et al., 2014).

Most importantly though, a pneumatic actuator can be intrinsically MR-Safe. According to Fisher et al. (2014) hospitals around the world are gradually moving from 1.5T magnetic field strength MR scanners to 3T or above. Thereafter, the MR compatibility and safety of an MRI conditional device will have to be re-evaluated for it to be certified in order to work in a higher field strength scanner. Since, as discussed earlier this actually boils down to the compatibility of the actuator, it is of paramount importance to come up with an inherently MR compatible design, so that the actuator's MR compatibility and safety are, as much as possible, independent from the surrounding environment conditions. This is the main guideline followed in this initial shrinkage of the design space, aiding the design of the general purpose multi modality actuator.

The challenge of this project takes form when taking a look at the "limitations" of the pneumatic actuation methods in Table 2.2. The air compressibility and delay make such kinds of actuators particularly difficult to control and difficult to achieve a desired position. Renn and Liao (2004) mention that "it is usually quite difficult to obtain a satisfactory and precise speed control of a servo-pneumatic motor at a low rotational speed because of the nonlinear deadband and stick-slip friction inside the proportional valve". Fortunately though, the issues of system delay and difficulty in smooth and controllable positioning have been addressed by special pneumatic actuator designs (Fisher et al., 2014), namely stepping actuation techniques.
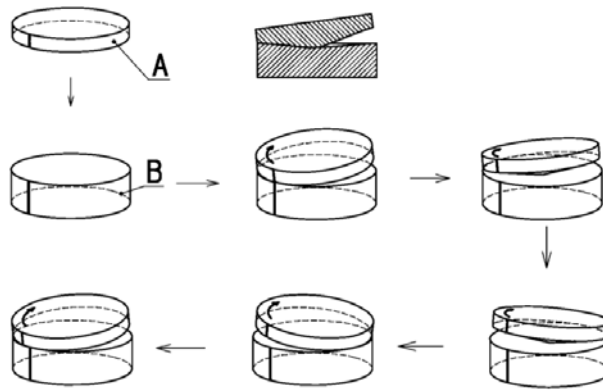
Figure 2.1: Nutation driving principle

Concluding, the initial design space examination described in this section, shrinks the scope of this project to the design of a pneumatic, back drivable actuator with discrete positioning. Next, the current state of the Art is presented in section 2.3.

2.3 State of the Art

As mentioned in the previous section, the conceptual design has been confined to pneumatic actuators with discrete positioning. Thereafter the state of Art contains nutation, wobble (harmonic drives) and stepper motors. However, it has been difficult to distinguish and assort MR compatible actuators since they are often designed and reported as parts of MR compatible mechanisms. Currently, there is no strong candidate for MR compatible COTS product in the market. Nevertheless, the most noteworthy ones are examined in this section. Interestingly, they span a range of sizes and specifications, depending on the requirements of the system they were designed for. Therefore, comparing these actuators is practically impossible, since there is no common basis to judge upon.

Suzumori et al. (2002) have designed a pneumatic nutation motor with three input lines. The driving principle is shown in figure 2.1 where a spherical bearing is used to keep the nutator (A) in place, while being pushed sequentially by cylinders arranged in a circular fashion. It is actually a cone-shaped bevel gear, paired to a cup-shaped bevel gear which acts as a rotor. The two gears are designed such that the nutator has more teeth than the rotor, which forces the later to shift with respect to the former after each nutation. The design comprises three pneumatic cylinders that act on the nutator, which are actuated in one of two modes: full-pitch drive or half-pitch drive. The former means that only one piston is actuated at each time, while the latter has two pistons actuated at a time, doubling the positioning resolution of the actuator. The authors claim that their motor comprises big torque, stable motion at low-speed operation and stepping control while having no slip. This design is however rather complex, due to the spherical bearing and it is fairly bulky since it measures 50x49mm and it weights 0.65Kg in order to achieve an impressive Torque of 1Nm at {10rpm, 5bar, 0.4m hose}.

The most remarkable, and still until now the most outstanding MR compatible actuator was reported five years later by Stoianovici et al. (2007). Although they call it a "step" motor, it is actually based on a wobble motor design using a rubber toothed diaphragm to transfer a wave formed motion from the stator to the rotor (see Figure 2.2). This motion is generated by three pneumatic cylinders which are sequentially actuated inflating their respective rubber chambers. Reaching 3.33deg positioning resolution with 0.028deg step error has since never been surmounted. The "PneuStep" as it has been named (see Figure 2.3), can achieve a torque of somewhere between 325 and 425mNm at {10rpm, 5bar, 3m hose} which is outstanding. To
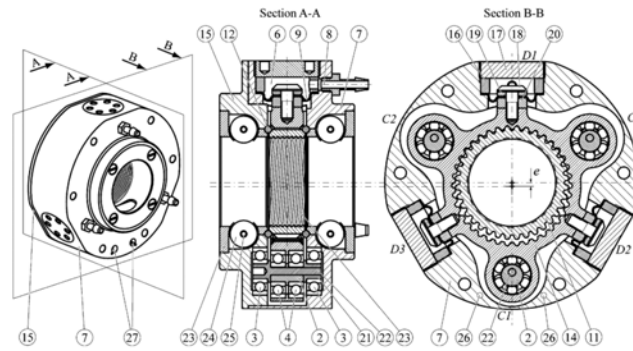
Figure 2.2: "PneuStep" schematic diagram

Figure 2.3: The "PneuStep" actuator comes in two sizes

add more, this actuator has also a built in position sensor, which uses fibre optic cables to transmit the signal outside the MR room. However, severe criticism has subsequently followed in literature, arguing that this design is very complex, with many parts. The list of materials used also contains a range of materials such as polymide and sapphire, that may comprise artefacts in the MRI images.

A much simpler design based on a different principle has been reported three years later by Sajima et al. (2010). The authors continued working on their actuator and developed a new version (Sajima et al., 2012) which they reported two years after the first one (see Figure 2.5). This actuator uses a principle where both the rotor and the actuator have toothed surfaces which are misaligned. Pistons on the stator push the toothed surface to interlock with the rotor's teeth, forcing them to get aligned, inducing a rotary motion (see Figure 2.4). Although at a first glance, this principle might look similar to the previous two actuators, it principally differs in one key aspect. The two actuators presented above comprise a continuous motion through one period's duration and they only proceed by one step when the period is finished. This allows for simultaneous actuation of more than one cylinders in order to control the position precision. However, this is not possible in the latter design. Only one cylinder can be actuated at a time, which makes it a true stepping actuator. Evidently, the simpler design and the ability to avoid using any elastic materials, which wear out by time, give this design a clear asset. Nonetheless, nothing comes at no cost, which in this case is the reduced positioning resolution of 4.29deg with 2.1deg step error. This actuator reaches a torque of 135mNm at {20rpm, 6bar, hose length not reported}.

Walking on the same path of discrete positioning, Chen et al. (2014b) designed a miniature actuator that works using the principle behind a typical pen mechanism (see Figure 2.6). They used one piston to push a rotor along a cylindrical bore and a copper spring to retract it. On the way back the toothed rotor meets teeth attached on the bore and it is forced to rotate. The
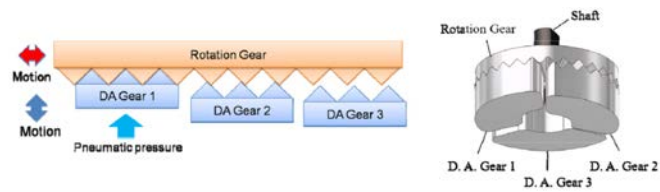
Figure 2.4: Rotational stepping principle
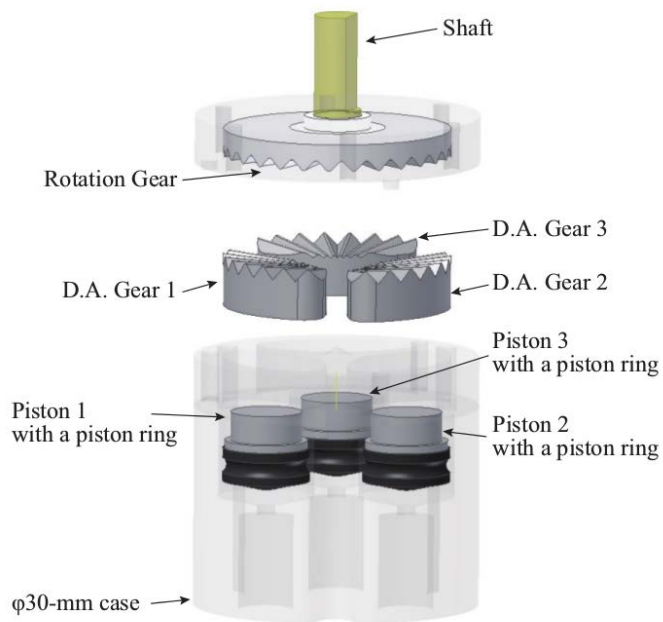
Figure 2.5: Rotational stepping actuator by Sajima et al. (2012)
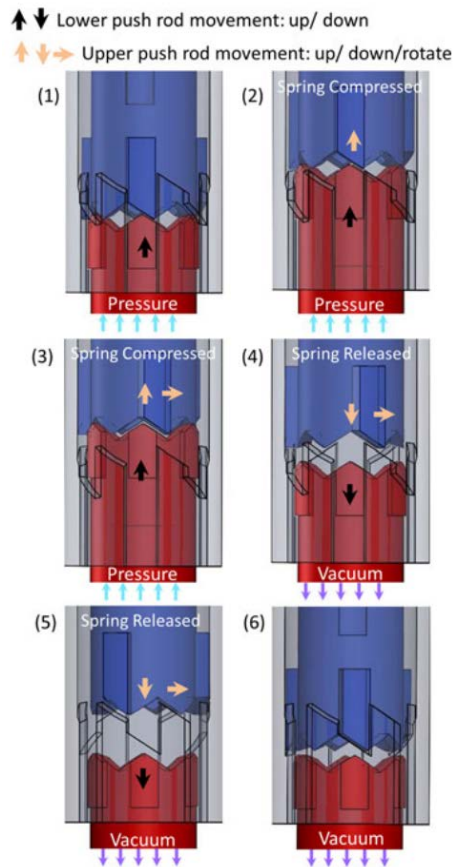
Figure 2.6: Chen et al. (2014b) 10mm actuator working principle

whole torque output is provided by the spring and some assisting vacuum created to pull it back. Therefore, the output torque is independent of the air pressure. This tiny mechanism of 10mm diameter can deliver a torque of 2.4mNm at {10rpm, pressure is irrelevant, hose length not reported}

On the very same year, Chen et al. (2014a) reported an alternative design choosing a completely different path, both when it comes to the actuation principle and the torque magnitudes involved. Their later actuator uses the familiar concept of the two stroke engine which provides a stepping action after each period (see Figure 2.7). Two pneumatic cylinders are driving a crankshaft with 90deg phase difference at very high speed. A gearbox which acts as a reduction mechanism is then used to provide the output of the actuator. The gearbox allows for an impressively high torque of 625mNm at {10rpm, 5bar, hose length not reported} and it also provides the flexibility of tuning the desired position error by carefully selecting the gear ratio. However, a high speed motion of the internal mechanism can not be avoided, which is potentially hazardous in a medical environment. The authors argue that their actuator vastly outperforms any other pneumatic motor when it comes to power efficiency. They claim that the experimental efficiency of their motor is equal to 69.8%, which is much higher than the average $20-30\%$ of "many sophisticated pneumatic actuators". On a comparison between (Stoianovici et al., 2007), (Sajima et al., 2012), (Chen et al., 2014b) and (Chen et al., 2014a) shown in Figure 2.8, they claim that their actuator is comparable to the "PneuStep" while being bigger in size but with higher torque output and tunable precision (using the gearbox).

Lately, Secoli et al. (2015) developed an actuator that delivers comparable torque with their main concern being focused on cost effectiveness and MR compatibility. They use the same concept (of a two stroke engine and a crankshaft) with three pneumatic cylinders arranged in

Part	Component Name
1	Planetary gearbox
2	Supporting structure
3	Connecting bush
4	Cylinder
5	Shaft
6	Crank
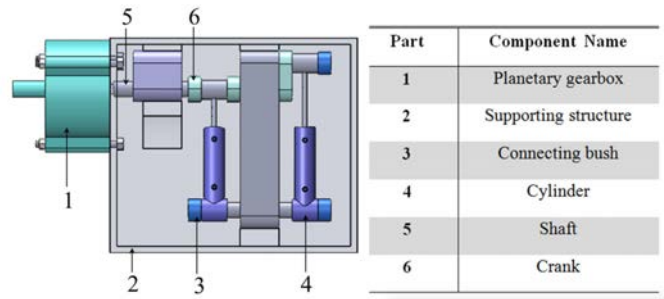
Figure 2.7: Chen et al. (2014a) High torque pneumatic stepper motor schematic

A: Motor dimension
B: Number of components
C: Step size
D: Motor output torque
E: Power
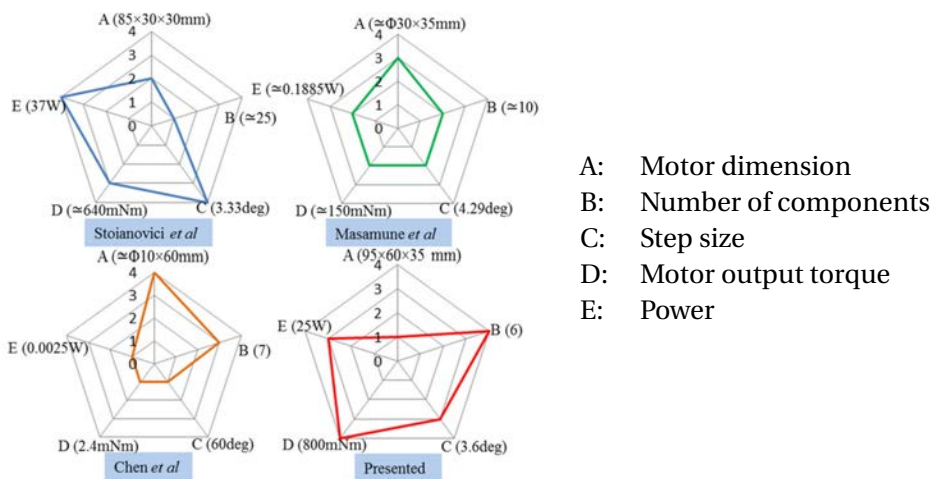
Figure 2.8: State of Art comparison by Chen et al. (2014a)

Author	Max Torque (mNm)	Angular Step (deg)	Max Step Error (deg)	Dimensions (mm)	Power (W)
Nutation: Suzumori et al. (2002)	2000	-	-	50x49	-
"PneuStep": Stoianovici et al. (2007)	640	3.33	0.028	85x30x20	37
Stepper: (Sajima et al., 2012)	150	4.29	2.1	30x35	0.189
Miniature: Chen et al. (2014b)	2.4	60	-	10x10x60	0.0025
High Torque: Chen et al. (2014a)	800	3.6	2	95x60x35	0.025
High Field: Secoli et al. (2015)	400	60	-	-	-
MotoP V1: Zhi (2015)	125	12	-		-

Figure 2.9: State of Art performance comparison

a 60deg fashion. Although their design avoids to use a gearbox and it is rather bulky, it can achieve a torque of 400mNm at {10rpm, 4bar, hose length not reported}. In order to enhance their control capabilities, they have also designed and implemented an MR compatible a position sensor which uses fibre optics to transmit the signal outside the MR room.

For the purposes of his master assignment, Zhi (2015) needed an MR-compatible actuator in order to drive McRobot, an MR-compatible patient mounted device for image guided minimally invasive interventions which is currently under development in the RaM lab. Naturally, he followed the literature, designed and implemented a basic version of a working MR-safe, pneumatic, stepper actuator, following the work of Sajima et al. (2010). The resulting actuator was tagged with the name "MotoP" and it can achieve a torque of 125mNm at {rotational speed not reported, 5bar, hose length not reported}. That was the beginning of the MotoP project, which aims to develop a multi modality compatible actuator, which should be able to be used as a COTS product, and comprise the flexibility of automated design for given desired specifications. This paper reports the development of the next version of MotoP.

Apparently the design space of such an actuator is vast. As examined above, the state of the art spans a huge range of designs and specifications. Since each actuator is developed within some very specific context, it is not possible to compare them referring to some common basis. Nevertheless, a collective representation of their characteristics is shown in Table 2.9[4]. However, the need of actuation in MR environments is extant, and since the requirements vary drastically, designing a universal actuator is rather utopian! Yet, it is towards this utopian direction that the MotoP project is proceeding, trying to alleviate these concerns through customisability. The resulting design should be such that given a set of desired specifications, the design parameters would be computed, producing the corresponding actuator to meet the requirements.

---

[4]After communication between Vincent Groenhuis and Yue Chen, a calculation mistake was discovered and the power of this actuator turns out to be 0.025W instead of the initially reported 25W.

3 Actuator Design

3.1 Problem Definition

Having as a starting point the desire of making a multi-modality compatible actuator (according to definition 2.1), the requirements of it being a non-metallic, non-magnetic, pneumatic, stepping motor have been derived in section 2.2. However, the list of requirements does not stop there. To start with, it must be possible to use the actuator in a broad range of applications, comprising different kind of mechanisms with versatile performance requirements. This means that it should be modular (designed as a mechanism to be mounted on other mechanical structures), embracing also widely used standards and protocols. Moreover, it must be customizable, i.e. the actuator must be dimensionalised properly to meet a given set of performance requirements. Apart from the modularity aspect though, it would be nice if commercial off the shelf products where used when possible in order to accelerate the design pace. To increase the range of possible applications, a requirement for the actuator to be bi-directional (ability to rotate both clock-wise and anti-clockwise) is included.

Naturally, the size must be as small as possible, in order to increase the application field. Moreover, since it is going to be used in medical environments, it is obvious that the design should follow applicable regulations and standards. In addition, the worst case scenario should guide the design so that it is assured that when failure occurs, the patient is not threatened by any harm. Complementing this, the requirement for back-drivability plays a role. For safety reasons, it must be possible for the surgeon to stop the procedure at any time and move the mechanism by hand. Therefore, the designed actuator should not lock at any point and it must allow for reverse motion when actuated by hand. Consequently, the back-drivability requirement induces uncertainty in the position of the actuator. When it is manually rotated, there is no way to estimate the new position, unless sensing is implicated. A position sensor would also improve the position estimation when a rotation step is missed due to any other possible reason. Next, comes the requirement for traceability/visibility in imagers. According to physicians, it would be nice if the actuator where visible in their images so that they can "see what they are doing" (radiologist Dr. Jeroen Veldman). However, as a rule of thumb, the MR-compatible materials are invisible to the imagers. Therefore, a way should be devised so that the actuator may be rendered on the imager's screen during the imaging procedure. Next, the requirements for MotoP v2.01 are summarised in a list, followed by the list of the emerging specifications.

Requirements

Must

>   This particular set of requirements is of high importance. Therefore, much effort and time should be invested towards achieving each and every one of them. Thus, the actuator must comprise the following characteristics:

Req1. Multimodality compatible

>   When the actuator is in the imager's field of view, it must yield no artefacts on the final images. Videlicet, the quality of the image must be affected as less as possible. The imagers of interest are primarily MRI & CT[1] scanners and secondarily PET scanners.

Req2. Modularity

>   It must be independent from the mechanism in which it will be integrated. The actuator should be designed such that it could become a module of a mechanical structure that could be designed in the future by a third party.

Req3. FDA/CE regulations compliance

>   It must satisfy sensitivity, reliability, accuracy, precision, sterilizability (or disposability), cost-effectivness and safety requirements for surgical procedures according to FDA/CE regulations.

Req4. Fail safe

>   The design must be based on the worst case scenario. The actuator must be designed such that it exhibits particular characteristics when some failure exists.

Req5. Customizability

>   It must be parametrically/modularly designed so that the CAD models or drawings may be updated by changing the parameters.

Req6. Back-Drivability

>   It must be possible to move the output shaft by applying certain force/torque. The stiffness of the actuator (as "seen" from the shaft) must must be adjustable. Videlicet, it must be possible to tune the static stiffness of the actuator, once, before it is put in action.

Req7. Compactness

>   The actuator must be as small and as light as possible.

Req8. Performance[2]

>   (a) It must deliver certain torque/force, precision/accuracy and speed.
>   (b) It must deliver certain strength/stiffness under certain loads.
>   (c) Backlash and lags must be as small as possible.
>   (d) It must outperform the currently available one, designed and implemented by Zhi (2015).

Req9. Position Feedback

>   The displacement of the actuator must be measured and provided as a sensory information.

Req10. Implementation

>   Prototypes must be delivered.

---

[1] CT scanners are a actually using a range of X-Ray images to recreate the 3D image of the scanned object. Making the actuator compatible with a CT scanner boils down to making it compatible with X-Ray scanners.

[2] The performance requirements are given as desired characteristics for each new actuator to be designed.

Req11. Demonstration
    The actuator must be operated digitally in a way that a proof of concept prototype
    may be demonstrated.

Should
    A set of requirements of secondary importance is outlined below. It is encouraged to
    work towards achieving these but failing to do so would not be considered as a big issue:

Req12. Functionality
    The actuator should be bi-directional.

Req13. Force Feedback
    The force exerted by the actuator to its load should be measured and provided as a
    sensory information.

Req14. Cost
    The overall cost of the actuator (implementation, maintenance, replacement)
    should be as low as possible.

Req15. COTS products policy
    Off the shelf products should be preferred than from the scratched designed com-
    ponents.

Req16. Standardization
    Standards, protocols and strategies promoted by companies which produce off the
    shelf products (e.g. Maxon) should be followed.

Req17. Traceability in imagers
    The actuator should be traceable in MR/CT images. There should be appropriate
    markers to allow for digital reconstruction of the actuator's pose.

Req18. Control
    A local controller/compensator/stabilizer should be included.

Could
    It is neither mandatory, nor important to fulfil the following requirements. They are taken
    as points to have in mind.

Req19. Visibility in imagers
    The actuator could be made such it is visible in MR/CT images.

Req20. Continuity
    Improving former designs is encouraged rather redesigning from scratch.

Abbreviation List		Importance Range
θ^o	θ degrees	High
rpm	Rotations Per Minute	Medium
SNR	Signal to Noise Ratio	Low

Table 3.1: Specifications list legend

Specifications

Technical

Id	Description	Value	Importance	Rel. Req.
Sp1.	**Angular Step:** The minimum possible angular displacement by which the actuator may increase its angular position.	$< 60^o$	High	Req8.
Sp2.	**Step Error:** The maximum difference between the desired new possition (angular displacement) and the actual new position when the position is increased by one step.	$< 0.9*$Sp1.	High	Req8.
Sp3.	**Nominal Speed:** The number of revolutions it should perform in a fixed amount of time, when providing its maximum torque.	< 10rpm	High	Req8.
Sp4.	**Min Torque:** The minimum twisting force that the actuator is capable to apply to its load when rotating at its nominal speed (Sp3.)	125mNm	High	Req8.
Sp5.	**Dimentions:** The dimensions of the convex hull of the volume occupied by the actuator should be minimized.	66x66x80mm[1]	Low	Req7. Req8.
Sp6.	**Weight:** The weight of the actuator must me minimized.	< 81g[1]	Low	Req7. Req8.

Safety

Id	Description	Value	Importance	Rel. Req.
Sp7.	**Multi-Modality Compatibility:** It should be Intrinsically "Multi-Modality Compatible" according to definition 2.1	–	High	Req1. Req3.
Sp8.	**Materials:** It should be made solely of Group1 materials (according to Stoianovici (2005)).	–	High	Req1. Req3.
Sp9.	**MR Safe:** It should be "MR Safe" according to ASTM International (2005).	–	High	Req1. Req3.

Special attention is to be paid throughout the design process in order to comply with the requirements that are not linked to some quantitative specification. Aspects such as modularity

---

[1]when delivering 125mNm

(Req2.) and functionality (Req12.) originate in design choices rather than particular measurable indicators. These design choices are discussed in sections 3.2 and 3.3 during the conceptual and the detailed design phases respectively.

3.1.1 Design Guidelines

The medical nature of application field of the actuator drives most of the design choices that are made. It is of paramount importance for the actuator to be inherently safe, which means that it should be safe when (almost) no assumptions are made as for any external factors and without the need of precise manufacture or by using any control methods to make it safe during operation.

To this end the design should be such that the actuator never clogs. Therefore at any point in time, at any point within the actuation period, the device should be able to move by applying certain inputs, regardless what the previous state had been. In addition, the materials and the way they are used will be chosen such that the functionality of the actuator does not change through time, while the mechanical properties of the materials might change.

Then, symmetry is intensively pursued when it comes to the shape, the involved forces or any other aspect. A symmetric actuator is beneficial for a variety of reasons. Symmetry in shape means uniform mass distribution, and consequently simplified dynamic behaviour of the mechanism on which the actuator will be attached. On the other hand, symmetry in forces means uniform wear of materials and thus, extended operational life and increased performance. Remarkably, the list of benefits of having a symmetric mechanism could keep going eternally. As a rule of thumb, symmetry is always saluted.

Another important design guideline is compactness. Maximal use of space not only reduces the size of the emerging actuator for a given performance requirement set, but it also reduces its weight and cost because of the lowered amount of material needed.

Finally freedom of customisability plays an important role. The design should be such, that it alleviates inherent constraints and allows for customisability according to a set of performance requirements.

Having these aspects in mind, during the conceptual design phase, it is attempted to derive the optimal shape of the actuator.

3.2 Conceptual Design

The designs examined in the literature review (section 2.3) include several actuation principles such as wobble motors, two stroke engines, nutation motors and direct acting stepper actuators.

A wobble motor, is similar to a harmonic drive with the difference that the outer rim, which is attached on the stator, is not rigid. Contrarily, it is composed of an elastic material which is deformed using linear actuators acting upon its circumference. The deformed outer rim' s shape is an oval, which is tangent to the rotor at two of its internal points. Thus, by sequentially activating the linear actuators, it is possible to change the orientation of the oval shape, imposing a rotation on the rotor. A characteristic example of a wobble motor is the "PneuStep" actuator examined earlier. This actuation principle can provide outstanding resolution with very smooth transition between the steps. However, it comes with some disadvantages. First and foremost, the linear actuators on the circumference induce an eccentric motion which creates oscillations outside the shaft axis. Moreover, it is important to carefully regulate the timing of actuation in order to maintain the proper oval shape and the desired rotational speed. This can be a major disadvantage when the pneumatic dynamics are considered. Also, the necessity of using the linear actuators on the circumference means that it is very difficult to reduce the size of such an actuator. Finally, the fact that rubber material is required results in reduced stiffness

and reduced precision in the output. The performance and mechanical characteristics of the rubber change through time, resulting in augmented actuator' s performance.

The two stroke engine principle is a typical way to transform translational to rotational motion while linear actuators are activated sequentially rotating a crankshaft. A typical example is the "High torque actuator" examined earlier, which showcases the principal advantage of this actuation principle. However, disadvantages similar to the wobble actuator exist. It is impossible to avoid eccentric vibrations, the input actuation timing is important and it is significantly bulky. Moreover, precision is reduced since holding the actuator in position directly depends on the pressure and implied forces of the linear actuators. Finally, its resolution is proportional to the number of linear actuators used, which means that achieving significant resolution requires significant increase in size.

The nutation principle involves a stator and a rotor always in contact to each other. The stator is suspended by a universal joint which allows it to roll without slipping with respect to the rotor (Uzuka et al., 2009), which is suspended by a rotational joint. It is possible to impose the nutation motion on a properly suspended stator using linear pneumatic actuators. Similarly to the wobble motor, this principle yields a very smooth motion with high resolution. The fact that the linear actuators have been moved to a position perpendicular to the rotor's plane allows for more compact designs. On the other hand, as discussed earlier, the device is still asymmetric imposing eccentric motions, the timing of actuation is important and the precision is reduced. Concluding, it is particularly difficult to implement the required universal joint, which complicates the design.

Last but most interesting of all, come the direct acting stepper actuators, such as the "10mm actuator" by Chen et al. and the "rotational stepping actuator" by Sajima et al. This principle involves "direct acting" gears which exert forces directly on the rotor. The gears are activated by linear pneumatic actuators and they rigidly interact with gears of the rotor. As a result, it is possible to reach high precision and high stiffness. At this point, it is worth to carefully examine the "10mm actuator" compared to the "rotational stepping actuator". The former avoids the eccentric motion by having the rotor/piston to follow a linear motion exerting all forces symmetrically. Moreover, in this design, the timing of actuation is not crucial since it will not compromise the functionality of the actuator. Nevertheless, both designs are simple to implement, compact and they avoid using rubber. On the other hand, the rotational motion is not smooth at all, and achieving high resolution is rather impossible. Finally, the most important disadvantage is that percussion is imminent in this design.

Certain advantages and disadvantages of each actuation principle have been singled out in Table 3.2, in an attempt to identify the most suitable solution. It is obvious that direct acting actuators comprise a range of important advantages. Thereafter, the new design will be based on this principle.

Taking Zhi (2015) actuator as a starting point, MotoP v2.01 is developed by following a step by step procedure. At each step, the prevailing problems are identified and a new design choice is made to fix them, tailgating the procedure to the next step. Naturally, what is described below is an ideal sequence of design steps, contradicting what happens in practice where a design choice might lead to a dead end.

Zhi (2015):

 MotoP v1 (shown in Figure 3.1) is composed by three pistons acting upon a rotor, forcing it to move by interlocking their respective teeth. Since the piston teeth are shifted w.r.t the rotor teeth, each stroke induces an angular shift. One piston is actuated at a time by pressurising its barrel following a sequence of piston actuations. This sequence defines the direction of rotation. In order to cope with leakage issues, Zhi decided to introduce an elastic diaphragm made out of rubber to separate the pressurized chamber in the barrel

	Wobble	Two stroke	Nutation	Direct acting
+	Very smooth Resolution	High power	Very smooth Resolution Compact	Simple design Precision Timing not important No rubber needed Compact Symmetry is possible
-	Asymmetric Timing is crucial Not precise Not compact Needs Rubber Compliant	Asymmetric Timing is crucial Not precise Not compact Small Resolution	Asymmetric Timing is crucial Not precise Complex design	Not smooth Percussion Small resolution

Table 3.2: Actuation principles comparison

and the chamber in which the piston moves. This diaphragm turns out to be not robust, failing constantly. As a retraction mechanism, laser cut rubber was used also. Here, the dynamic behaviour and the retraction speed are imposed by the (slow) behaviour of the rubber, which is undesired. Nevertheless, the most important issue with using rubber in key points that define performance is the fact that the rubber's mechanical properties change through time, thereafter compromising the actuator's performance. The last, but most important aspect lies in the structure of the design itself; it is asymmetric both in shape and the implied forces. Each piston stroke induces a force acting on the circumference, inducing a torque that tries to rotate the actuator around one of its radial axes, which induces vibrations. Finally, it is worth to examine the design freedom regarding the step size provided by the structure of the design:

$$StepSize^{-1} \propto \#Teeth * \#Pistons$$

which means that in principle, it should be possible to reduce the step size as much as necessary. However, this is not the case, since the sum of the areas of the pistons should be less than the bore area. This leads to unavoidably reducing the force exerted by each piston when increasing the number of pistons. Moreover, the number of pistons is also bounded from below, since the minimum number for bi-directional motion is three. In practice, this is the only choice which in turn means that the area of each piston is even less that one third of the bore' s area due to implementation reasons (wall thickness, clearances).

Problems:

- Geometrical constraint leads in reduced force.
- Stroke asymmetry leads to vibrations.
- Shape asymmetry leads to varying moment applied on the mechanism to be driven depending on orientation.
- Rubber usage induces slow dynamics and change of performance through time.
- The diaphragm is not robust.
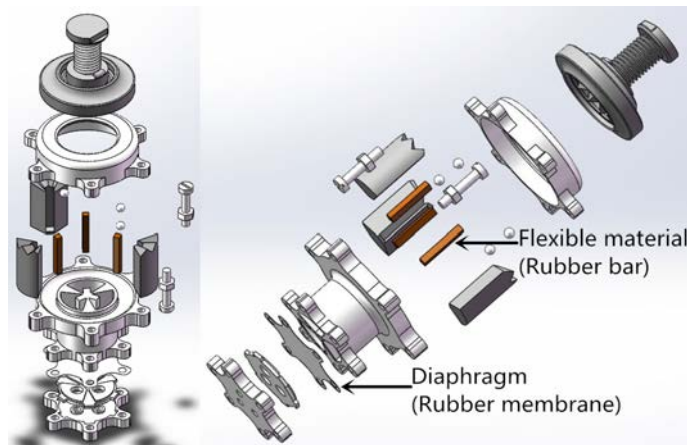
Figure 3.1: MotoP v1 exploded view
Courtesy: Zhi (2015)

Solution:
The whole actuation principle is redesigned introducing symmetry and reducing the piston number, as described next:

Rotor Design:
Compromising the number of pistons choice freedom, the rotor is redesigned by incorporating a fixed number of two pistons, one opposite of the other as shown in Figure 3.4. However, the fact that there is no choice over the piston number any more is not that critical since the choice had never been there in the first place, as discussed earlier. The mislay here is the increase of the step size, since the number of pistons is decreased by one and fixed to two. Yet, this design choice provides a range of advantages and fixes all the problems of the previous design. The step size may be decreased by using a gear box where necessary, in order to compensate for this design choice.

The rotor design introduces the so much craved for, symmetry. Not only upon the rotor itself, but on the whole design as well; a fact that will become apparent later on. The symmetry in shape not only serves in providing uniform moments exerted on the mechanism to be driven, but it comprises one more important advantage. Latent in the design of the opposing chambers driving the rotor, is a negative feedback mechanism. When a given chamber is pressurised, the rotor moves towards the opposing chamber which was pressurised earlier. It now de-pressurises through its driving valve towards the environment, thus resisting the motion. This mechanism, reduces in principle the percussion force when the rotor reaches its extreme positions. Moreover, there is no need to dump any excess air to the environment around the actuator any more.

The assets of the rotor design do not stop here, yet it provides force symmetry at each stroke as well. The exerted force is always on the axial direction, which means that the vibrations are constrained to the shaft axis. Most importantly though, it maximises the area usage of the bore making the piston area roughly three times larger. Apart from the much bigger force in the axial direction, the number of teeth that are in contact on each stroke is vastly increased, resulting in exerted torque multiple times larger than earlier.

Next, the irregular cross section shape of the pistons used in MotoP v1 is replaced by a circular shape, discarding the corners which used to hinder the ceiling. Thereafter, the need of the diaphragm is now alleviated.
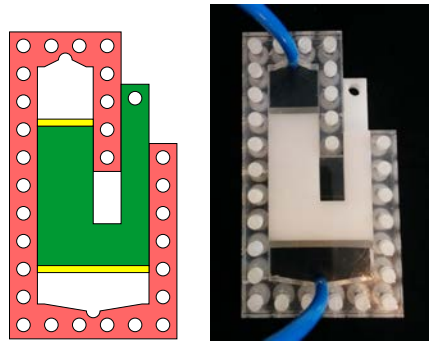
Figure 3.2: Chamber Vs Shaft separation principle.
Courtesy: Groenhuis and Stramigioli (2016)

Problems:
Beneficial as it might be, the new design introduces two new problems:

- The merging of the piston and rotor functionalities in one part, creates the problem of a proper design of the shaft that provides the output torque while decoupling the translational and rotational motion of the rotor. The solution of this problem is discussed right below (see "Shaft Design")

- Loss of direction selection mechanism. It is no longer possible to impose the direction of rotation using the sequence of piston actuation. Instead, the rotation teeth (the teeth of the rotor and the matching teeth on the stator) have to be redesigned, as discussed in ("Rotation Teeth Design")

Shaft Design:
V. Groenhuis dealt with the design and implementation of pneumatically actuated mechanisms (Groenhuis and Stramigioli, 2016). In order to cope with proper sealing of moving pistons, he used a rubber material which he could laser-cut and he devised an ingenious way of separating the pressurised chamber and the shaft as shown in Figure 3.2. He argues that this way, the ceiling of the pressurised chamber can be achieved more easily and effectively than having the shaft sliding within a pressurised chamber through an orifice towards the outer environment.

The same principle is used here in order to construct the rotor/shaft. To start with, the piston of Figure 3.2 is mirrored w.r.t the large yellow line, creating the template illustrated in Figure 3.3a. Then, that template is revolved in order to create the rotor/shaft and the question emerges: around which edge is it better to revolve? The two outcomes are shown in Figure 3.3.

Choice 3.3b yields a shaft of wider radius but it is much more difficult to decouple the translational and rotational motion in that case. Moreover, it is well known that the cylindrical shell shape is not stiff in radial directions (Soemers, 2011). Finally, but most importantly, according to lemma A.0.1, increasing a piston' s radius R by dr yields a bigger area increase than increasing a smaller piston with radius $r < R$ by the same dr. Thereafter, it is better to place the shaft at the inner side, providing the freedom of radius expansion over the larger, outer radius. This allows for torque output increment at a lower volumetric cost, which yields a more compact design.

Problem:
Of course, it is not clear yet neither how the translational back and forth motion is transformed to rotation, nor how the rotor and the shaft are separated. These aspects are described in "Rotation Teeth Design" and "Motion Decoupling" paragraphs respectively.

(a) Template to be revolved

(b) Revolution around piston

(c) Revolution around shaft
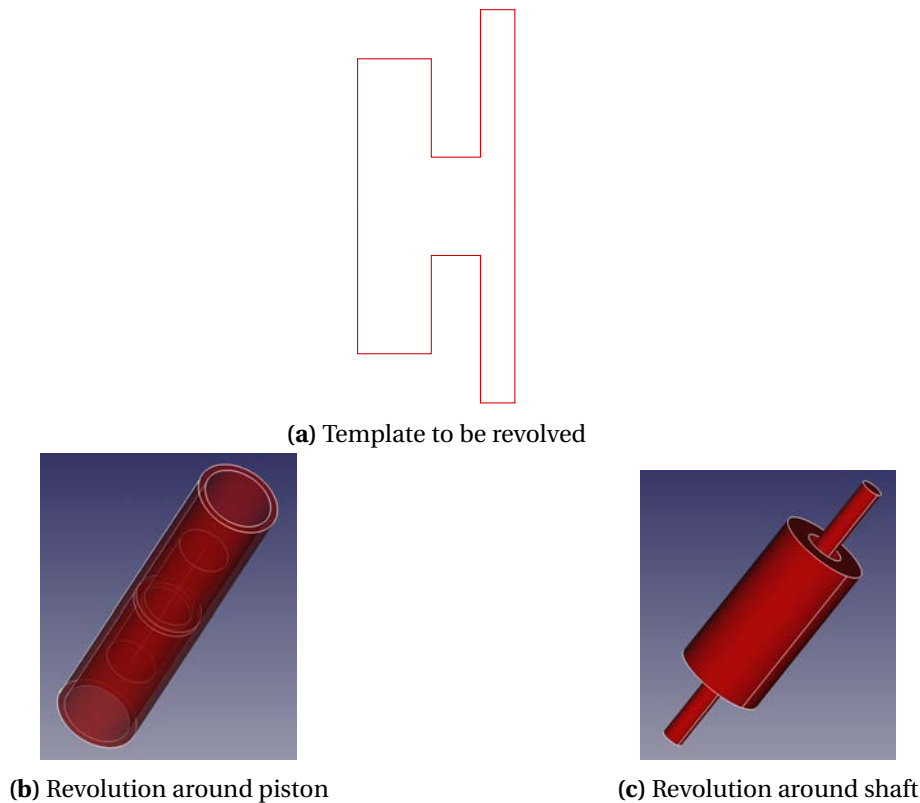
Figure 3.3: Rotor Construction

Rotation Teeth Design:

MotoP v1 works based on the principle shown in Figure 3.7. The pistons are actuated in sequence $\{P_1, P_2, P_3, P_1, \dots\}$ for anti-clockwise rotation and $\{P_3, P_2, P_1, P_3, \dots\}$ for clockwise rotation. The new principle involves rotation teeth fixed on the stator which is composed of the two bores one opposing each other (see Figure 3.4). When sequentially pressurising the chambers, the rotor moves back and forth between the two bores (translational motion). When it reaches the extreme position, the rotor' s teeth rack engages the bore' s teeth rack, which forces it to rotate.

Since the new rotor design includes only two pistons, the previous actuation technique can not be applied any more. In order to fix this, one must make three observations:

- According to Proposition A.0.2, the rotation teeth must be symmetric.
- The rotor/stator teeth can not be perfectly aligned.
  There has to be a tiny offset in order to misalign the vertices of the teeth and allow for respective sliding as shown in Figure 3.5
- The required offset can not be provided by misaligning the stator' s teeth as shown in Figure 3.6
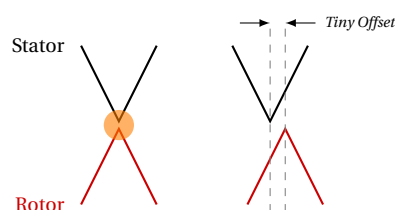
Figure 3.5: Rotor/stator teeth misalignment is necessary
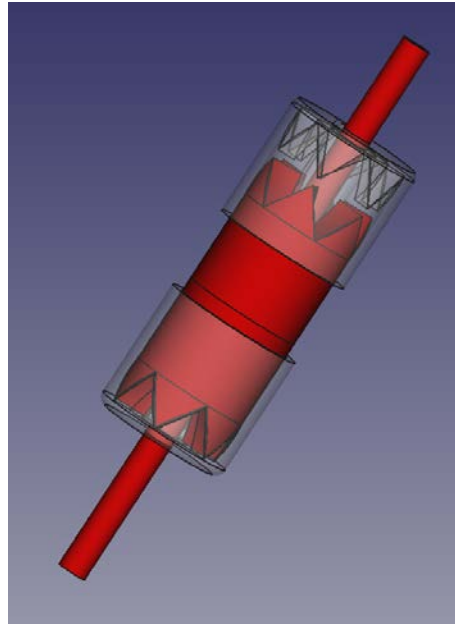
Figure 3.4: Rotor new actuation principle rendering
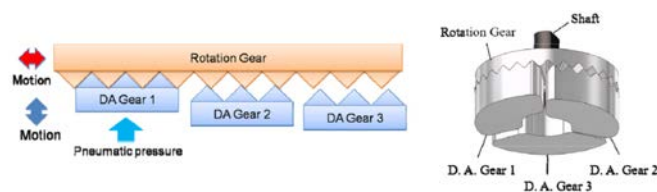
Figure 3.7: MotoP v1 actuation principle
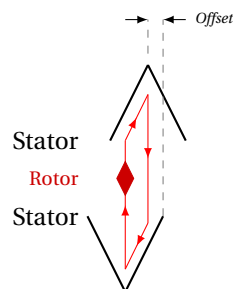
Figure 3.6: Stator teeth misalignment comprises a deadlock hazard

The above mentioned constrains, when combined together, compose a problem which can not be solved by tuning the current configuration. The need of misalignment between the rotor/stator teeth (Figure 3.5) and the deadlock hazard when the stator's teeth are misaligned (see Figure 3.6) signify that the tiny offset has to be provided from a structure in some other dimension. This might be abstract and difficult to understand at a first glance, but it becomes clear when the solution is examined at "Direction Selector Design"

Motion Decoupling:
 It is apparent that the rotor performs a combined rotational and translational motion. However, the output shaft must only transfer the rotation to the load. Thereafter, a way must be devised so that the combined motion of the rotor is decoupled.
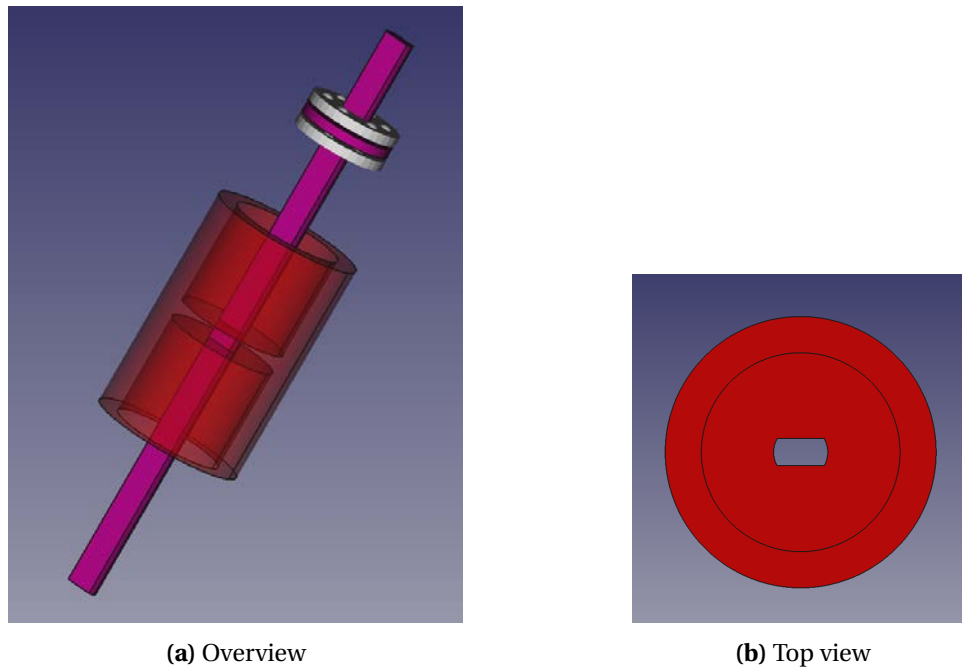
(a) Overview

(b) Top view

Figure 3.8: Rotor/Shaft motion decoupling

When it comes to precision, the best choice would be to use flexures in order to constrain the rotation between the rotor and the shaft, while allowing the rest of the motions free. Ideal as it would be, this solution is postponed because not only it requires proper material choice, but it also imposes a limitation on the stroke length. Flexures require small deflections in order for the analysis to hold, which means that they should be made long enough so that their end moves little when compared to their length. In a customisable actuator where the stroke length varies depending on the performance requirements, the design of a proper flecture would be not worth the trouble; at least not in the first development phase.

Instead, the much simpler solution shown in Figure 3.8 is chosen. The non-circular profile of the rotor/shaft interlocking mechanism allows for sliding but not rotating between the two parts. Of course, the friction and the wear will eventually play a role, ending up in backlash at the output. These are issues that have to be dealt with in a successive development phase. The translational motion is constrained using a couple of ball bearings which allow rotation but hold the shaft in place.

Direction Selector Design:

As discussed earlier, a module is necessary in order to shift the rotor w.r.t. the stator. The direction selector serves this purpose, as well as providing a mechanism in order to chose direction of rotation. It is practically a rim which holds an extra teeth rack responsible for the tiny offset required at each stroke. While the rotor moves from one extreme to the other, a pin attached on it comes in contact with the shift teeth on the direction selector, forcing it to rotate by a tiny offset and misalign the rotation teeth rack of the rotor w.r.t. the rotation teeth rack of the stator. The principle is depicted in Figure 3.9. The direction selector may be fixed on one of two positions, thus defining the position of the shift teeth w.r.t. the stator' s rotation teeth. This imposes which side of the shift teeth comes in contact with the rotor pin, and consequently the direction of rotation. Notice that Figure 3.9 is actually not complete. In fact, one rotor pin is not enough, but at least two pins are necessary. One is engaged on the forward and the other on the backward stroke. The two pins must abstain a fixed offset in order to finely align with the direction selector pins.

However, these design details are currently left out for the sake of simplicity and they are examined thoroughly in section 3.3
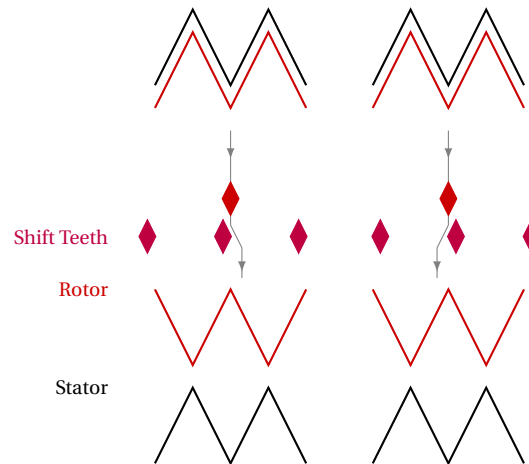
Figure 3.9: Direction selector principle. Left: Anti-Clockwise rotation (towards the right side). Right: Clockwise rotation (towards the left side)

Problem:
Of course, the direction selector is only designed because it is necessary for the whole concept to function. No such module would be used, unless it was absolutely necessary, which is unfortunately the case as proved above. Latent in the direction selector module is the Achilles' heel of the new design. Firstly, the shift teeth should be as small as possible while being strong enough to withstand the percussion and the exerted forces. This introduces a dependency on the used material's mechanical properties, a fact which is rather unpleasant. Moreover, it will be proved in the detailed design (Chapter 3.3) that the number of these teeth is inversely proportional to the resolution of the actuator. Therefore, the more precise the actuator is, the more shift teeth must be stacked in the direction selector's circumference. Since there will always be a minimum manufacturable shift tooth size, the circumference of the direction selector must increase to accommodate the increased shift teeth number. Nevertheless, it has been decided to examine this design choice further since it allows for the implementation of the new concept, whose numerous advantages have been discussed earlier in this section.

Three new issues emerge from this design:

- How is the direction selector going to be actuated. (Discussed in "Direction Selector Actuation").
- How is this design going to be modified to become back-drivable. This is examined in "Shift Teeth Design".
- Since the direction selector radius depends on the step size, and the rotor' s (so the piston' s) radius depends on the available pressure and the desired torque output, these two radii do not match in principle. Therefore, a new structure must be designed to allow for the rotor' s pins to come in contact with the shift teeth, which is the job of the "Rotor Pin Holding Rim".

Shift Teeth Design:
The shifting mechanism has already been described above and illustrated in Figure 3.9. However, it is not yet clear how the actuator is going to be back-drivable. Indeed, the mechanism in Figure 3.9 has to be augmented in order to allow for free rotation in either

side when the two chambers are not pressurised. To do that, the shift teeth are split in half to create a channel in which the rotor pin can freely move when the rotor is in the neutral position, i.e. in the middle between its two extremities. This concept is shown in Figure 3.10(Left). However, this design is still not satisfactory since it carries a clogging hazard. When the rotor pin is at a random position in the channel in between two of the shift teeth, it might stick on the flat side of a tooth when the rotor is pushed towards either of the extreme positions. The clogging hazard is alleviated, by redesigning the teeth to take a rhombus shape, so that there is always a way out of the channel by pushing the rotor either upwards or downwards, as shown in Figure 3.10(Right).
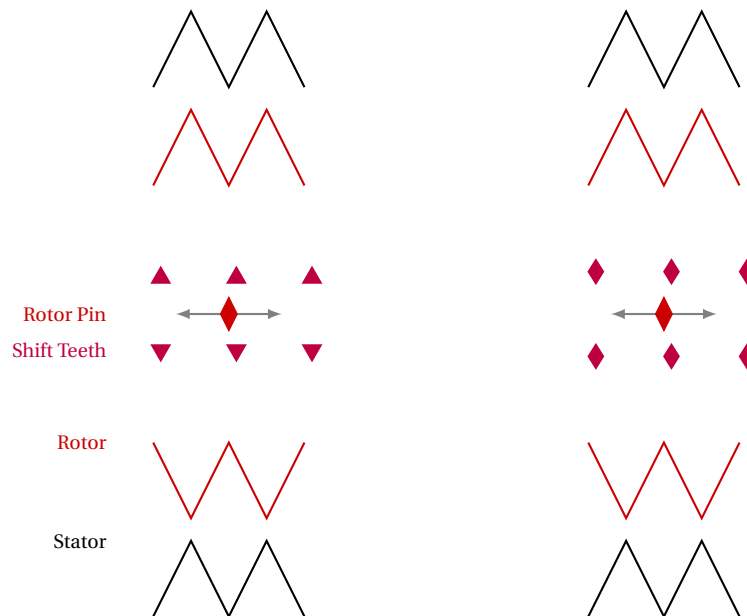
Figure 3.10: Shift teeth principle. Left: Allows back-drivability but contains clogging hazard. Right: Clogging hazard alleviated.

Problem:
Although this was not clear in the beginning, the last steps in the shift teeth design increase the height of the actuator significantly. Particularly, during the detailed design phase became also apparent that the stroke length of the rotor should be big enough so that the rotor pin travels through the whole height of the direction selector. This significantly increases the size of the actuator as well as the momentum gained by the rotor while moving, and consequently the percussion forces.
Solution:
To minimise the effect of this, the rotor must be made as light as possible and the shift teeth must be as small as possible.

Rotor Pin Holding Rim Design:
As mentioned earlier the radii of the piston and the direction selector are in principle not the same. It will become clear later on, during the detailed design, that the output torque is proportional to the piston area and the actuation air pressure. Also, the area is obviously proportional to the radius of the piston. Thus, given a desired output torque and an operational air pressure, the piston radius can be defined. On the other hand, the direction selector radius must be big enough to create a circumference able to accommodate all the shift teeth. The number of the shift teeth though, is directly related to the desired resolution. Consequently, given a resolution specification, the direction selector radius is defined.
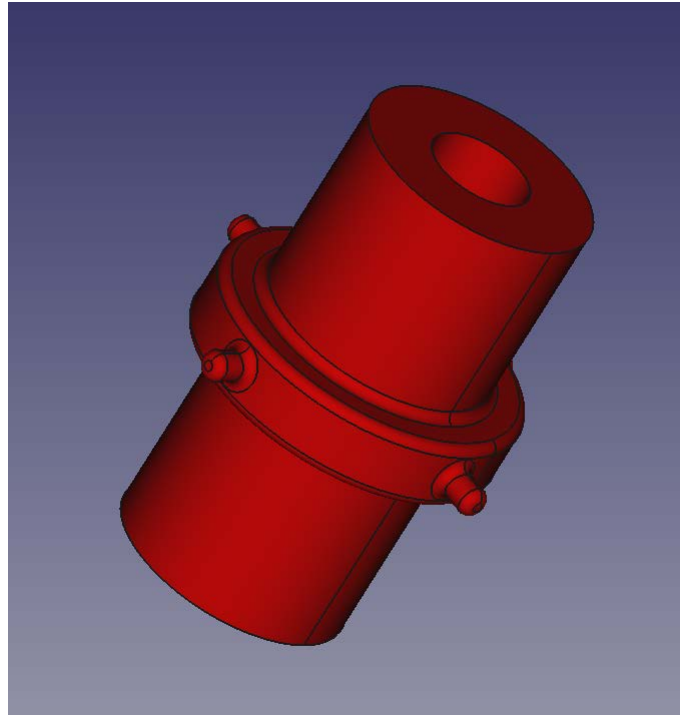
Figure 3.11: Rotor pin holding rim principle

The fact that these two radii are different, creates the need of designing a structure to hold the rotor's pins so that they can come in contact with the shift teeth. To this end, a rim was designed in the middle of the rotor which can be expanded as much as necessary, as shown in Figure 3.11

Direction Selector Actuation:
As discussed earlier and depicted in Figure 3.9, the position of the shift teeth with respect to the stator's rotation teeth imposes the direction of rotation. This can be achieved by switching between two fixed positions of the direction selector. Figure 3.12 shows a new structure, called the assembly rim which was created to ensure that the direction selector can only take one of the two mentioned positions. The two cuts on the assembly rim's circumference have the precise arc necessary in order to fix the direction selector at the desired positions when its pins reach either end of the assembly rim's cut.

Of course, this motion must be remotely actuated somehow. It is indeed possible to drive both back and forward rotations by two opposing pistons, similarly to the rotor's actuation principle. This solution requires two air hoses added to the already required two hoses for the rotor, summing up to a total of four. Moreover, the assembly rim must hold all the parts of the actuator together. Therefore, it is made such that it encircles the dir selector and the two bores are mounted on the top and bottom sides. A "slide and lock" mechanism is used which allows the bore to be easily fixed into position and constrains the axial motion. Two bolts are used at each side in order to constrain the rotation. This provides the advantage of taking away the percussion forces from the bolts to the assembly rim, while on the rotational motion, the tangential forces are counter acted by both the bolts and the friction between the assembly rim and the bores.

Retraction mechanism:
When the actuator is in back-drivable mode, the rotor should be kept in the neutral position (middle), such that the rotor pins are kept between the shift teeth. Two opposing springs are used as a retraction mechanism to serve this purpose, as shown in Figure 3.13.
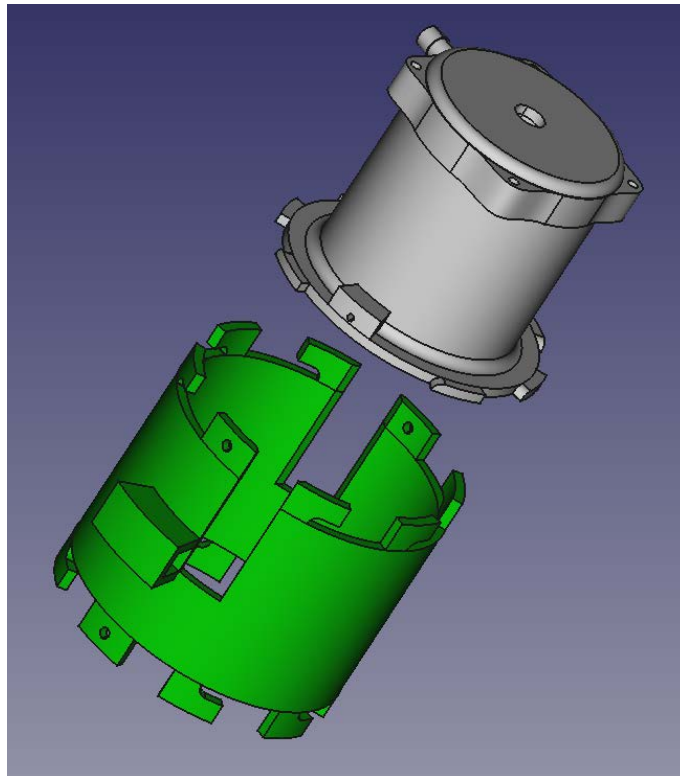
Figure 3.12: Assembly rim principle

Although this method was not favourable because it induces unwanted dynamics in the system and it also reduces the output torque, it was unfortunately impossible to avoid. The alternative solution would be to allow the rotor to slide back to the neutral position by rotating the output shaft. However, there is an inherent locking condition which imposes the rotation teeth's slope, thus preventing the slope to be designed for maximal output torque. Therefore, this solution was abandoned.

Back-Drivability Rubbers:

A very significant issue that has to be dealt with, is the loss of traction while the rotor passes through the neutral section on its way from one end to another. Naturally, it is back-drivable in this area, thus no element prevents it from rotating in either direction. Nevertheless, this is undesired when the actuator is actually driving a load. In this case, the load would force the rotor through the gap between the shift teeth on its way from one end to another, making the actuator useless in practice. This issue is addressed by the Back-Drivability Rubbers (BDR), depicted in Figure 3.14. These rubbers actually serve a second purpose as well. By selecting rubbers of different stiffness, it is possible to adjust the actuator's output stiffness in back-drivable mode, as described in the requirements. In practice, it is possible to engrave the rubbers using a laser-cutter, tuning their stiffness on demand. Moreover, this design choice allows for a stepwise back-drivable mode, making sure that any manipulator driven by this actuator is kept in place when the back-drivable mode is activated.

Sealing:

Naturally, the rotor/bore interface needs to be sealed in order to prevent air leakage and de-pressurisation of the chamber. Avoiding the use of standardised sizes of o-rings, since this would confine the design space of the actuator, laser cut rubber is used as a sealer. A channel is engraved on the rotor in order to hold the sealer in place, as shown in Figure 3.15. Following the work of Groenhuis and Stramigioli (2016), the sealer has to be
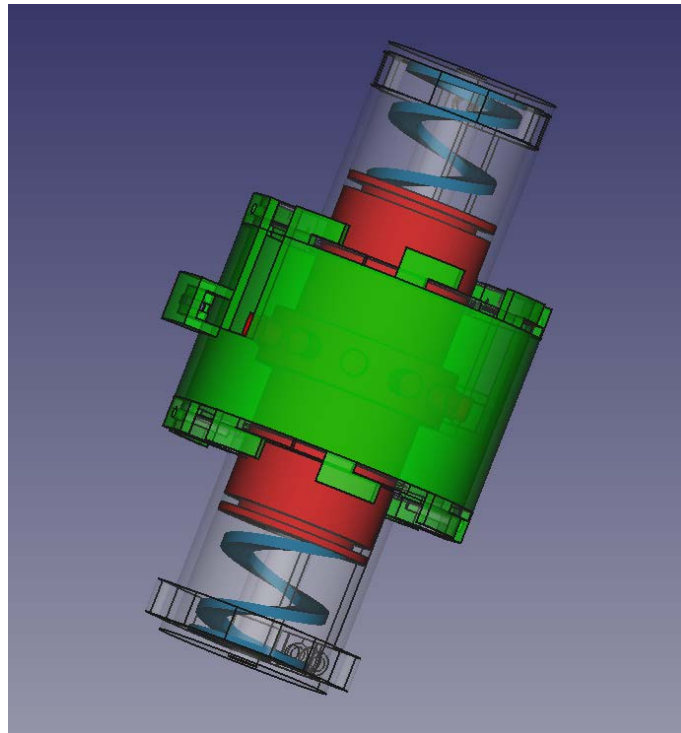
Figure 3.13: Rotor retraction principle
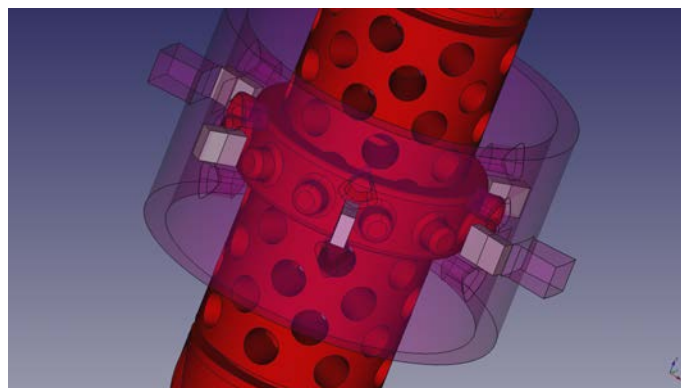
Figure 3.14: Back-Drivability Rubbers principle
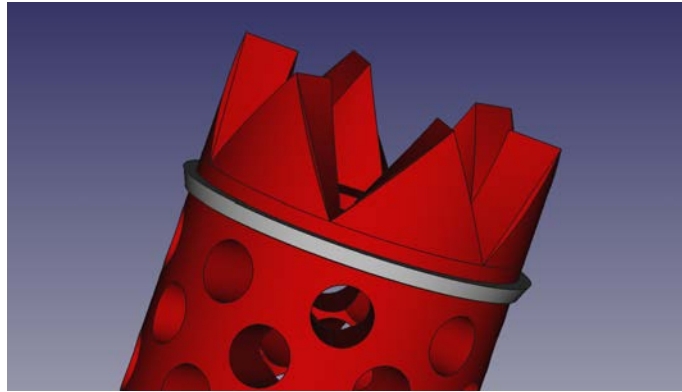
Figure 3.15: Sealing principle
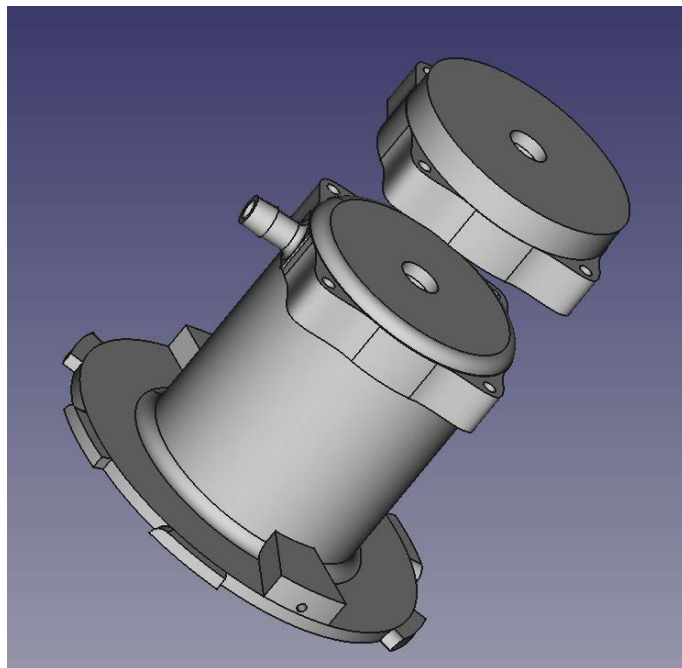
Figure 3.16: Modular interface principle

attached properly (i.e. the wider part in the side of pressure), in order to achieve optimal results.

Modular interface:

In order to accommodate the interfacing between heterogeneous modules, a rim is designed as shown in Figure 3.16. It should be the same for any module that is going to be designed in the future (e.g a gear-box, an encoder), so that the module can be seamlessly attached on the actuator in a modular manner. Moreover, it may serve as a mounting interface between the actuator and the mechanism to be driven.

The working principle of the final design is depicted in Figure 3.17.

3.3 Actuator Detailed Design

3.3.1 Actuator

After defining the shape of the new actuator during the conceptual design phase, it has to be modelled so that the dimensions of each part are properly defined. Thus, a structural model is

(a)   **(b)**   **(c)**   **(d)**   **(e)**
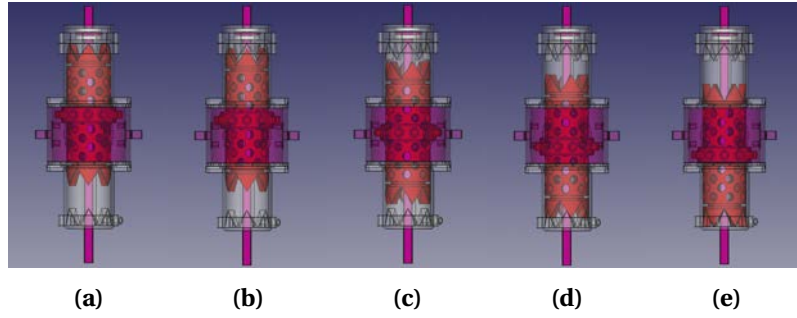
Figure 3.17: MotoP 2 working principle: a) Moving downwards. b) Shift right. c) Downwards through back-drivable region. d) Rotating right. e) End of stroke.

hereby developed which will enable the derivation of all the dimensions of an arbitrary MotoP 2.01 actuator, given a minimal set of desired parameters.

As shown in Figure 3.18, when the barrel is pressurised, the net force f is acting on the rotor in the axial direction. This force includes both of the force due to the pressure pressure acting upon the rotor's surface and the spring forces. The static friction force is disregarded for simplicity. While the rotor is sliding, since it is in contact with the inner surface of the bore, a kinetic friction force f_{kf} is exerted on it. Naturally, the direction of the kinetic friction force is opposite the direction of the velocity u of the rotor, which is following a screw motion. Then, the net force applied on the stator by the rotor, results in a pair of normal forces f_n acting on both bodies. Due to this normal force, a friction force is also acting on the interface between the teeth. Therefore the forces acting on the rotor can be summarised as follows:

$$\sum f_z = f - f_{kf}S_{\theta u} - f_f C_\theta - f_n S_\theta$$
$$\sum f_x = -f_{kf}C_{\theta u} - f_f S_\theta + f_n C_\theta$$

(3.1)

$$f = P(\pi r^2 - \pi r_{in}^2) + f_{springs}$$
$$f_{springs} = k(z_0 - z) - k(z_0 + z) = -2kz$$
$$f_n = (f - f_{kf}S_{\theta u})S_\theta + f_{kf}C_{\theta u}C_\theta$$
$$f_f = \mu f_n$$

(3.2)

Where[3]

f :	Net force due to pressure and springs
f_{kf} :	Kinetic friction force between bore and rotor
u :	Rotor velocity
θ_u :	Angle between vectors **u** and **z**
f_f :	Net tangential kinetic friction force
θ :	Rotation teeth steepness angle
f_n :	Normal force between teeth
P :	Air pressure in chamber
r :	Outer rotation teeth radius
r_{in} :	Inner rotation teeth radius
μ :	Kinetic friction coefficient
n :	Number of rotation/shift teeth
k :	Spring constant
z_0 :	Initial spring displacement
z :	Spring displacement

---

[3]Notation: The $\sin(\theta)$ and $\cos(\theta)$ functions are abbreviated as S_θ and C_θ respectively.
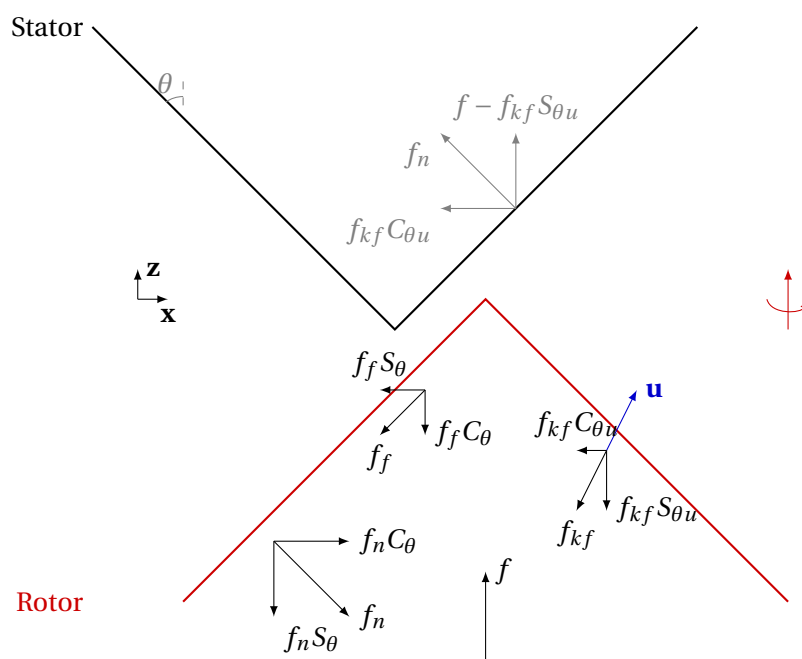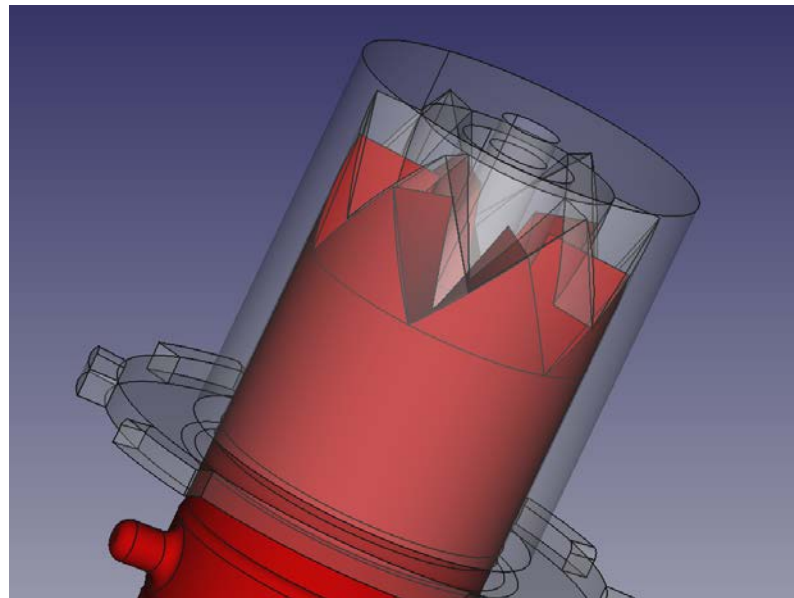
Figure 3.18: Force analysis on rotation teeth

The net tangential force (force on the x axis) is responsible for the rotation, which combining Equations 3.1 and 3.2 becomes:

$$
\begin{aligned}
f_t := \sum f_x &= -f_{kf}C_{\theta u} + f_n(C_\theta - \mu S_\theta) \\
f_t &= -f_{kf}C_{\theta u} + [(f - f_{kf}S_{\theta u})S_\theta + f_{kf}C_{\theta u}C_\theta](C_\theta - \mu S_\theta) \\
f_t &= f_{kf}(-C_{\theta u} - S_{\theta u}S_\theta C_\theta + C_{\theta u}C_\theta^2 + \mu S_{\theta u}S_\theta^2 - \mu C_{\theta u}C_\theta S_\theta) + f(S_\theta C_\theta - \mu S_\theta^2)
\end{aligned}
\tag{3.3}
$$

When the rotor is travelling from one extreme position to another, its motion is linear, and θ_u is almost equal to $\pi/2$. Thus, Equation 3.3 becomes:

$$
\begin{aligned}
f_t &\approx f_{kf}(-S_\theta C_\theta + \mu S_\theta^2) + f(S_\theta C_\theta - \mu S_\theta^2) \\
f_t &\approx (f - f_{kf})(S_\theta C_\theta - \mu S_\theta^2)
\end{aligned}
\tag{3.4}
$$

On the other hand though, when the rotor has reached its extreme position and already stopped, its velocity is equal zero and the kinetic friction force does not exist any more. Therefore, Equation 3.3 becomes in this case:

$$
f_t \approx f(S_\theta C_\theta - \mu S_\theta^2)
\tag{3.5}
$$

The torque applied by the actuator may then be derived considering that each of the n teeth applies the tangential force mentioned above. Assuming for simplicity that all forces are applied on the outer radius of the teeth. the torque then becomes:

$$
T = nrf_t
\tag{3.6}
$$

Combining Equations (3.4) and (3.6), an approximation of the dynamic torque is derived:

$$
T \approx nr(f - f_{kf})(S_\theta C_\theta - \mu S_\theta^2)
\tag{3.7}
$$

which is subsequently used in order to find the optimal rotation teeth steepness angle θ, which maximizes the dynamic torque:

$$
\begin{aligned}
\frac{\partial T}{\partial \theta} &= 0 \\
\frac{\partial}{\partial \theta}\left[nr(f - f_{kf})(S_\theta C_\theta - \mu S_\theta^2)\right] &= 0 \\
nr(f - f_{kf})(C_\theta^2 - S_\theta^2 - 2\mu S_\theta C_\theta) &= 0 \\
\Rightarrow (C_\theta^2 - S_\theta^2 - 2\mu S_\theta C_\theta) &= 0
\end{aligned}
\tag{3.8}
$$

Notice that starting from the static torque would yield the same condition. Therefore, the angle $\hat\theta$ that satisfies Equation 3.8 maximises both the dynamic and static torque. It is thus proven (A.0.4) that the optimal angle is given by

$$
\hat\theta = \arccos\left\{\pm\sqrt{\frac{1 \pm \sqrt{1 - \frac{1}{1+\mu^2}}}{2}}\right\}
\tag{3.9}
$$

At each stroke, i.e. when the rotor moves from one extreme to another, it rotates by an angle corresponding to half a tooth. Thus, the tooth step angle θ_s is computed after the desired resolution θ_{res} as follows:

$$
\theta_{s_{desired}} = 2\theta_{res}
\tag{3.10}
$$

Then, the number of rotation teeth that satisfies this resolution may be calculated. Referring to Figures 3.19 and 3.20:

$$\left.\begin{array}{c} S_T = \theta_s r \\ n S_T = 2\pi r \end{array}\right\} \quad \tilde{n} = \left\lceil \frac{2\pi}{\theta_{s_{desired}}} \right\rceil \tag{3.11}$$

Of course, n must be even, in order to have the same number of gaps and teeth, so the expression in Equation (3.11) becomes:

$$n = \begin{cases} \tilde{n} & \text{if } \tilde{n} \text{ is even} \\ \tilde{n}+1 & \text{if } \tilde{n} \text{ is odd} \end{cases} \tag{3.12}$$

and the actual step angle is recomputed:

$$\theta_s = \frac{2\pi}{n} \tag{3.13}$$

The inner radius of the rotation teeth r_{in} is imposed by the desired shaft radius. Then, the outer radius must be computed so that the actuator delivers the desired torque. Combining Equations (3.2) and (3.7) yields:

$$nr\left[\pi P(r^2 - r_{in}^2) - 2kz - f_{kf}\right](S_\theta C_\theta - \mu S_\theta^2) - T = 0 \tag{3.14}$$

which when solved gives the outer radius r and the depth of the rotation teeth may be calculated by:

$$d_T = r - r_{in} \tag{3.15}$$

(a) Overview

(b) Top view

$n = 8$ Teeth
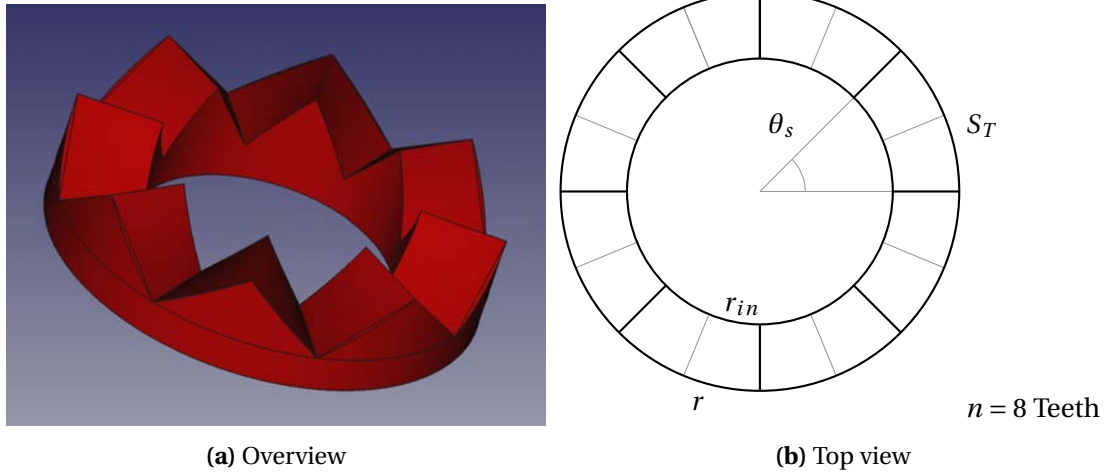
Figure 3.19: Rotation teeth

Referring to Figures 3.20 and 3.21 and lemma A.0.3, the rest of the dimensions of the rotation teeth may then be calculated:

$$\sin\frac{\theta_s}{2} = \frac{l_T/2}{r} \quad \Rightarrow \quad l_T = 2r\sin\frac{\theta_s}{2} \tag{3.16}$$

$$\tan\theta = \frac{l_T/2}{h_T} \quad \Rightarrow \quad h_T = \frac{l_T}{2\tan\theta} \tag{3.17}$$
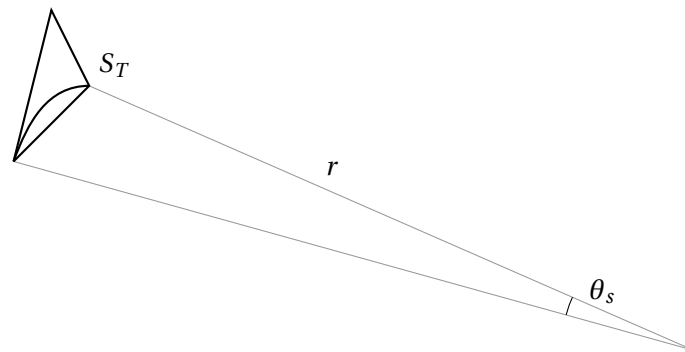
Figure 3.20: Arc of rotation teeth
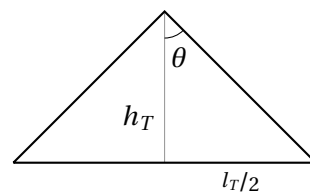
Figure 3.21: Rotation teeth dimensions

Where:
  S_T :   Rotation teeth outer arc
  θ_s :   Rotation teeth step angle
  θ :   Rotation teeth steepness angle
  d_T :   Rotation teeth depth
  l_T :   Rotation teeth length
  h_T :   Rotation teeth height

Next, the shift teeth, which are attached on the dir selector, are designed. Examining Figure 3.22 closely, one can draw Figure 3.24. It focuses on the case where the rotor passes through the shift teeth travelling from one extreme position to another. In that case, since the rotor pins must pass between the shift teeth, some clearance must be allowed. Notice also that the shift teeth sides follow the radial direction allowing for a wider base surface on the dir selector. Contrarily, the rotor pins comprise an unaltered circular profile in order to allow for larger base surface on the rotor. Of course, this situation is exaggerated in the schematics. In practice, the surfaces are almost co-linear.
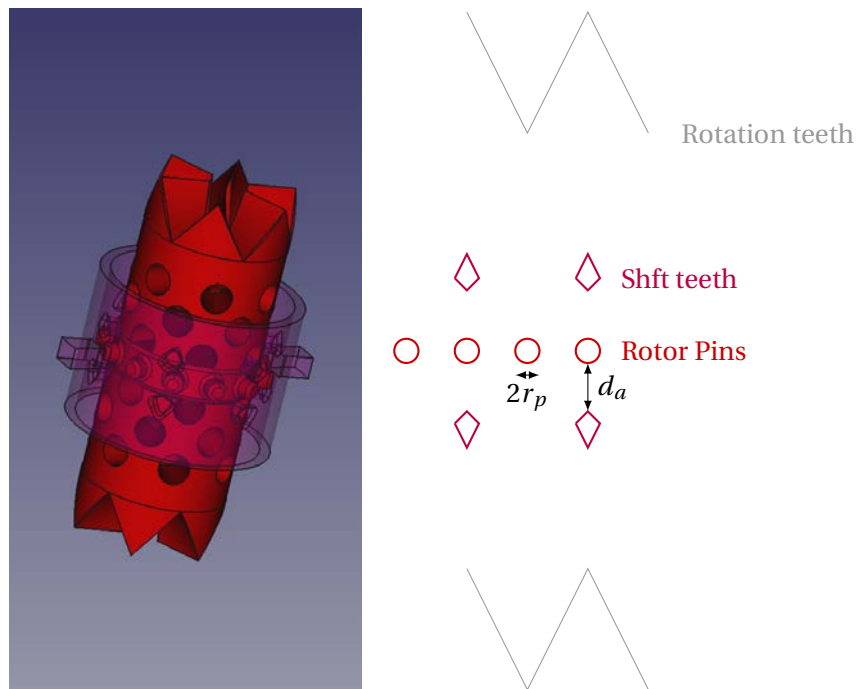
Figure 3.22: Shift teeth overview
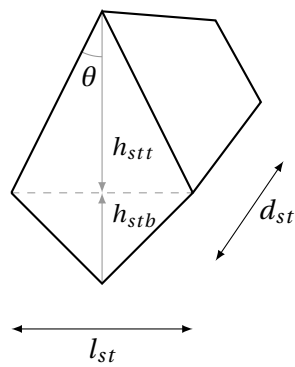
Figure 3.23: Shift teeth dimensions

(a) Side view   **(b)** Top view
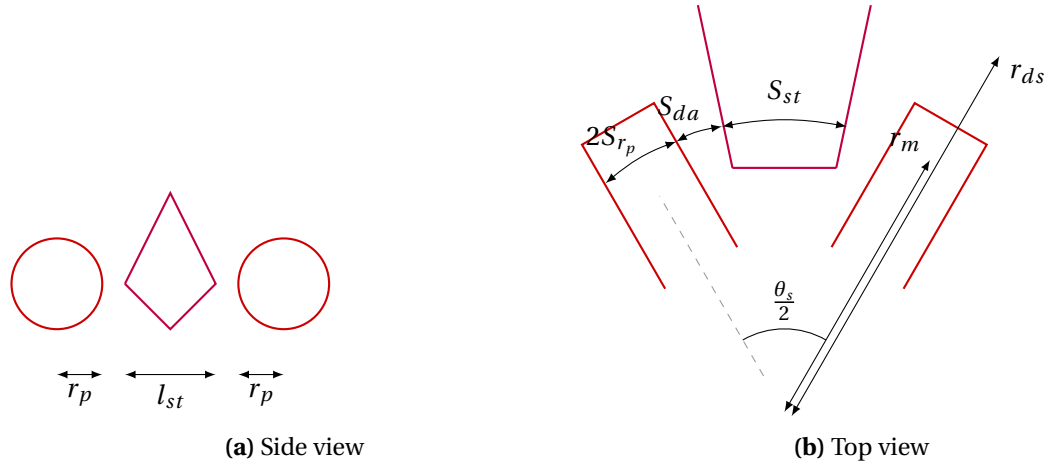
Figure 3.24: Shift teeth clearance

Where:
r_p :   Rotor pin radius
r_{ds} :   Dir selector radius
d_a :   No-Contact clearance
h_{st} :   Shift teeth height
l_{st} :   Shift teeth length
d_{st} :   Shift teeth depth (in the radial direction)
r_m :   Midway radius
S_{r_p} :   Arc of r_p at r_m
S_{d_a} :   Arc of d_a at r_m
S_{st} :   Arc of l_{st} at r_m

A careful look at Figure 3.22 reveals that the angle between two rotor teeth has to be equal to $\frac{\theta_s}{2}$ for the mechanism to function properly. Then, Figure 3.24b suggests that in order to allow the required clearance, the following relation must be satisfied:

$$\frac{\theta_s}{2} r_m = 2S_{d_a} + 2S_{r_p} + S_{st}$$

which by lemma A.0.3 becomes:

$$\frac{\theta_s}{2} r_m = 2r_m \left[2 \left(\arcsin \frac{d_a}{2r_m} + \arcsin \frac{r_p}{2r_m} \right) + \arcsin \frac{l_{st}}{2r_m} \right] \tag{3.18}$$

$$2r_m \left[2 \left(\arcsin \frac{d_a}{2r_m} + \arcsin \frac{r_p}{2r_m} \right) + \arcsin \frac{l_{st}}{2r_m} \right] - \frac{\theta_s}{2} r_m = 0$$

This clearance condition must be evaluated at the most perilous case, which is when r_m coincides with the edge of the shift teeth. In order to ensure this, the following must hold:

$$r_{ds} = r_m + d_{st} \tag{3.19}$$

Therefore, r_m is calculated via Equation (3.18) so that the clearance condition is satisfied. Then, using Equation (3.19), the radius of the dir selector is derived.

Focusing on the design of the shift teeth shown in Figure 3.23, two issues must be dealt with. Firstly, notice that the role of the shift teeth is to turn the rotor by a tiny angle on its way from one extreme to another. Theoretically, an infinitesimal shift should do. However, in practice there is a limitation on the minimum size that can be made, such that the tooth is strong

enough. In order to take this into account, the shift teeth size is set relative to the rotation teeth size:

$$l_{st} = \max\{l_T/3, l_{min}\} \tag{3.20}$$

Second, but most important, is designing the slope of the upper part of the tooth. When the rotor engages the rotation teeth on the way from one extreme to another, it will follow a screw motion. Inevitably, the rotor pin will follow the corresponding trajectory while being in a vicinity around the shift tooth. Thus, imposing the same slope on the upper part of the shift teeth to be equal to the slope of the rotation teeth, ensures that the rotor pin will move freely avoiding an imminent clogging hazard:

$$h_{stt} = \frac{l_{st}/2}{\tan\theta} \tag{3.21}$$

$$
\begin{aligned}
h_{st} &= h_{stt} + h_{stb} \\
h_{stb} &= \frac{h_{stt}}{2}
\end{aligned}
\tag{3.22}
$$

The cut on the assembly rim depicted in Figure 3.25 is designed such that it precisely stops the pin at two extreme positions that shift the dir selector by $l_{st}/2$. Lemma A.0.3 gives the shift arc required for this to hold:

$$S_{shift} = 2r_{ds}\arcsin\frac{l_{st}}{4r_{ds}} \tag{3.23}$$

Of course, the dir selector pin takes some space also. Its arc is given again by Lemma A.0.3:

$$S_{ds_p} = 2r_{ds}\arcsin\frac{l_{ds_p}}{2r_{ds}} \tag{3.24}$$

The cut arc is the given by:

$$S_{cut} = S_{shift} + S_{ds_p} \tag{3.25}$$

Where:

l_{ds_p} :	Dir selector pin length
S_{shift} :	Dir selector shift arc at r_{ds}
S_{ds_p} :	Dir selector pin arc at r_{ds}
S_{cut} :	Dir selector cut arc at r_{ds}

The stroke length is defined as follows, so that the rotor moves across the dir selector from the neutral to one extreme position, while assuring that it is large enough to cover for the rotation teeth height:

$$l_s = \max\{2r_p + 2d_a + h_{st},\ h_T\} \tag{3.26}$$

Where h_T is the height of the rotation teeth. Then, the height of the dir selector is defined as:

$$
\begin{aligned}
h_{ds} &= 2l_s + h_{cr} \\
h_{cr} &= 2r_p + 2d_a
\end{aligned}
\tag{3.27}
$$

Where h_{cr} is the height of the connecting rim. Figure 3.26 illustrates the detailed design of the rotor. The seal rubber dimensions are defined by the thickness of the available rubber. Similarly, the radius of the available spring (if a COTS product is to be used) defines the radius
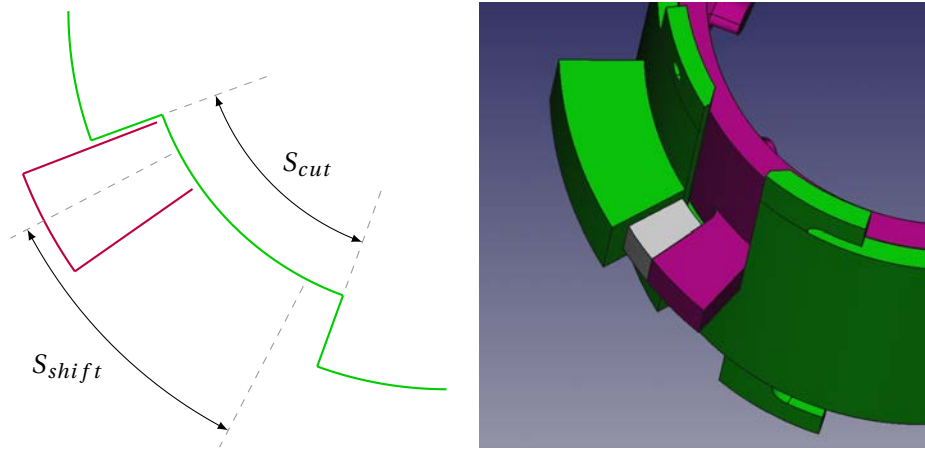
Figure 3.25: Assembly rim cut

of the inner cut. The radius of the connecting rim r_{cr} is defined by the dir selector radius as $r_{cr} = r_{ds} - d_p - da$. Finally, the height of the piston must be such that when the rotor is one of the extreme positions, the piston is still inside the opposing barrel, thus keeping it pressurised. Therefore

$$h_P = h_{pc} + h_{psc} + h_T$$
$$h_{pc} = h_{ds} - h_{cr} + da$$

(3.28)

Where:

h_P :	Piston height
h_{pc} :	Piston column height
h_{psc} :	Piston sealer cut height
h_{ds} :	Dir selector height

In order to decrease the volume of the rotor, holes following the pattern of Figure 3.27 are drilled. The diagonal distance between the holes is defined to be the same as their radii in an attempt to maintain strength while cutting away as much material as possible. This results in a 90° pattern.

$$\cos \frac{\pi}{4} = \frac{r_o + a/2}{3r_o}$$
$$a = \left(3\cos\frac{\pi}{4} - 1\right)2r_o$$

(3.29)

Each pattern is composed of primary and secondary rows/columns. Primary rows/columns comprise holes that abstain distance a apart on the vertical/horizontal direction respectively. Secondary rows/columns abstain distance $a/2$ apart on the vertical/horizontal direction respectively. Each piston of the rotor is drilled by n_H number of primary columns, and n_V number of primary rows. Consequently also n_H number of secondary columns and $n_V - 1$ number of secondary rows.

The sum of hole and spacing arcs in the horizontal direction must be equal to the rotor circumference, whereas in the vertical case, they should sum up to height H. Notice that H is defined
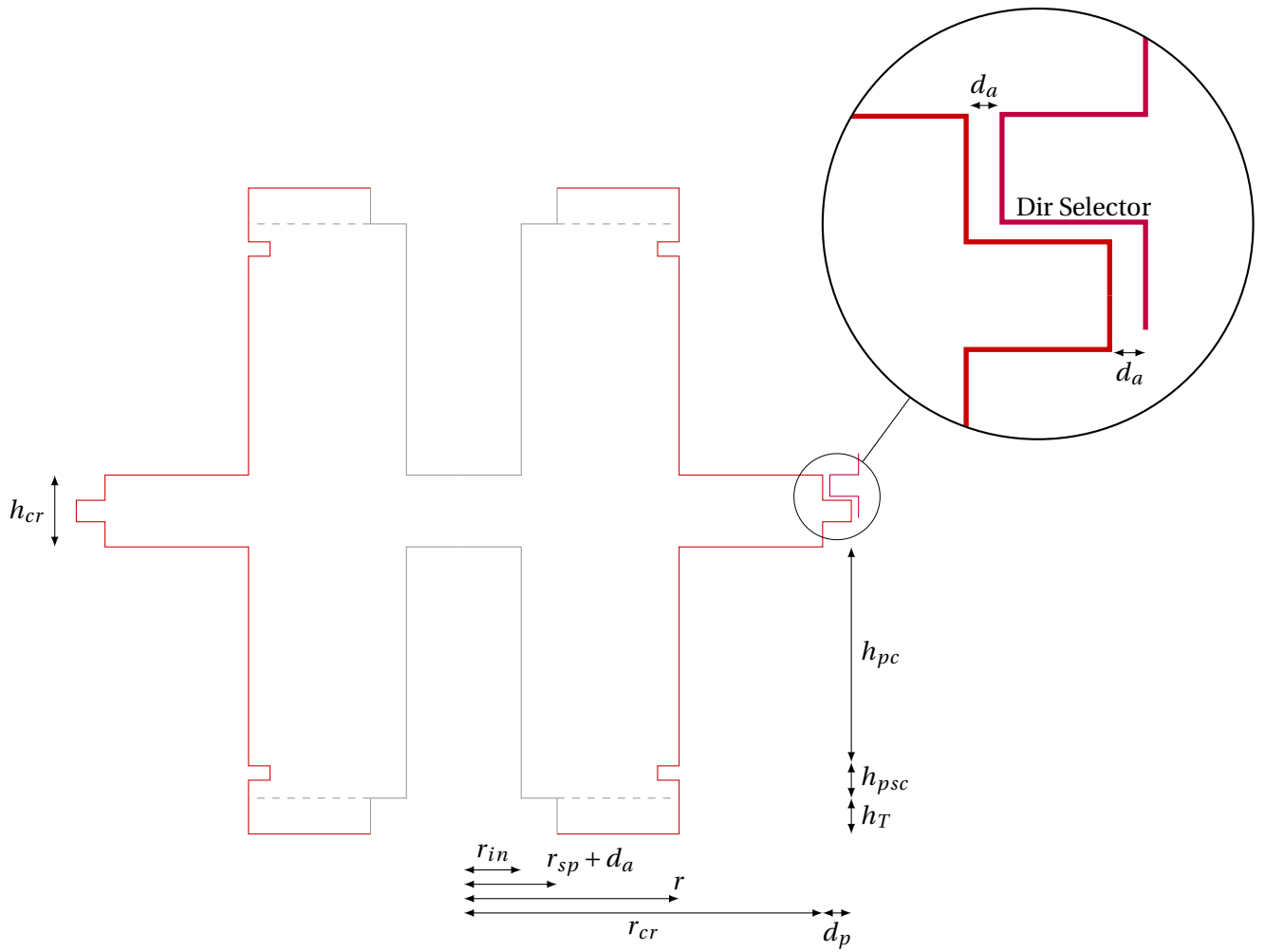
Figure 3.26: Rotor design
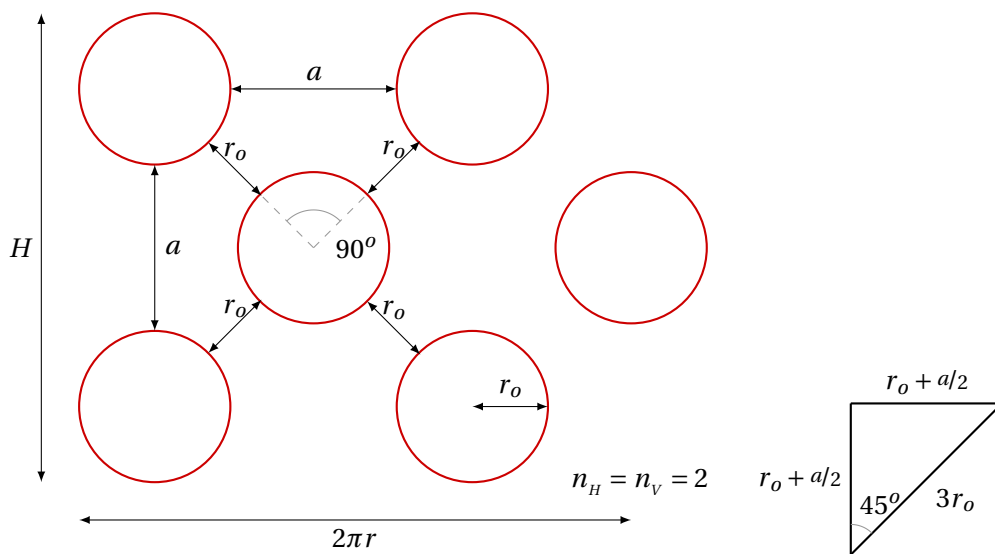
Figure 3.27: Perforated rotor design

such that the first hole below the rotor rotation teeth is far enough from the teeth in order to allow for a solid base.

$$n_H S_{2r} + n_H S_a = 2\pi r$$
$$n_H (S_{2r} + S_a) = 2\pi r \tag{3.30}$$

$$n_V S_{2r} + (n_V - 1)S_a = H \tag{3.31}$$

Following lemma A.0.3 and using Equation 3.29, the relations for S_{2r} and S_a are obtained:

$$S_a = 2r \arcsin \frac{\left(3\cos\frac{\pi}{4} - 1\right) r_o}{r} \tag{3.32}$$

$$S_{2r} = 2r \arcsin \frac{r_o}{r} \tag{3.33}$$

Substituting Equations (3.29) and (3.33) in Equation (3.30) yields:

$$n_H (S_{2r} + S_a) = 2\pi r$$
$$n_H (S_{2r} + S_a) - 2\pi r = 0$$
$$n_H \left[2r \arcsin \frac{r_o}{r} + 2r \arcsin \frac{\left(3\cos\frac{\pi}{4} - 1\right) r_o}{r} \right] - 2\pi r = 0 \tag{3.34}$$
$$\arcsin \frac{r_o}{r} + \arcsin \frac{\left(3\cos\frac{\pi}{4} - 1\right) r_o}{r} - \frac{\pi}{n_H} = 0$$

which when solved gives r_o

Of course, in order to solve Equation (3.34), n_H is necessary. Given an r_o the pair $\{n_H, n_V\}$ may be chosen such that the hole surface area is maximal and consequently the rotor volume is minimised.

$$A = n_H n_V \pi r_o^2 + n_H (n_V - 1)\pi r_o^2$$
$$A = (2n_H n_V - n_V)\pi r_o^2 \tag{3.35}$$

$$\{n_H, n_V\} = \arg\max A \tag{3.36}$$

In order to avoid solving this complex system, in practice it is possible to sweep through a range of pairs $\{n_H, n_V\}$, calculate the corresponding r_o from Equation (3.34), and A from Equation (3.35). Then, the pair that maximizes A is selected.

Finally, the bore is designed as a composition of a pressurisation barrel, the rotation teeth and a rim matching the assembly rim. As mentioned earlier, a shell surrounding the shaft is created in the center of the bore so that the piston is properly sealed. Air enters the chambers through inlets attached on the sides of the top and bottom bores as shown in Figure 3.28. A gap around the shaft shell is responsible for even air distribution acting upon the pistons, as well as avoiding the case where a very small air gap prevents the piston from moving and locks it in place. The radius of the air gap is calculated such that the total area is at least equal to the inlet area:

$$A_{gap} = A_{inlet}$$
$$\pi r_{rot\_teeth'}^2 - \pi r_{shell}^2 = A_{inlet} \tag{3.37}$$
$$r_{rot\_teeth'} = \sqrt{\frac{A_{inlet}}{\pi} - r_{shell}^2}$$
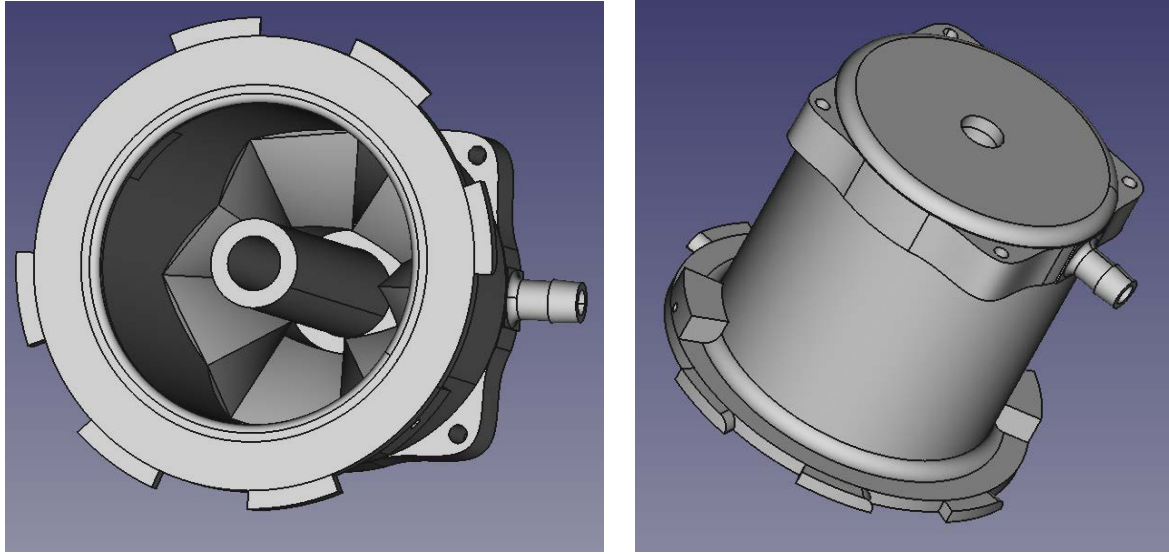
Figure 3.28: Bore overview
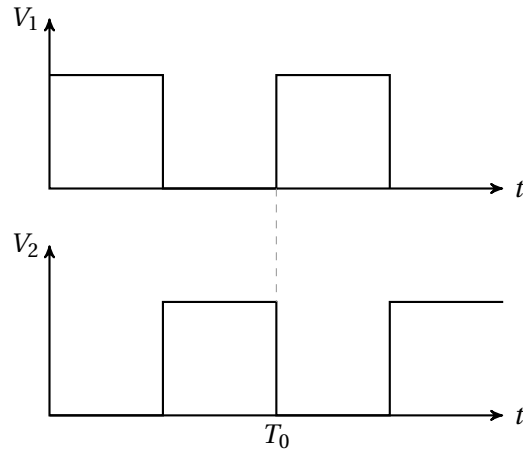
Figure 3.29: Valve input signals

$$r_{rot\_teeth} = \max\{r_{rot\_teeth'},\ r_{sp} + d_a\} \tag{3.38}$$

where r_{sp} is the radius of the retraction spring, which should fit inside the gap.

Figure 3.29 shows the input signals of the valves that drive the chambers of the actuator. The signals are complementary, so that when one chamber is pressurised, the opposing chamber is not. Thus, during a principal period of the input signal T_0, the rotor moves from one extreme to another and back, advancing by $\theta_s\ rad$ (one rotation tooth). Therefore, the shaft will perform a complete rotation when the rotor has passed through all of the teeth, so the actuation period is given by:

$$T = nT_0 \tag{3.39}$$

Introducing the angular velocity of the actuator yields:

$$nT_0 = T$$
$$T_0 = \frac{2\pi}{nw} \tag{3.40}$$

Eventually, the model is solved by following the equations causality graph of Figure 3.30 and the complete actuator looks like the one depicted in Figure 3.31
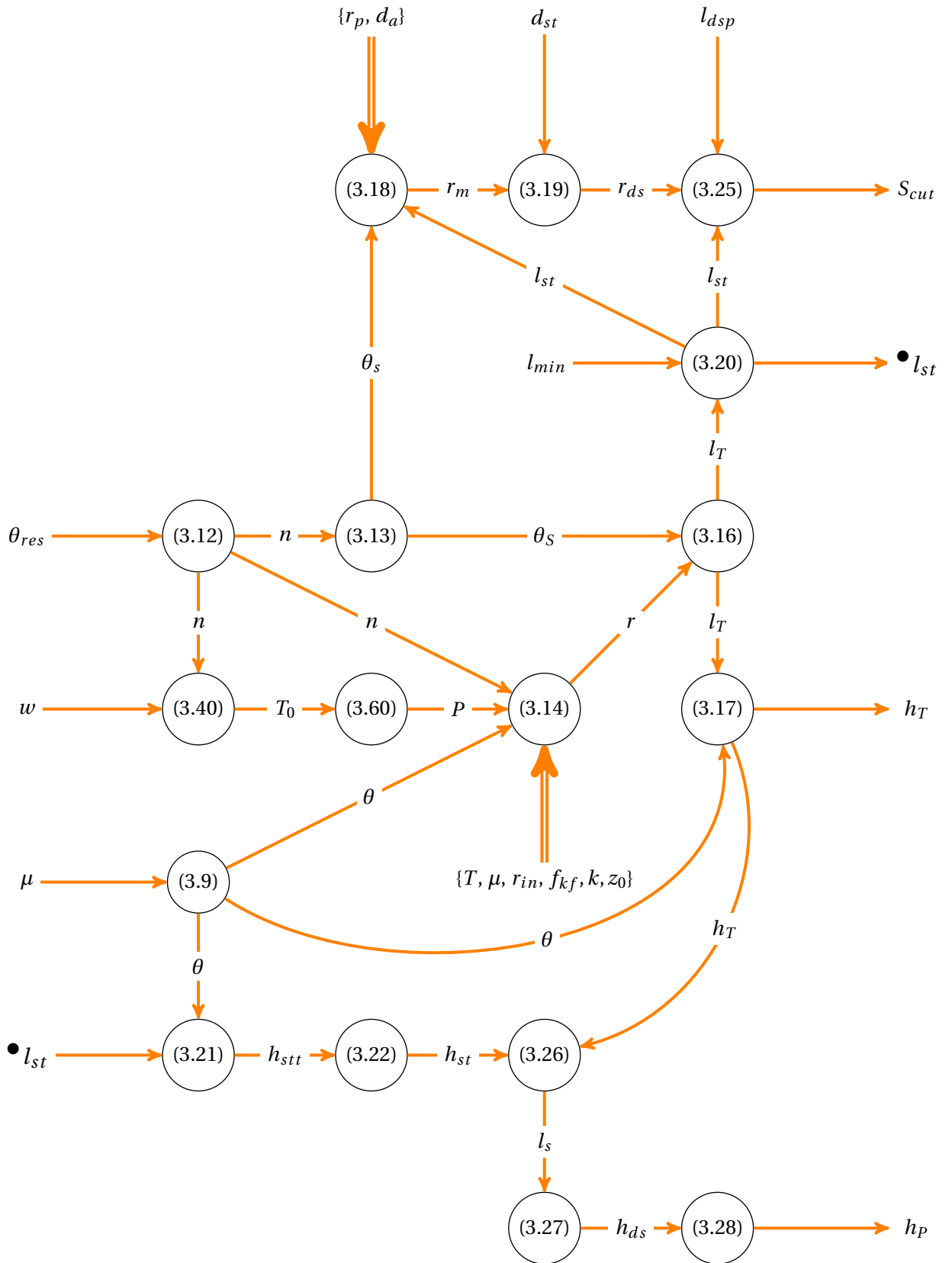
Figure 3.30: Mathematical relations causality graph
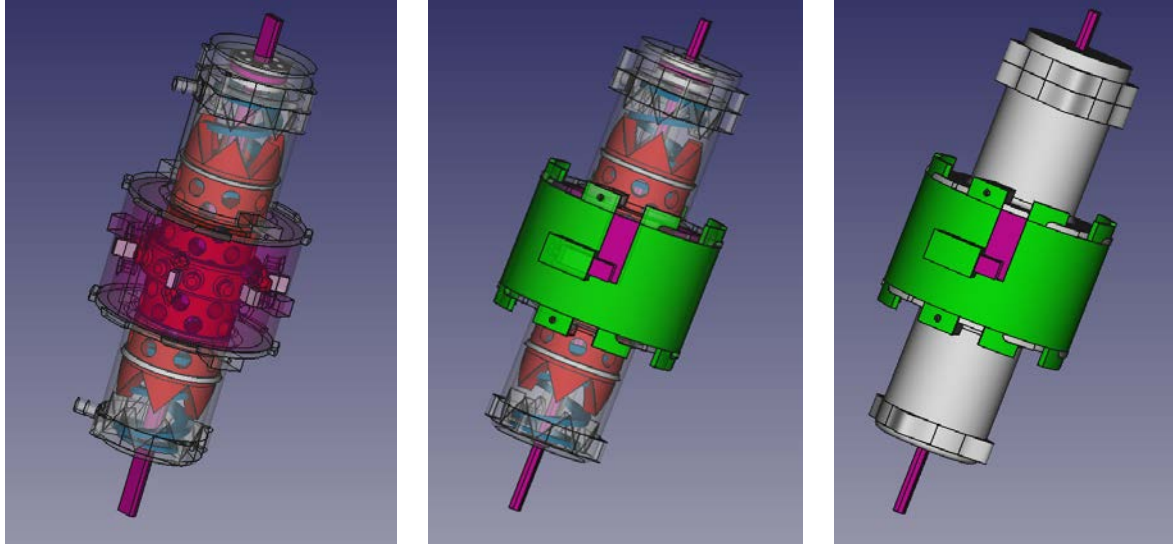
Figure 3.31: MotoP 2.01 overview

3.4   Sensor Detailed Design

Next, an MR compatible quadrature position encoder is designed as a module that can be attached on MotoP 2.01 series. According to (Fisher et al., 2014), "custom position and force sensors generally take an optical approach where signals are transmitted via optical fibers". This approach is followed here as well in order to develop a proof of concept encoder. Fibre optic cables are used to transmit optical signal inside the MRI bore to the optical encoder. The beam is periodically interrupted by the encoder disk depicted in Figure 3.32 and then read back by a returning fibre optic cable.

In order to satisfy the Shannon's theorem of sampling, the resolution of the encoder should be at least twice as much as the resolution of the actuator. Since a quadrature encoder design is implied though, the resulting resolution is actually double the resolution of a linear encoder:

$$
\begin{aligned}
\theta_e &< 2\frac{\theta_s}{2} \\
\theta_e &< \theta_s
\end{aligned}
\tag{3.41}
$$

In practice, the encoder segments tend to be significantly small, introducing difficulty in manufacturing. For the purposes of this project, a proof of concept prototype was created by 3D printing. Therefore, the desired resolution is set to be relatively big (big angle increments), in order to allow for the disk to be printed:

$$
\hat{\theta}_e = \frac{\theta_s}{3}
\tag{3.42}
$$

The number of segments, i.e. either hollow or solid circular arcs, is of course an even number, so that the circular arrangement has equal number of hollow and solid segments:

$$
\begin{aligned}
\hat{n}_{seg} &:= \left\lceil \frac{2\pi}{\hat{\theta}_e} \right\rceil \\
n_{seg} &= \begin{cases} \hat{n}_{seg} & \text{if } \hat{n}_{seg} \text{ is even} \\ \hat{n}_{seg} + 1 & \text{if } \hat{n}_{seg} \text{ is odd} \end{cases}
\end{aligned}
\tag{3.43}
$$
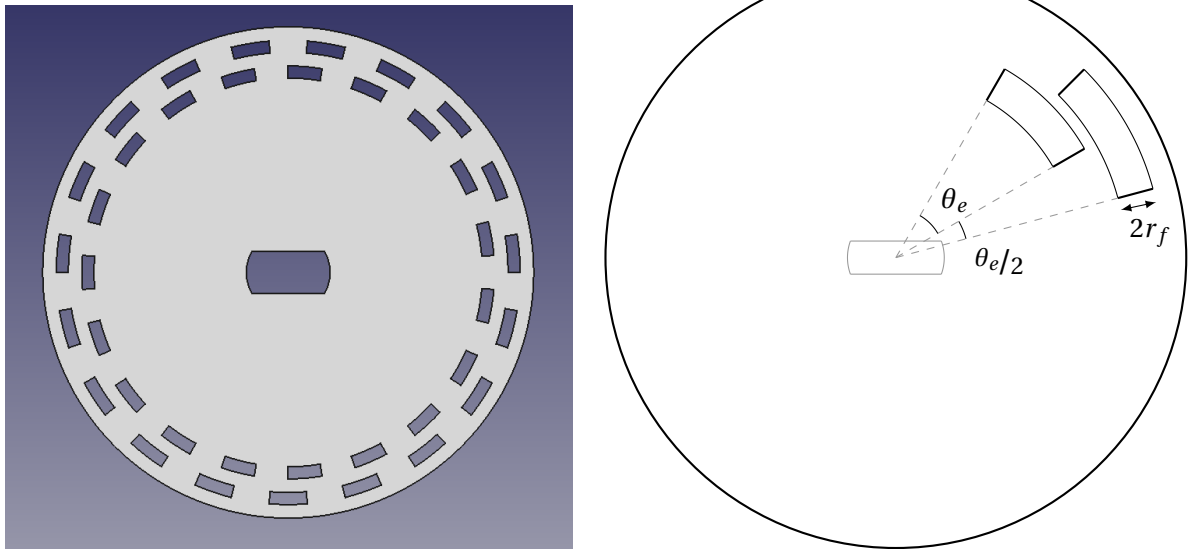
Figure 3.32: Encoder disk design

and the final resolution of the encoder is given by:

$$StepSize_{enc} = \frac{\theta_e}{2} = \frac{\pi}{n_{seg}} rad \tag{3.44}$$

Since it is a quadrature encoder, two lines of segments are required. Their radii are not actually of importance, so they are chosen as large as possible (i.e. the closest to the disk's circumference), in order to increase the segment arc sizes.

Once the encoder disk is designed, then it is only necessary to have a housing that holds everything in place. Figure 3.33 shows such a housing which allows the actuator's shaft to pass through and rotate the encoder disk. The disk itself is suspended using two commercial plastic ball bearings and centred by being in contact with the housing on its circumference. The fibre optic cables are kept in place using four holding caps. The outer radius of the housing is defined by the outer radius of the actuator it is being designed for. That, imposes in turn the radius of the encoder disk.

3.5 Air Hose Modelling

Prevailing in literature is the problem of pressure drop along the pneumatic line that powers the actuators. The dynamics introduced by the air hose which supplies the actuators with pressurised air, are such that researchers were forced to use metallic pneumatic valves inside the MRI room in order to reduce the hose length down to at maximum $1m$ (Chen et al., 2014b), (Secoli et al., 2015), (Chen et al., 2014a), (Sajima et al., 2012) in an attempt to obtain sufficient air pressure to drive their actuator at higher frequencies with reduced delay (Gassert et al., 2006).

In order to acquire more insight in the effect of the air hose on the system's dynamics, a macroscopic model is derived, aiding in the process of selecting tubes of optimal dimensions depending on the application. The model encompasses characteristics of the hose such as its length, diameter and material properties, as well as the supply pressure. Next, it is validated on a range of experiments by varying the principal model parameters.

Structure:
The developed model corresponds to the setup depicted in Figure 3.34. Since this model will be used in order to describe the behaviour of the pneumatic line that drives an MR compatible
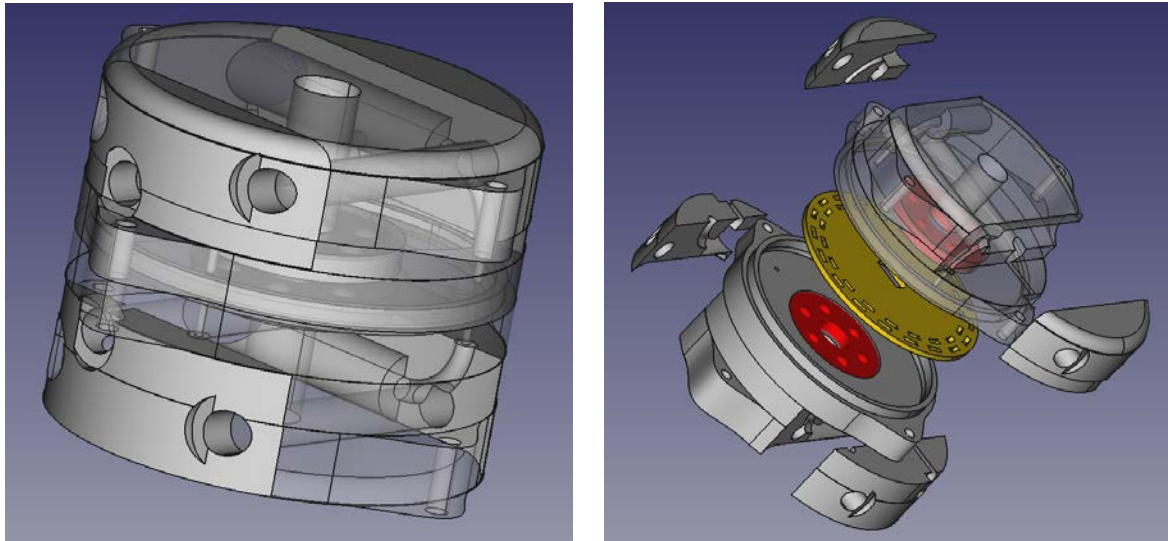
Figure 3.33: Encoder overview

Figure 3.34: Pneumatic model structure

actuator inside the MR room, the air source is assumed to be the existing pneumatic network of the hospital. A plastic hose of circular cross section is attached on the inlet through a valve and its other end is assumed to be closed (for simplicity). Notice that when the actuator is attached, the other end can not be assumed close but it is loaded with a volume which varies through time.

Assumptions:

- The thermodynamic process of air flow through the hose is assumed to be **isometric** (constant volume).

- The thermodynamic process of air emission from the source to the hose is assumed to be **isentropic**, i.e the source acts as an ideal compressor.

- Compressed air is assumed to behave as an **ideal gas**.

- It is a **pinhole model**, i.e. the hose is assumed to be "adequately short" so that:

$$\left. \begin{array}{l} u_{(t,l)} = u_{(t)} \\ \rho_{(t,l)} = \rho_{(t)} \end{array} \right\} \text{ constant across } l \tag{3.45}$$

where u is the air velocity, ρ is the air density and l the distance from the source across the hose. Notice that this assumption is undoubtedly wrong, but it is introduced in the sense that the change inside the tube may be neglected.

- The air flow type inside the hose does not change. Therefore, the **Reynolds number** is relatively **constant**.
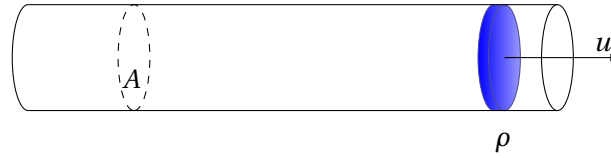
Figure 3.35: Pneumatic tube cross section

Model

Notation:

P [Pa] :	Air pressure	$\mu = 19.83$ [$\mu Pa\,s$] :	Air dynamic viscosity
m [kg] :	Air mass	u [m/s] :	Air velocity
ρ [kg/m^3] :	Air density	A [m^2] :	Tube cross section area
T [K] :	Air temperature	V_a [m^3] :	Volume of air hose
$R = 287$ [J/kgK] :	Air gas constant	g [m/s^2] :	Acceleration of gravity
$\gamma = 1.4$ [–] :	Air specific heat ratio	z [m] :	Height across direction of g

It is desired to express the pressure at the end of the hose (output pressure) as a function of the pressure at the origin (input pressure) and of course other parameters of the hose such as its length and diameter.

In order to derive an expression for the pressure, it is assumed that the air emission from the source to the pipe can be modelled as an isentropic process. Then, the fraction of $\frac{P}{\rho^\gamma}$ remains constant, and the following relation holds:

$$\frac{P_{(t+\Delta t)}}{\rho_{(t+\Delta t)}{}^\gamma} = \frac{P_{(t)}}{\rho_{(t)}{}^\gamma} = const \tag{3.46}$$

$$\frac{P_{(t+\Delta t)} V_{(t+\Delta t)}^\gamma}{m_{(t+\Delta t)}^\gamma} = \frac{P_{(t)} V_{(t)}^\gamma}{m_{(t)}^\gamma}$$

where γ is the specific heat ratio of air, ρ is the density of air and V is air volume. Since the volume of the tube, consequently the air volume inside the tube also, does not change through time, the process is isometric and the equation above becomes:

$$\frac{P_{(t+\Delta t)} V^\gamma}{m_{(t+\Delta t)}^\gamma} = \frac{P_{(t)} V^\gamma}{m_{(t)}^\gamma}$$

$$\frac{P_{(t+\Delta t)}}{m_{(t+\Delta t)}^\gamma} = \frac{P_{(t)}}{m_{(t)}^\gamma}$$

$$P_{(t+\Delta t)} = \left(\frac{m_{(t+\Delta t)}}{m_{(t)}} \right)^\gamma P_{(t)} \tag{3.47}$$

where P is some pressure, m is the air mass and t is the time since the valve has opened. Proceeding from equation (3.47) it is necessary to obtain an expression for the mass. At the output of the tube, the mass exits the tube with velocity u, as shown in Figure 3.35, and the mass flow rate is given by:

$$\dot{m}_{(t)} = A \rho_{(t)} u_{(t)} \tag{3.48}$$

where A is the cross section area of the hose, l is distance across the hose and u is air velocity. Equation 3.46 also suggests that at any two different time instances the following holds:

$$\frac{P_{(t0)}}{\rho_{(t0)}{}^{\gamma}} = \frac{P_{(t1)}}{\rho_{(t1)}{}^{\gamma}}$$

which can be reformulated to give an expression for the density as a function of the environmental pressure and the air density at the environmental conditions:

$$\rho_{(t)} = \rho_0 \left(\frac{P_{(t)}}{P_e} \right)^{1/\gamma} \tag{3.49}$$

where ρ_0 is the air density at the environmental conditions where the absolute environmental pressure P_e is measured. Combining equations (3.48) and (3.49) while considering an air tube with circular cross section area of diameter D yields:

$$\dot{m}_{(t)} = \pi \left(\frac{D}{2} \right)^2 \rho_0 \left(\frac{P_{(t)}}{P_e} \right)^{1/\gamma} u_{(t)} \tag{3.50}$$

Therefore, it is now necessary to obtain an expression for the air velocity in the tube. Considering the energy conservation at the two ends of the tube, a modified Bernulli law states:

$$\frac{u_0{}^2}{2g} + \frac{P_0}{\breve{\rho}_0 g} + z_0 = \frac{u_L{}^2}{2g} + \frac{P_L}{\breve{\rho}_L g} + z_L + \Delta h \tag{3.51}$$

where P_0, P_L are the input and out pressure respectively, z_0, z_L the height (across the direction of g) of the origin and the end of the tube respectively, and Δh is the energy loss due to friction in the tube. Also, $u_0 := u_{(t,0)}$, $u_L := u_{(t,L)}$ which according to 3.45 $u_0 = u_L =: u$ and $\breve{\rho}_0 := \rho_{(t,0)}$, $\breve{\rho}_L := \rho_{(t,L)}$ which is $\breve{\rho}_0 = \breve{\rho}_L =: \rho$
Thus:

$$\frac{P_0 - P_L}{\rho g} = z_L - z_0 + \Delta h$$

Darcy-Weisbach equation:

$$\frac{P_0 - P_L}{\rho g} = \Delta z + f \frac{L u^2}{2 D g} \tag{3.52}$$

where f is the friction factor and L, D is the length and the diameter of the tube respectively.

The friction factor is a function of the Reynolds number Re (which describes the flow type of air in the tube), and the relative roughness of the tube ϵ/D (ϵ is the tube roughness): $f = \phi(Re, \epsilon/D)$

The complete formula (Colebrook Equation) which adequately describes the friction effects is not in a closed form. Thereafter, approximations by Haaland and Alsdul simplify the formula obtaining more usable forms

Colebrook Equation:

$$\frac{1}{\sqrt{f}} = -2 log \left(\frac{\epsilon/D}{3.7} + \frac{2.51}{Re\sqrt{f}} \right)$$

Haaland approximation:

$$\frac{1}{\sqrt{f}} \approx -1.8 log \left(\left(\frac{\epsilon/D}{3.7} \right)^{1.11} + \frac{6.9}{Re} \right)$$

Alsdul approximation:

$$f \approx 0.11 \left(\frac{\epsilon}{D} + \frac{68}{Re} \right)^{1/4}$$

A closed form expression for the velocity is desired, which is directly proportional to the Reynolds number. Unfortunately, Alsdul approximation is not convenient enough to solve for the Reynolds number and consequently for the velocity. To this end, the Reynolds number may be considered approximately constant, i.e. the type of air flow does not change, and the approximation for friction factor is is given by:

$$f \approx 0.11 \left(k \frac{68}{Re} \right)^{1/4} \tag{3.53}$$

As shown in Figure 3.36, this approximation will hold in a vicinity around the intersection point of the two lines. In practice, for smooth tubes, the roughness factor ϵ is approximately zero. Therefore, the two lines are almost identical, yielding a larger range across which the approximation holds. The introduced "roughness scaling factor" k can be determined experimentally.
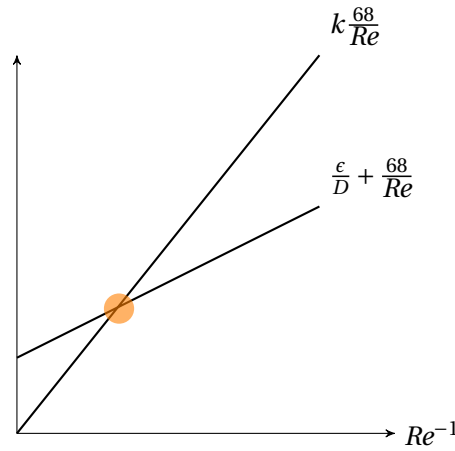
Figure 3.36: Approximation for approximately constant Reynolds number

Next, the Reynolds number is given by the following formula:

$$Re = \frac{\rho D u}{\mu} \tag{3.54}$$

where μ is the dynamic viscosity of air in room temperature and pressure close to the pressures of interest. In practice, the mid pressure between the source and the environment may be used. Combining equations 3.52, 3.53 and 3.54, it is possible to derive an estimation of the air velocity in the hose:

$$\frac{P_0 - P_L}{\rho g} = \Delta z + 0.11 \left(k \frac{68\mu}{\rho D u} \right)^{1/4} \frac{L u^2}{2 D g}$$

$$u = \left[\left(\frac{P_0 - P_L}{\rho g} - \Delta z \right) \frac{2g}{0.11 L} \left(\frac{\rho D^5}{68 \mu k} \right)^{1/4} \right]^{4/7}$$

$$u = \left[\frac{2}{0.11 L} \left(P_0 \frac{1 - \frac{P_L}{P_0}}{\rho_0 \left(\frac{P_L}{P_e} \right)^{1/\gamma}} - g \Delta z \right) \left(\frac{\rho_0 \left(\frac{P_L}{P_e} \right)^{1/\gamma} D^5}{68 \mu k} \right)^{1/4} \right]^{4/7} \tag{3.55}$$

which when is replaced in equation (3.50) yields the relation for the mass derivative:

$$\dot{m}_{(t)} = \pi \left(\frac{D}{2} \right)^2 \rho_0 \left(\frac{P_L}{P_e} \right)^{1/\gamma} \left[\frac{2}{0.11 L} \left(P_0 \frac{1 - \frac{P_L}{P_0}}{\rho_0 \left(\frac{P_L}{P_e} \right)^{1/\gamma}} - g \Delta z \right) \left(\frac{\rho_0 \left(\frac{P_L}{P_e} \right)^{1/\gamma} D^5}{68 \mu k} \right)^{1/4} \right]^{4/7} \tag{3.56}$$

Next the phenomenon of critical (choked) flow is taken into account, where the mass flow will not increase with further increase in P_0 according to:

$$\frac{P_L}{P_0} < \left(\frac{2}{\gamma+1}\right)^{\frac{\gamma}{\gamma-1}} \tag{3.57}$$

Thus:

$$\dot{m} = \begin{cases} \dot{m}|_{\frac{P_L}{P_0}} & \frac{P_L}{P_0} > \left(\frac{2}{\gamma+1}\right)^{\frac{\gamma}{\gamma-1}} \\[4mm] \dot{m}|_{\frac{P_L}{P_0}=\left(\frac{2}{\gamma+1}\right)^{\frac{\gamma}{\gamma-1}}} & \text{Otherwise} \end{cases}$$

Of course, air will flow from the end of high pressure towards the end of low pressure. Therefore, at each moment, P_L is considered to be the low pressure and P_0 the high one while the sign is imposed by the flow direction:

$$\dot{m} = \begin{cases} \check{k} \cdot \dot{m}|_{\frac{P_{min}}{P_{max}}} & \frac{P_{min}}{P_{max}} > \left(\frac{2}{\gamma+1}\right)^{\frac{\gamma}{\gamma-1}} \\[4mm] \check{k} \cdot \dot{m}|_{\frac{P_{min}}{P_{max}}=\left(\frac{2}{\gamma+1}\right)^{\frac{\gamma}{\gamma-1}}} & \text{Otherwise} \\[4mm] P_{min} = \min\{P_L, P_0\} \quad \check{k} = sgn\{P_0 - P_L\} \\[2mm] P_{max} = \max\{P_L, P_0\} \end{cases} \tag{3.58}$$

In order to derive the mas at each time step, a numerical integration technique may be used, with the 3rd order Runge-Kutta being the method of preference as far as this project is concerned:

$$\begin{aligned} m_{(t+\Delta t)} &= m_{(t)} + \frac{1}{6}(k_1 + 4k_2 + k_3)\Delta t \\ k_1 &= \dot{m}_{(t,\ P_L,\ P_0)} \\ k_2 &= \dot{m}_{(t+\frac{\Delta t}{2},\ P_L+k_1\frac{\Delta t}{2},\ P_0)} \\ k_3 &= \dot{m}_{(t+\Delta t,\ P_L-k_1\Delta t+2k_2\Delta t,\ P_0)} \end{aligned} \tag{3.59}$$

Notice that in equation 3.59 the notation is simplified for convenience as follows: $P_L \equiv P_L(t)$ and $P_0 \equiv P_0(t)$. Finally, the pressure at the end of the tube at time $t + \Delta t$ is computed using equation (3.47):

$$P_L(t + \Delta t) = \left(\frac{m_{(t+\Delta t)}}{m_{(t)}}\right)^{\gamma} P_L(t) \tag{3.60}$$

with initial conditions:

$$\begin{aligned} P_L(0) &= P_e = 0.1017 x 10^6\ Pa \\ m(0) &= P_L(0)\frac{V_a}{RT} = P_e\frac{\pi (D/2)^2 L}{RT} \qquad \text{ideal gas law} \end{aligned} \tag{3.61}$$

3.5.1   Experimental validation

Next, the model is validated by experimentation. The set-up of Figure 3.34 was used in two types of experiments. Firstly, the step response of polyurethane tubes of four different (inner) diameters $\{1.4, 2, 2.5, 4\}mm$ and three different lengths $\{1, 5, 7\}m$ has been measured at three different source (absolute) pressures $\{2, 5, 6\}bar$. Based on the results and the prospective use,
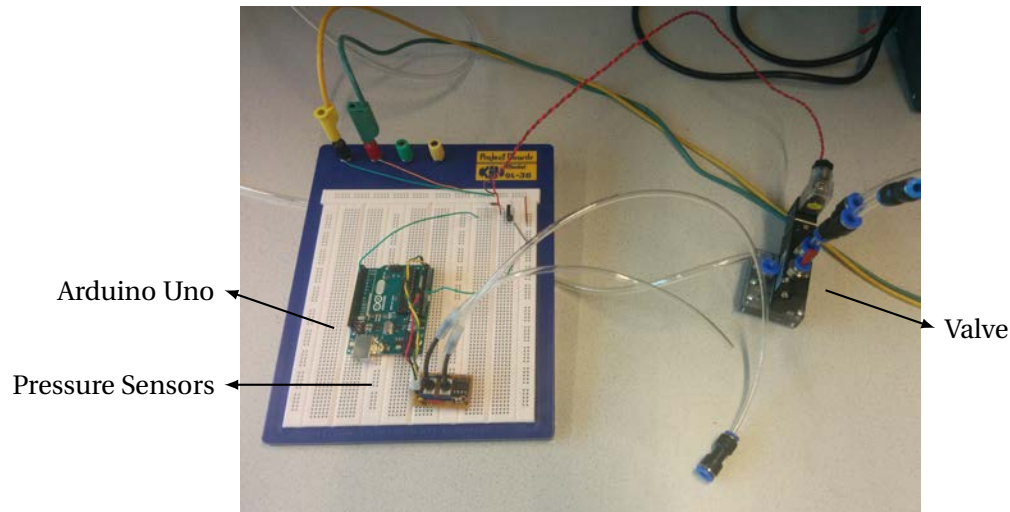
Figure 3.37: Experimental setup

Diameter [mm]	k
1.4	1.1896556
2.0	0.0222667
2.5	0.0141765
4.0	0.0035740

Table 3.3: Roughness scaling factors (k) of the used tubes

the hoses of $2mm$ and $2.5mm$ diameter have been selected for the next step, where the tubes of $5m$ and $7m$ lengths have been excited with a random signal at $5bar$ and $6bar$ absolute pressures.

A solenoid 5/2 valve with retraction spring and two pressure sensors were connected to an Arduino Uno as shown in Figure 3.37. Depending on the experiment, a control signal was sent to the valve and the pressures at the beginning and at the end of the tube were measured. These measurements were analysed with Scilab, a free and open source software for scientific programming. An estimation of the output pressure is obtained by exciting the model with the measured input pressure[4]. Then, the model estimation is compared to the measured output.

Firstly, a fitting procedure is performed, in order to identify the optimal "roughness scaling factor" (k) of each tube. To do this, for a given tube diameter, the values of k are swept manually over a range. The resulting models are used in order to estimate the step responses mentioned above and the total error over each tube material is measured. Eventually, the k that yields the smallest total error is selected (see Figure 3.3). According to the definition of the "roughness scaling factor" (Equation 3.53), k should be a positive value, close to and greater than one. However, the fitting in this case yields significantly different results. Apparently, diverse error sources and possibly model incompetencies are absorbed in k during the fitting process. If k is constrained to be greater than one, the model becomes slower during the transient period. During this particular phase, the assumption about constant density and velocity throughout the hose is actually violated.

The results are summarised here and only a subset of indicative plots is presented. However, the full collection of the plots can be found in Appendix B. As mentioned earlier, literature

---

[4]In order for the model to converge, the sampling time must be much smaller than the measurement intervals. Thus, the model is excited with an interpolated version of the input measurements, yielding a signal with significantly more points than the measurements. Wherever a comparison is necessary between signals of unequal lengths (e.g. error calculation) the shorter one is interpolated to get signals of the same size.
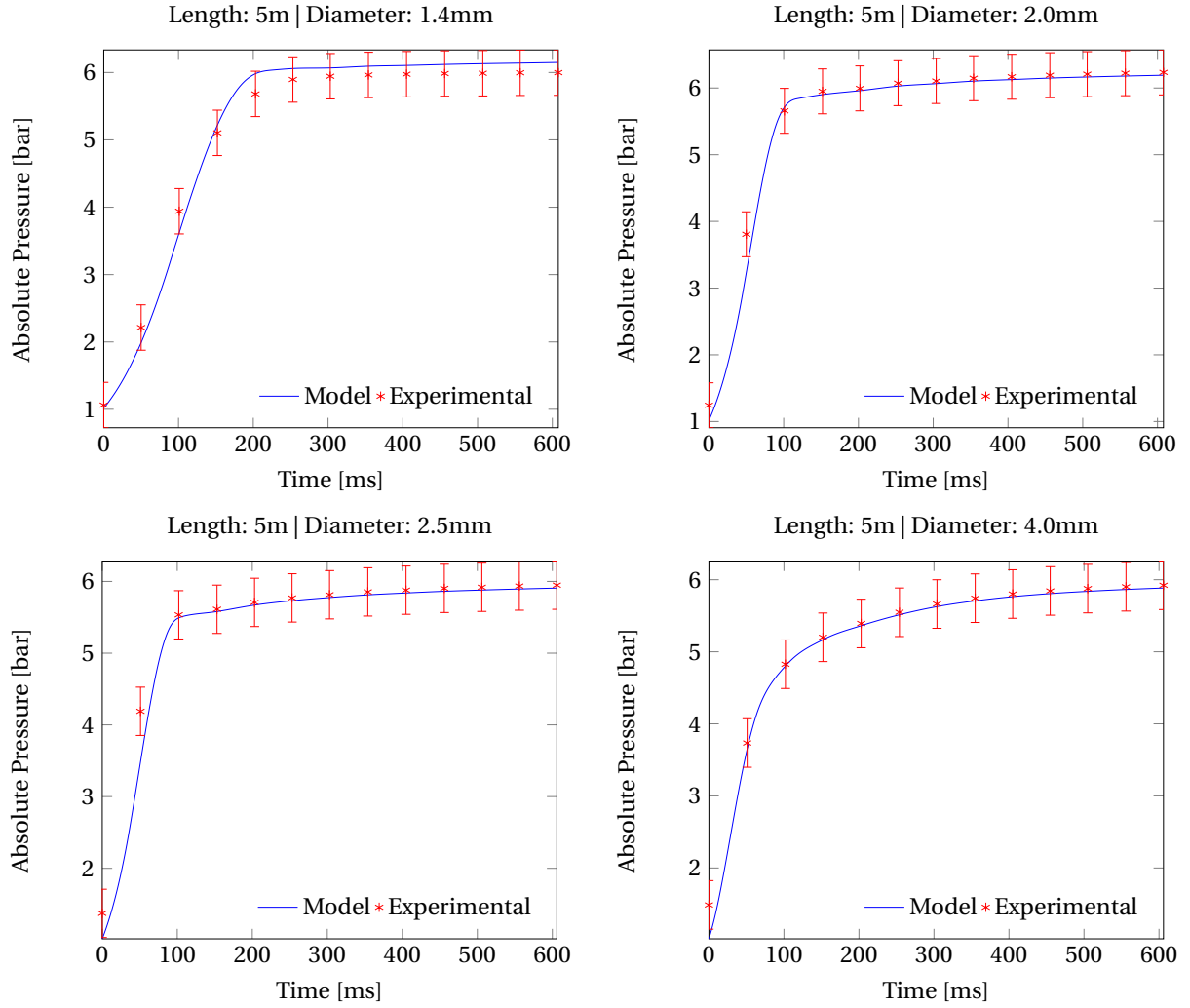
Figure 3.38: Diameter sweep with 6 bar source pressure and 5 meter long tube

suggests that a hose of $5-7m$ is necessary in order to reach the MRI bore from outside the Faraday cage. Moreover, it is stated that the nominal pressure in hospitals is $5barG$, i.e. $6bar$ of absolute pressure. Therefore, these cases are examined here. Figure 3.38 shows the step response of $5m$ long tubes of different diameters at $6bar$ source pressure, while Figure 3.39 shows the step response of $7m$ long tubes of different diameters at $6bar$ source pressure.

As a fitting evaluation metric, the following normalised error norm is used:

$$e_{\{P_s,L,D\}} := \frac{\|P_{meas} - P_{est}\|_2}{\|P_{meas}\|_2} \tag{3.62}$$

where P_{meas} is the measurement point vector, P_{est} is the model prediction vector, P_s is the source pressure, L is the tube length and D is the tube diameter.

Collecting the errors of all experiments, the error vector E can be defined:

$$E := [e_{\{P_s,L,D\}}]^T \qquad P_s \in \{2,5,6\}bar, \ \ L \in \{1,5,7\}m, \ \ D \in \{1.4,2,2.5,4\}mm \tag{3.63}$$

The mean fitting error over all experiments is

$$\bar{E} = 0.0305825$$
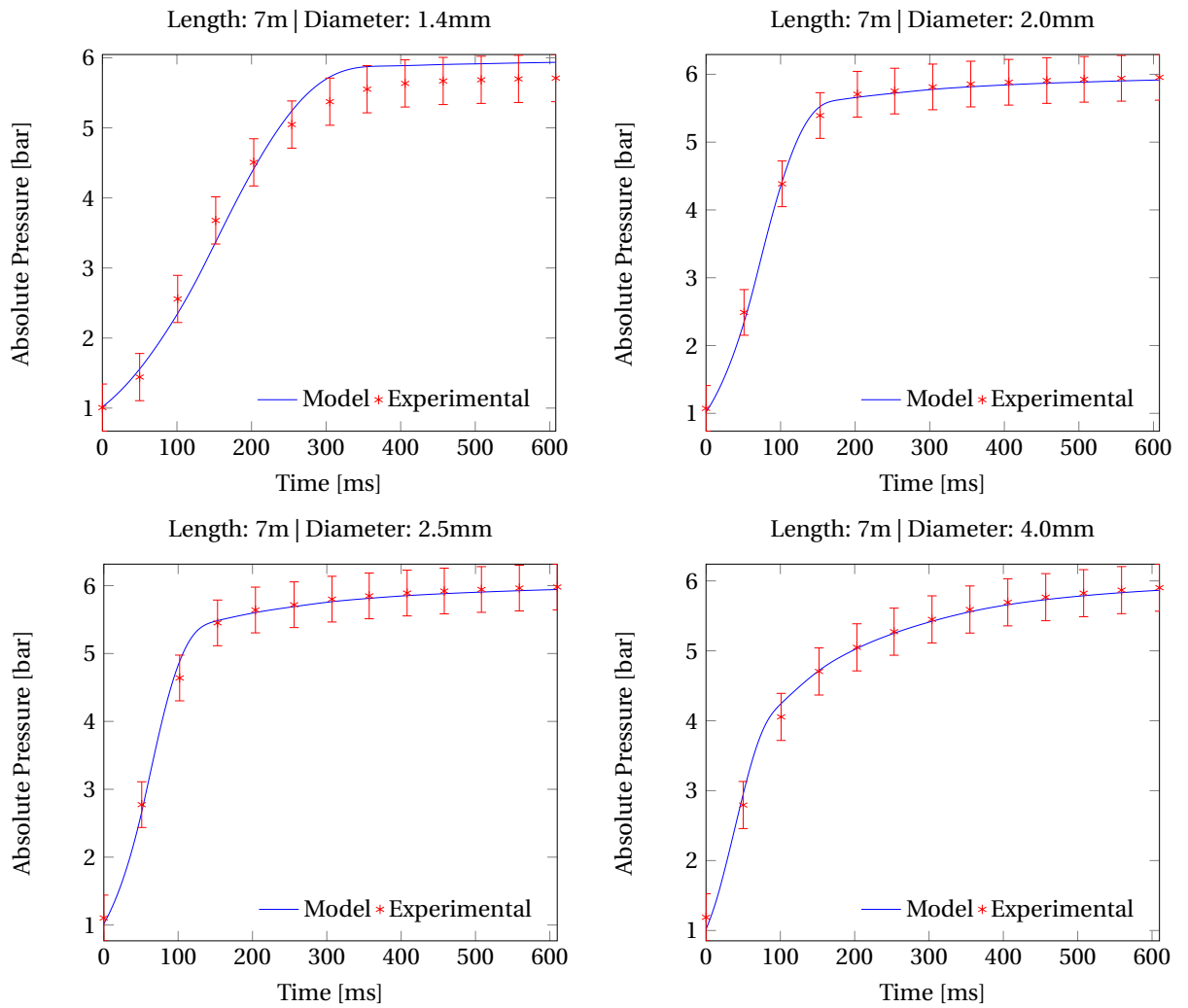
Figure 3.39: Diameter sweep with 6 bar source pressure and 7 meter long tube

$D[mm]$ $L[m]$	1.4	2.0	2.5	4.0
1	31.039039	30.43043	29.165165	29.870871
5	148.5005	72.17017	71.57958	74.128128
7	226.53654	104.85285	94.7998	131.41642

Table 3.4: Rise time (in ms) for source pressure of $2bar$

$D[mm]$ $L[m]$	1.4	2.0	2.5	4.0
1	35.241241	31.335335	30.43043	33.473473
5	168.63664	91.748749	82.634635	149.47147
7	257.86486	141.57257	135.11111	244.46246

Table 3.5: Rise time (in ms) for source pressure of $5bar$

with variance

$$var(E) = 0.0002589$$

Then, the rise time is defined as the time it takes for the response to go from 10% of its final value to 90% of its steady state value:

$$t_r := t_{90\%} - t_{10\%} \tag{3.64}$$

Examining the plots, one can see that as expected, the response is faster for shorter tubes. What is of interest though, is to examine the parameters that one has control over when designing such a system, i.e. the effect of the tube diameter on the system's response. The experiments and the model, suggest that as a rule of thumb, increasing the tube diameter yields an increase in the rise time. However, this is not the case for an increase from $D = 1.4mm$ to $D = 2.0mm$. Apparently, the resistance due to the tube walls inside the smaller diameter tube is larger than the rest of the tubes. This happens because the wall area with respect to the hose cross section area is significantly larger than the rest of the cases.

Due to this phenomenon, the smallest diameter is rejected since it behaves worse than its successor. Tables 3.4, 3.5 and 3.6 suggest that, the tube with the largest diameter ($D = 4.0mm$) is significantly slower than the rest. Finally, the tubes of $D = 2.0mm$ and $D = 2.5mm$ yield comparable results in all cases, with a maximum rise time difference of about $10ms$. Conclusively, it is safe to consider the tubes of $D = 2.0mm$ and $D = 2.5mm$ as equivalent. This gives reason to chose tubes of $D = 2.5mm$ for the air supply of MotoP 2.01 in order to maximise the volume of the supplied air while avoiding any compromise in the frequency response.

Next the model is evaluated on a random input signal. The two diameters of interest $\{2, 2.5\}mm$ are selected and experiments are made with hoses of $\{5, 7\}m$ lengths, as shown in Figures 3.40 and 3.41. This time, the mean fitting error was increased to:

$$\bar{E} = 0.1402298$$

with variance

$$var(E) = 0.0006277$$

The above mentioned results suggest that the model can adequately follow the actual response even for high frequent signals. The presented experimental data support the competence of the developed model.
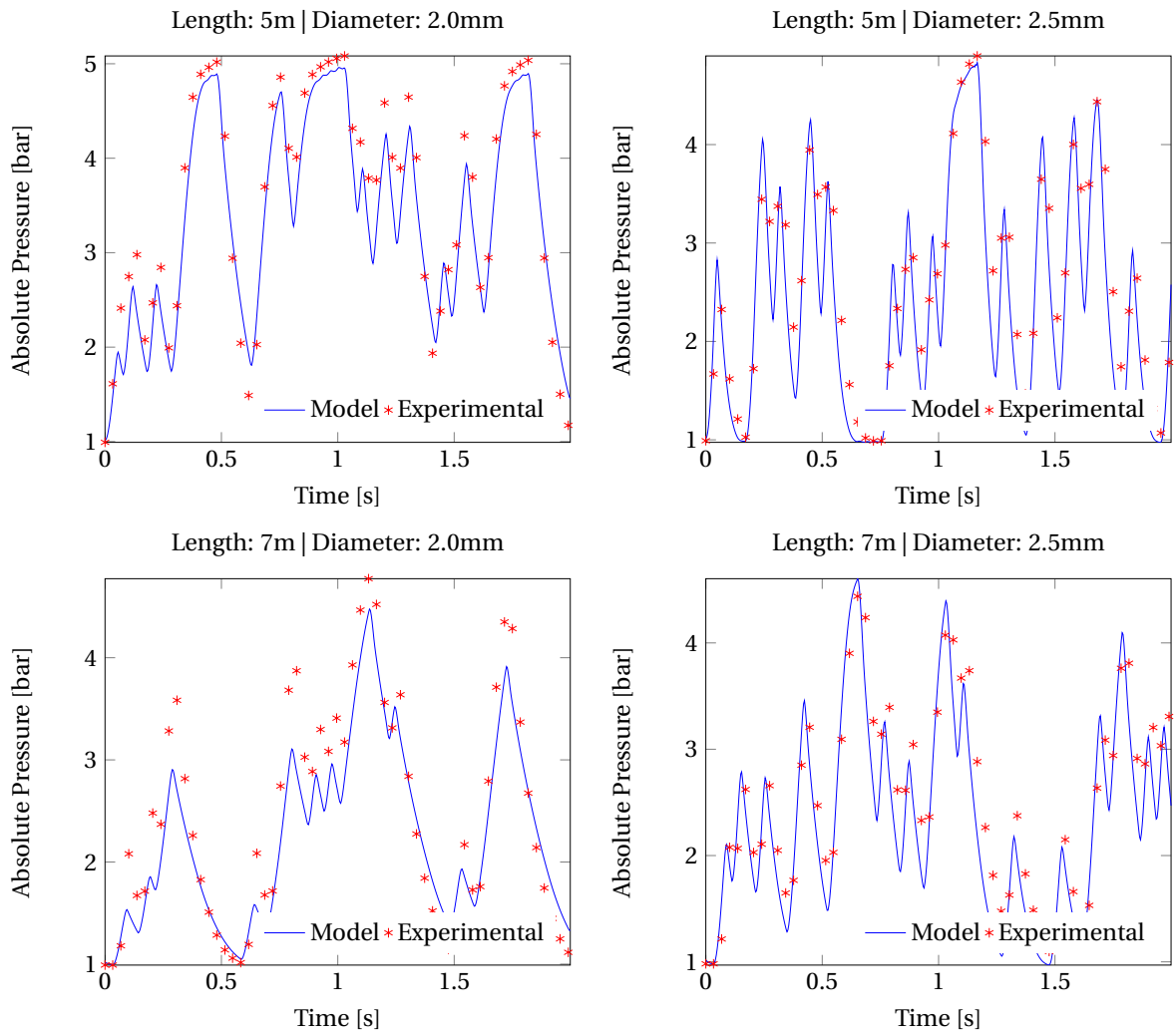
Figure 3.40: Random input with 5bar source pressure
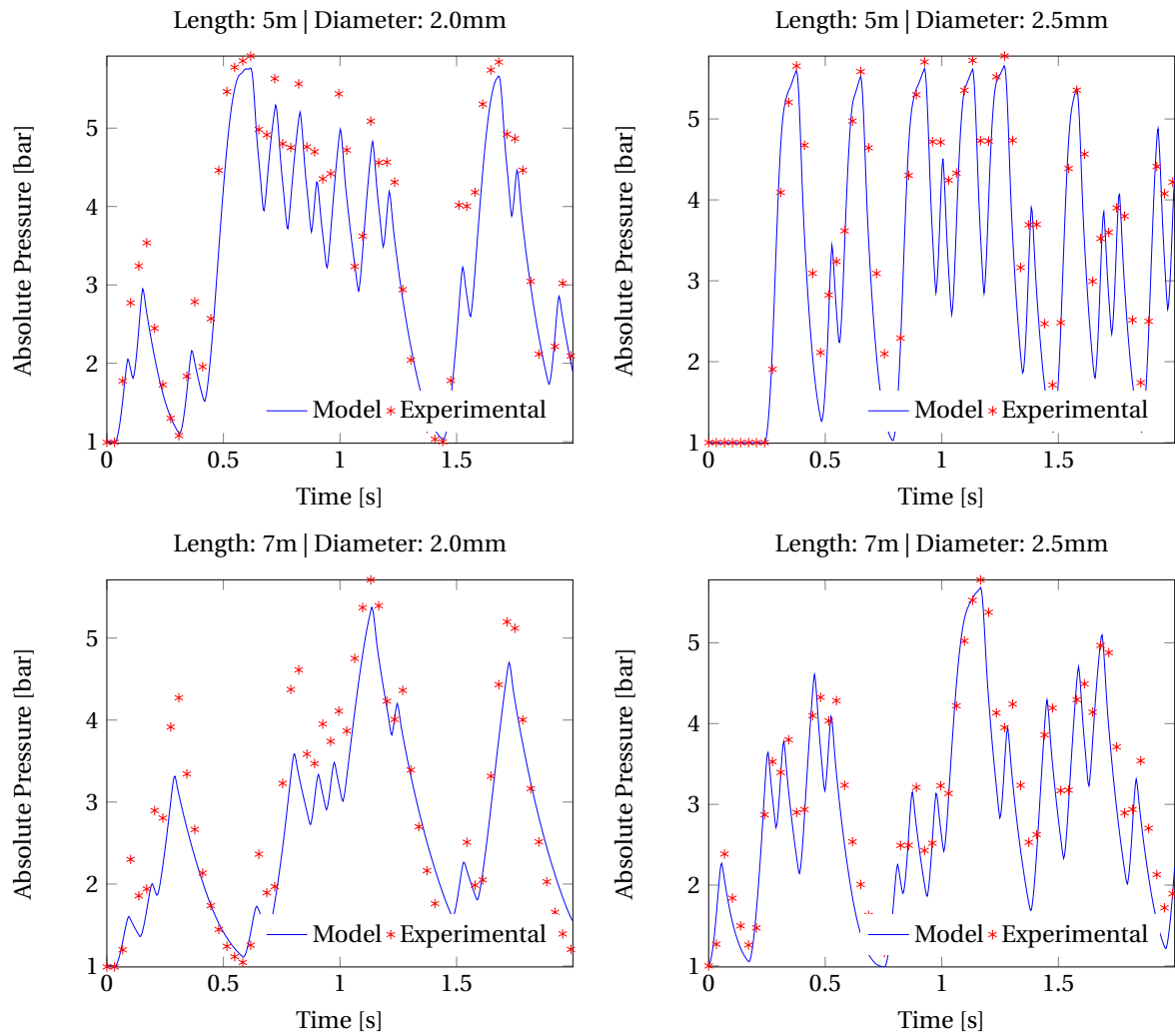
Figure 3.41: Random input with 6bar source pressure

$D[mm]$ $L[m]$	1.4	2.0	2.5	4.0
1	35.357357	31.595596	31.543544	34.576577
5	171.01902	94.942943	85.531532	162.57057
7	262.91892	145.45746	139.82983	252.79279

Table 3.6: Rise time (in ms) for source pressure of $6bar$
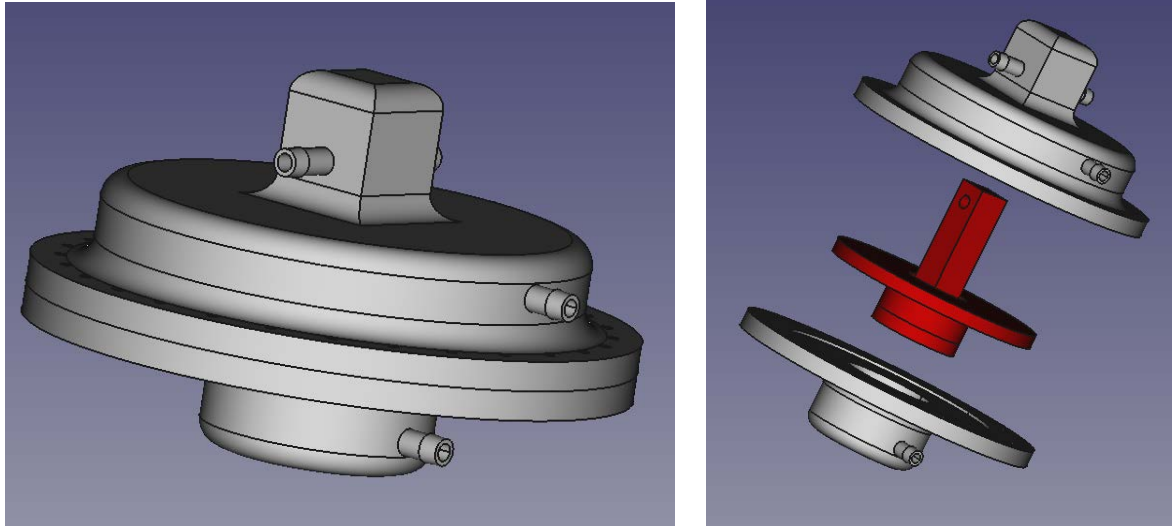
Figure 3.42: ValveP overview

3.6 Valve Detailed Design

As discussed in section 3.5, there is a pressure drop at the end of the tube when the input pressure is not a constant signal. Since this pressure drop depends also on parameters that can not be freely selected, i.e. the tube length, as well as the desired output power, it is not possible to run the actuator at any desired pressure. This becomes a constraining factor when a high power actuator with compact size is to be designed.

In order to solve this issue, a multi-modality compatible pneumatically actuated pneumatic valve is designed (ValveP). It is triggered by a signal of minimal pressure, releasing highly pressurised air towards the actuator, performing like a relay. Therefore, it can be placed inside the MRI room, close to the imager (approximately $1m$ away).

This configuration allows for a highly frequent control signal to trigger the valve from long distance, which in turn powers the actuator from a closer distance. Therefore, a high pressure and fast actuator provides both high torque and high speed, which yields increased power.

ValveP is a normally closed plastic valve. Two opposing pistons of different sizes are responsible for the forward and backward motion as shown in Figure 3.42. The small chamber is always pressurized, acting as a retraction mechanism that closes the valve without the need of actuation. A pin slides through a compartment where it either closes or opens the air gap between two inlets of highly pressurised air as shown in Figure 3.44 driving the actuator. When the bigger chamber is pressurised, the force on the big piston counteracts the small piston force and the valve opens. Figure 3.43 shows a more detailed view of the bore and the pistons.

When it comes to designing the valve, one aspect is of importance, the force applied on the big piston must be bigger than the force applied on the lower one. As mentioned above, the small barrel is always pressurised at a constant pressure P_s, while the big barrel is actuated by a

highly frequent signal P_b. If the same source is used, the big barrel will have significantly lower pressure than the small one. The implied forces are then given by:

$$f_s = A_s P_s$$
$$f_s = \pi r_s^2 P_s$$

(3.65)

$$f_b = A_b P_b$$
$$f_b = (\pi r_b^2 - \pi r_i^2) P_b$$

(3.66)

where:
  f_s :   Force acting on small piston
  A_s :   Area of small piston
  r_s :   Radius small piston
  P_s :   Pressure inside the small barrel
  f_b :   Force acting on big piston
  A_b :   Area of big piston
  r_b :   Outer radius big piston
  r_i :   Inner radius big piston
  P_b :   Pressure inside the big barrel

Combining Equations (3.65) and (3.65) and imposing the relative size condition yields:

$$f_b > f_s$$
$$(\pi r_b^2 - \pi r_i^2) P_b > \pi r_s^2 P_s$$
$$r_b^2 > r_s^2 \frac{P_s}{P_b} + r_i^2$$

(3.67)

which of course should hold for any value of P_b through time, so the extreme case should be taken into account:

$$r_b > \sqrt{r_s^2 \frac{P_s}{P_{bmin}} + r_i^2}$$

(3.68)

where r_i and r_s are practically imposed by manufacturability constraints, and P_s is defined by the source pressure and the ability to control it (using for example a pressure regulator). In order to determine P_{bmin}, the tube model is to be used. The model could be configured for the used tube characteristics and excited with the desired actuation frequency. Then, the minimum value of the output pressure at steady state could be measured.
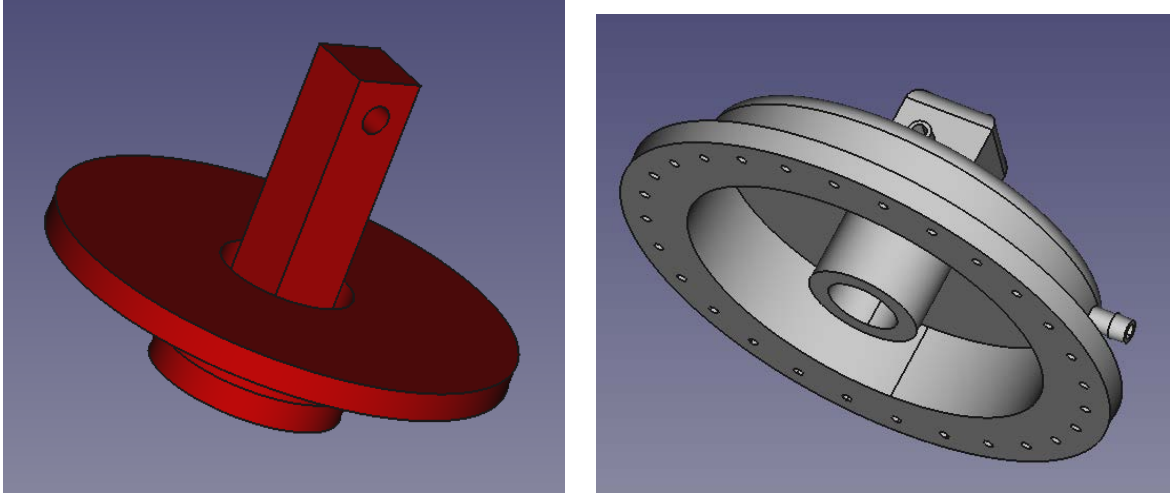
Figure 3.43: ValveP piston and bore views
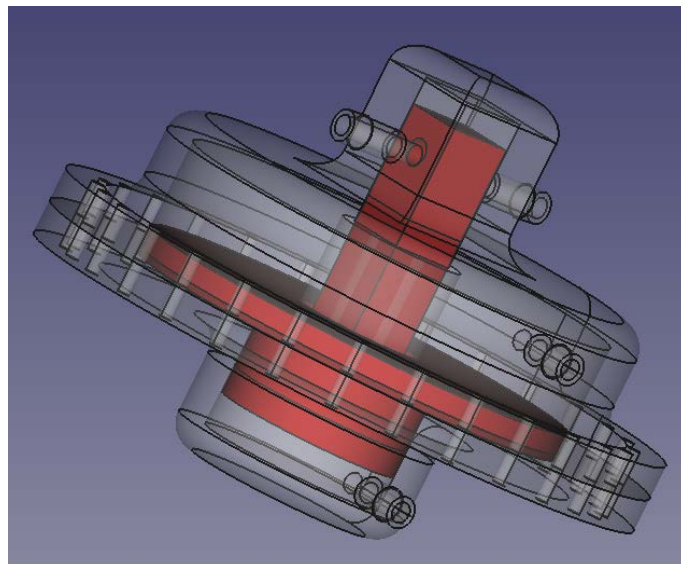
Figure 3.44: ValveP assembled

4 Prototyping

4.1 Hardware Tools

A functional prototype has been developed for each of the designs presented in previous chapters. Eventually, a MotoP 2, a ValveP 1 and an EncEFOQ 1 have been built in house, using rapid prototyping techniques (3D printing and laser-cutting). Depending on the particularities of each design, either an Objet Eden 250 (url, 2016c) with Fullcure 720 resin, or an Ultimaker 2 (url, 2016h) with ABS plastic have been used for prototyping. Specifically, the Objet has been preferred for MotoP, ValveP, and the encoder disc of EncEFOQ because of its superior resolution, which allows for smaller clearances. The housing of EncEFOQ has been printed using the Ultimaker, since no special performance was required, while the ABS plastic is lighter and cheaper than Fullcure 720 resin. Any rubber material needed was cut using a Trotec Speedy 300 (url, 2016g), and the pneumatic tube experiments were performed using an Arduino Uno (url, 2016a). Finally, the actuator is driven by pneumatiek voordeel valves (url, 2016d).

4.2 Software Tools

Throughout this thesis project only free, open source software has been used under open licences. This ensures that the project may be continued by anyone without the hassle of software licensing and unavailability.

Since customizability is a basic requirement for MotoP 2.01, special care has been taken in order to derive a fully parametric model of the actuator as described in section 3.3.1. Having this model in hand, appropriate software has to be used also in order to benefit from this versatility. FreeCAD (url, 2016b) is a choice that respects the criteria described above. Python scripting for FreeCAD (url, 2016e) was chosen in order to construct the CAD model on the actuator and execute the script for any desired configuration, each time producing a MotoP2.01 according to the given requirements.

SciLab (url, 2016f) was also the choice of preference for the simulation of the tube pneumatic model described in section 3.5. All the scripts can be found in the attached directory "/scripts/<>" and execution instructions in the respective "readme.txt" files.

4.3 Process

Conceptual Design

 During the conceptual design phase, each of the main underlying principles was proven using a Proof of Principle (POP) Prototype. Naturally, some ideas were discarded after failing to pass the tests and others would be selected to be incorporated in the design. Some of the such proof of principle prototypes are shown in Fiqure 4.1
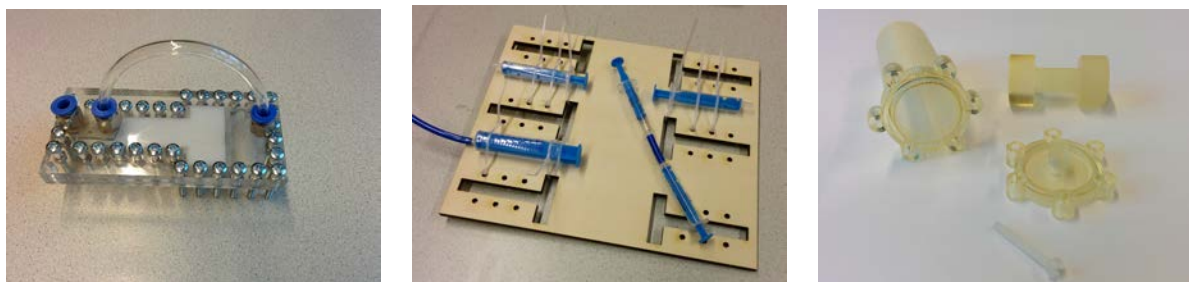
Figure 4.1: Some Proof of Principle Prototypes
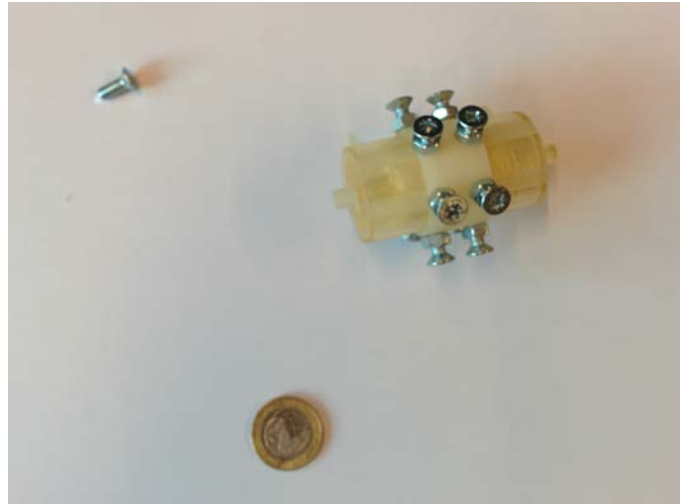
Figure 4.2: Assembly rim POP prototype

MotoP 2 abandoned designs

Before finalising the design, a range of failed shapes has been implemented, until the design was robust enough. Figure 4.2 shows an abandoned idea on the assembly technique while Figure 4.3 shows a neglected design of the rotor pin holding rim.

This assembly idea was not preferred mainly for two reasons. Firstly, the alignment of the rotation teeth is maintained by the screws which hold the assembly rim in place. This means that after some actuation periods, when the screws would loosen up, the functionality of the actuator would have been compromised. Secondly, this design is not flexible enough. It later became apparent that an arbitrary size rotor pin holding rim was necessary in order to accommodate different radius for the shift teeth, as discussed in the conceptual design phase.

Both issues were confronted by the next prototype. The new design involved matching fases of the bores, so that the rotation teeth alignment would be guaranteed, while a rotor pin holding rim was introduced. This design, allowed for the shift teeth radius to be smaller than the piston radius, an element which turns out to be not necessary. In order to achieve this, the rotor was split in two pieces, which made the task of assembling it, a weak spot of the design. The rotor was too fragile, while it is not clear in this phase how the rotational and translational motion would be decoupled.

MotoP 2.011

During the premature designs it was already apparent that the shift teeth were too fragile. None of the produced POP prototypes was functional before significantly increasing the shift teeth size, thus making the actuator pretty bulky. Nevertheless, "MotoP 2.011" shown in Figure 4.4 was the first functional prototype. For the first time, the shift teeth where robust, giving an indication on their minimum manufacturable size. Also the wall thickness was acceptable. At this point, it was decided to go from a triangular shift teeth profile to rhombus shaped teeth. Moreover, a design mistake was discovered indicating that the pistons were too short. This means that the piston going out of the barrel when an extreme position was reached, which resulted in de pressurisation and zero output torque.

MotoP 2.012

During the next iteration, the above mentioned problems have been fixed. Also, the final assembly design has been incorporated which alleviated the need of excess use of bolts while significantly reduced the necessary wall thickness, thus the radius of the assembly

Figure 4.3: Rotor pins POP prototype
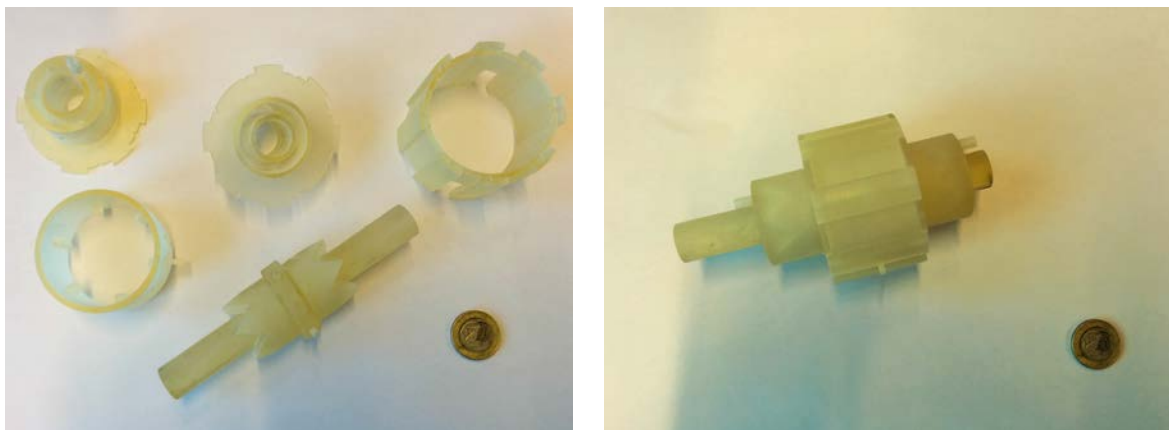
Figure 4.4: MotoP 2.011
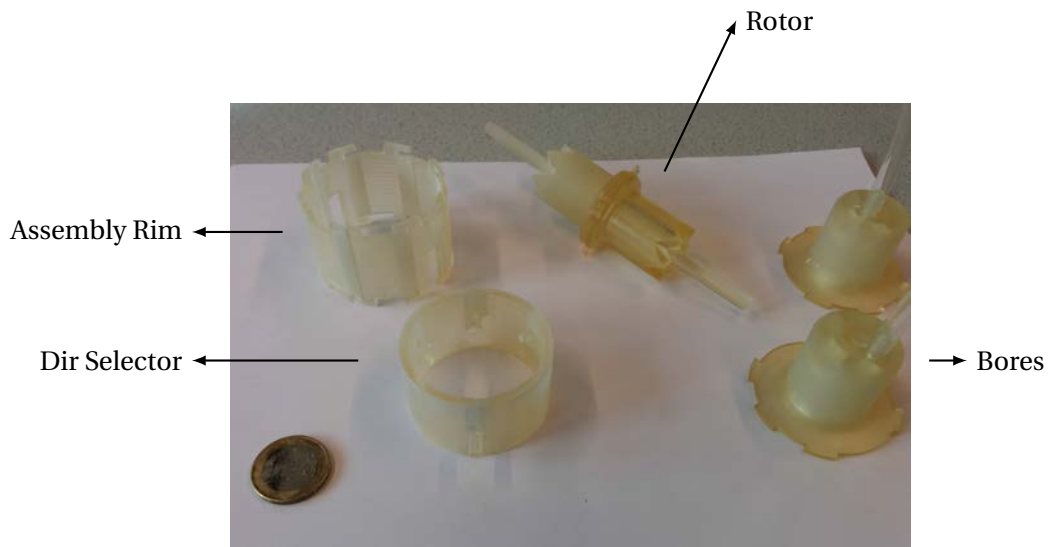
Figure 4.5: MotoP 2.012
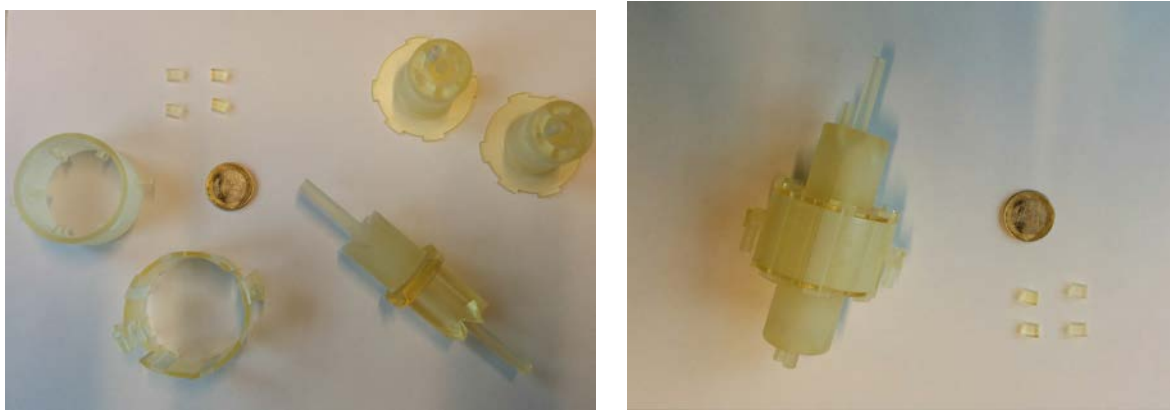
Figure 4.6: MotoP 2.013

rim. The percussion forces are now accounted by the pins on the assembly rim, a design which comes with a range of advantages as discussed in the conceptual design chapter. Moreover, fillets have been introduced and the dimensions have been better tuned towards a more compact design. In this iteration, one more mistake was discovered. The rotation teeth were poorly designed, such that the rotor rotation teeth did not match the rotation teeth on the bore. This version was not functional.

MotoP 2.013

After solving the significant problems of the previous iterations, it was time to introduce the dir selector actuation mechanisms. Initially, the concept assumed that actuating using one barrel alone, would clog the dir selector. To this end, two barrels were placed symmetrically, pushing towards the same direction. The retraction would have been taken care of, using rubber bands. This version was finally fully functional. This allowed for continuous actuation over a couple of rotations, until the resin gave up and the actuator broke apart as shown in Figure 4.7. Apparently, both the assembly rim pins and the shaft were too fragile.

MotoP 2.014

Although the previous version was so fragile that it was not possible to demonstrate the actuator's functionality, it was evident that the design was acceptable. Thus, during the
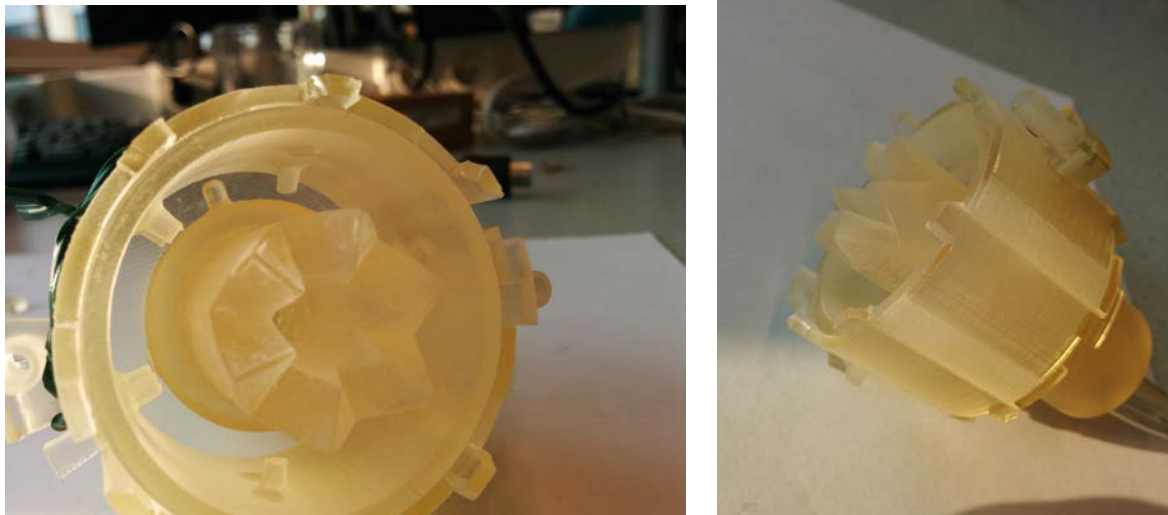
Figure 4.7: MotoP 2.013 was too fragile
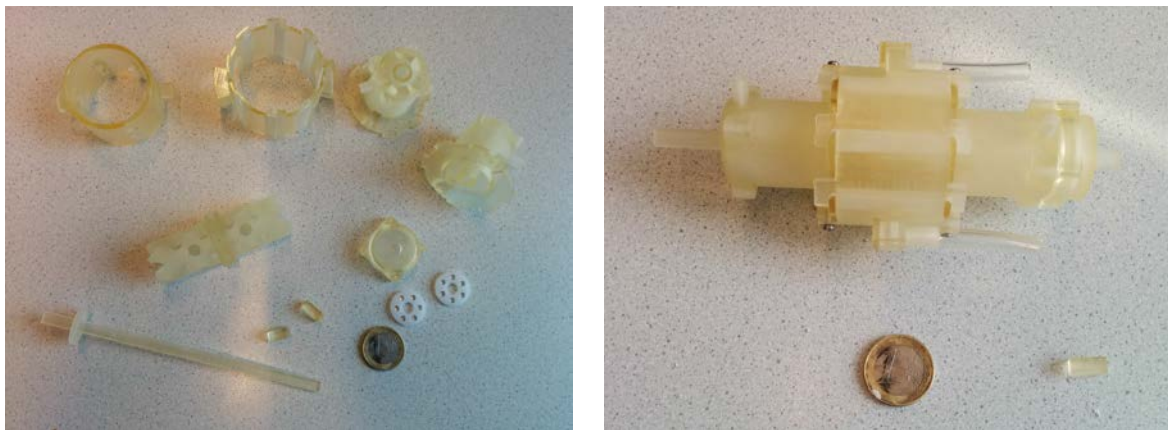
Figure 4.8: MotoP 2.014

next iteration, the rotor and the shaft have been finally decoupled. Also, the air inlets were moved to the sides of the bores and the dimensions of the pins and the wall thickness have been tuned further. This version was operational for a while.

Eventually, it was proven that it is possible to rotate the dir selector using only one barrel. Also, this version was operational for any input pressure from $2barG$ up to $6barG$. However, at this point became evident that it was necessary to introduce sealers between the rotor and the bores, since the leakage was excess.

MotoP 2.015

Due to time constraints, MotoP 2.015 (shown in Figure 4.9) was the last prototype. Therefore, all the design elements that could maximize its performance have been included. The back drivability rubbers as well as the sealers and the retraction mechanism are introduced in this version. The size of both the shift teeth as well as the rotor pins has been increased. Moreover, a total of $n = 6$ rotor pins have been incorporated, following the detailed design section. The changes above contribute to the robustness of the actuator and enclose all the experience obtained throughout this thesis. This prototype was functional, yet the performance was not satisfactory. For more details, refer to the characterisation section (5.2)
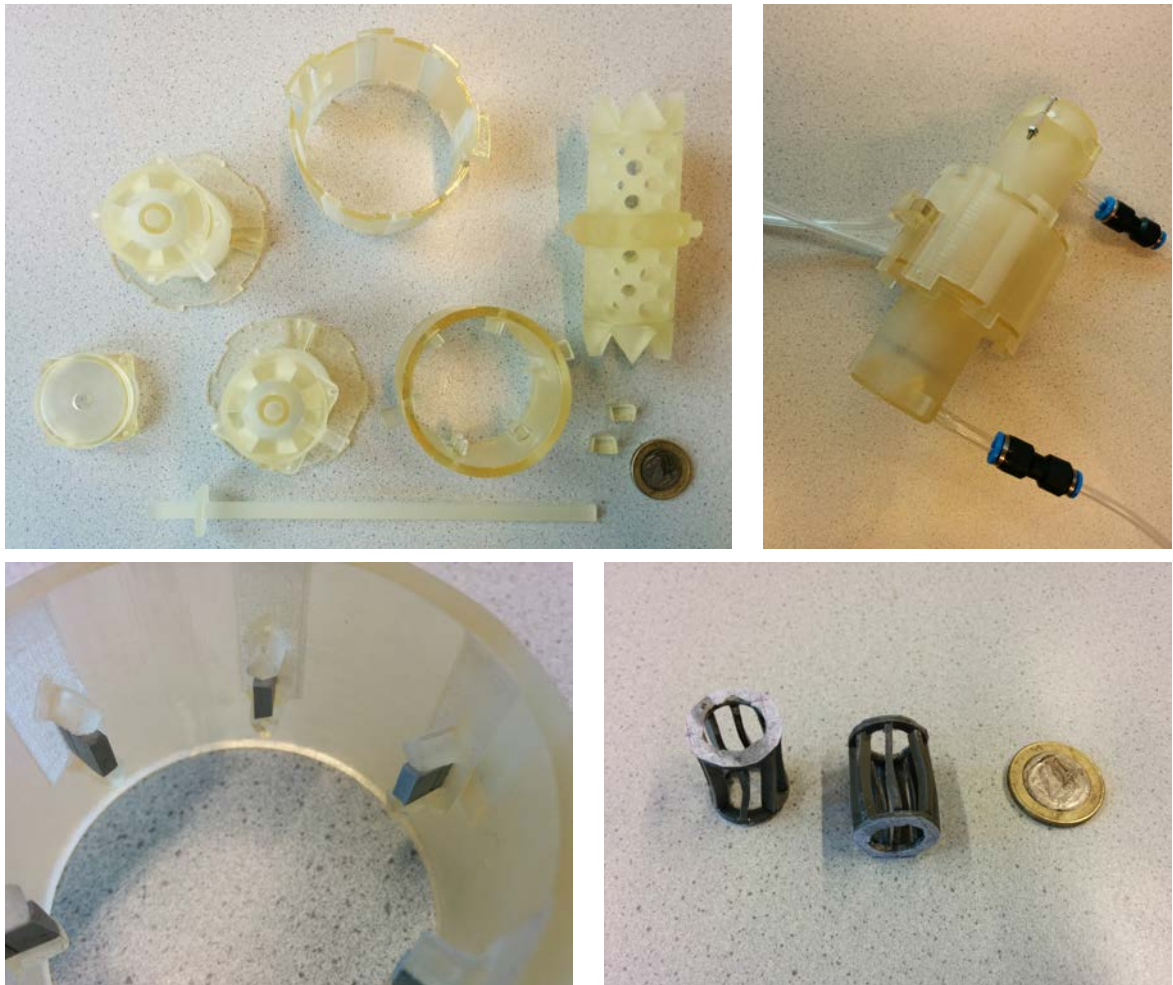
Figure 4.9: MotoP 2.015

Figure 4.10: EncIFOQ 0.11

Figure 4.11: EncIFOQ 0.12

EncIFOQ 0.11

Figure 4.10 shows the first attempt to implement the Incremental Quadrature Fibre Optic Encoder designed earlier. Commercial Off The Shelf audio fibre optic cables were used, along with their transmitters. The housing and the encoder disk were printed out of ABS plastic using the Ulitmaker 2. Due to its reduced size, and restricting of 3D-printing resolution, this version of the EncIFOQ was not functional. Initially, a custom made ball bearing was implemented by creating a (3D printed) channel on the encoder bore. Because of this bearing, the air gap that the light beam should pass through in order to reach the opposite fibre optic cable was too big, resulting in significant signal loss.

EncIFOQ 0.12

Next, the custom bearing was replaced by the same commercial bearing used for MotoP 2. Also, the encoder disk was now printed with the Objet printer instead of the Ultimaker, fact which significantly improved the result. Of course, the Fullcure resin is transparent, thus the disk was painted using a permanent black marker. The resulting encoder, shown in Figure 4.11, has resolution of 4.74 degrees.

ValveP

ValveP, shown in Figure 4.12, was seriously affected by air leakage. Excess air was leaking out of the bores unless metallic screws were used to apply increased pressure. This prob-

Figure 4.12: ValveP 0.2

lem can be fixed by increasing the number and diameter of the nylon screws (for MRI compatibility) and introducing some sealing paste. Again, in the case of the valve, the resin was too fragile. Once the valve was sealed properly and pressurised, it failed spectacularly. Moreover, there is leakage from the high pressure pin inlet (top left) towards the big piston bore. This results in the valve being normally open when the big bore inlet (top middle) is closed. A redesign of the valve could take advantage of this phenomenon, reducing the number of inlets by one.

5 Actuator Testing

Naturally, the final product is not ready yet. However, five prototypes were developed in-house using the highest resolution 3D-printer available. It was already apparent, before even characterising the final prototype, that the mechanical properties of the used resin were not satisfactory. Nevertheless, this chapter copes with the validation and characterisation of the latest prototype "MotoP 2.015". Therefore, the results should only be used in order to provide an insight on what can be achieved rather than an indication of performance.

5.1   Validation

In this section, the requirements list initially presented in Chapter 3.6 is reviewed in order to validate that "MotoP" complies with it:

Must

> This particular set of requirements is of high importance. Therefore, much effort and time should be invested towards achieving each and every one of them. Thus, the actuator must comprise the following characteristics:

> **Req1.   Multimodality compatible**
> As discussed earlier, multi-modality compatibility boils down to absence of metalic and magnetic parts. This is the case for the developed prototype, as shown in Figures 5.1 and 5.2. An "ILUMA Ultra Cone Beam CT" dentistry scanner (Model No: E-40R HF X20P L, 120KV) and an eSAOTE "G-Scan Brio" (0.24T) MRI scanner were used to verify the multi-modality compatibility of the developed actuator. MotoP 2.015 is visible to the X-Ray scanner but invisible to the MRI. It is possible to make it traceable in the MRI by using markers attached on it (fish oil capsules in this case). Including metallic parts is harmless to the X-Ray but it distorts the image.

> **Req2.   Modularity**
> Fulfilled.

> **Req3.   FDA/CE regulations compliance**
> The compliance with medical regulations is not verified yet. Undoubtedly the used materials will play a significant role.

> **Req4.   Fail safe**
> The design is such that all fragile parts are contained inside the bores. Therefore, the risk of fragments being flung in case of failure is minimised. The fact that the actuator comprises adjustable back drivability stiffness yields stable behaviour in case of power cut-off. Tuning the stiffness one can define the supplied torque when the actuator is not pressurised, therefore maintain the configuration of the whole mechanism. Certainly though, a thorough failure analysis must be performed in order to validate the design from the safety perspective.

> **Req5.   Customizability**
> Fulfilled.
> The script that produces the CAD design takes as input three performance parameters: "Working air pressure", "Output torque" and "Resolution" and outputs .stl files according to the model described in the detailed design section.

> **Req6.   Back-Drivability**
> Fulfilled.
> The back drivability stiffness may be tuned by the back drivability rubbers and the depth of the laser engraving on them.

Req7. Compactness
Fulfilled.
Maximal use of space is obtained by design. The prototypes were oversized due to the inadequate material properties, but the choice of proper material would alleviate this necessity.

Req8. Performance

   (a) It must deliver certain torque/force, precision/accuracy and speed .
      Fulfilled by design.

   (b) It must deliver certain strength/stiffness.
      Fulfilled by design.

   (c) Backlash and lags must be as small as possible.
      Fulfilled by design. Literally no backlash.

   (d) It must outperform the currently available one, designed and implemented by Zhi (2015).
      Fulfilled by design. An actuator of greater torque may be designed by specifying the desired torque as an input.[1]

Req9. Position Feedback
Fulfilled.
A position encoder was designed and implemented.

Req10. Implementation
Fulfilled.

Req11. Demonstration
Fulfilled.
A demonstrative platform was implemented, integrating the encoder and one actuator.

Should

A set of requirements of secondary importance is outlined below. It is encouraged to work towards achieving these but failing to do so would not be considered as a big issue:

Req12. Functionality
Fulfilled.

Req13. Force Feedback
Not fulfilled.

Req14. Cost
It was attempted to minimise the development cost during prototyping, by introducing changes as early as possible during the iterative procedure as well as reducing the sizes and the material used.

Req15. COTS products policy
Fulfilled.
COTS MRI compatible bearings (igus® xirodur® B180 - thrust race BB-626TW-B180-GL) have been already used, as well as MRI compatible springs (LeeP Plastic Composite Springs LL 100 125 U000) have been ordered (although due to delays they were not received yet).

Req16. Standardization
Not fulfilled.

---

[1]MotoP 2.015 does not fulfil this requirement, but as discussed later this is due to material properties.

(a) Overview

(b) Including metallic parts

(c) Glass balls of COTS bearing

(d) The dir-selector teeth
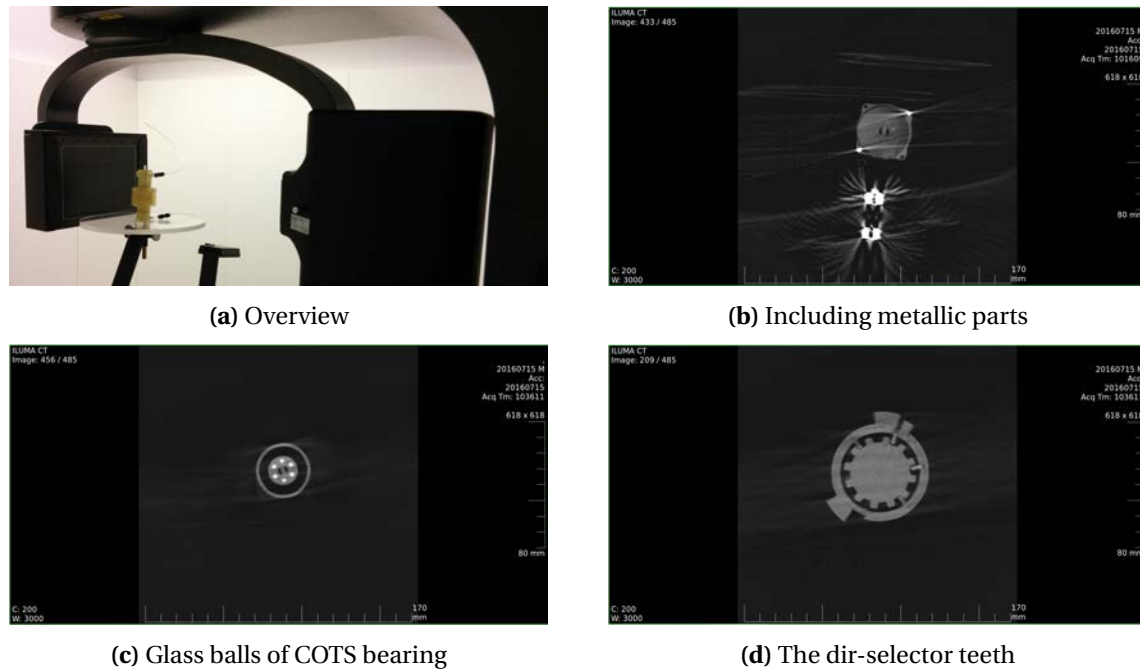
Figure 5.1: X-Ray scan

Req17. Traceability in imagers
Not fulfilled.
It was proved than it is possible to make it traceable in MRI by introducing markers, but the markers were not integrated.

Req18. Control
Not fulfilled.
This must be done after a functional and robust prototype is developed.

Could

It is neither mandatory, nor important to fulfil the following requirements. They are taken as points to have in mind.

Req19. Visibility in imagers
Fulfilled.

Req20. Continuity
Not fulfilled.
The new actuator was actually designed from scratch.

5.2   Characterisation

It has been attempted to properly characterise MotoP 2.015. Figure 5.3 shows the demonstrative platform used to control four electronically controlled actuation valves connected to MotoP 2.015. The air pressure provided to the valves is set from the source by a manually operated valve. Then, using an Arduino script, the actuation frequency is defined as discussed in Chapter 3.6. The load torque is applied by changing the load mass using a bottle of water.

Unfortunately, it was not possible to swipe through different working pressures, because two of the shift teeth failed and the actuator was not functional any more. Excess leakage yielded significantly reduced performance as well as unacceptably large pressure drop from the source to the actuation valves (3.5bar). Due to this reason, the actuator was not functional until the retraction springs were removed.

(a) MRI scanner
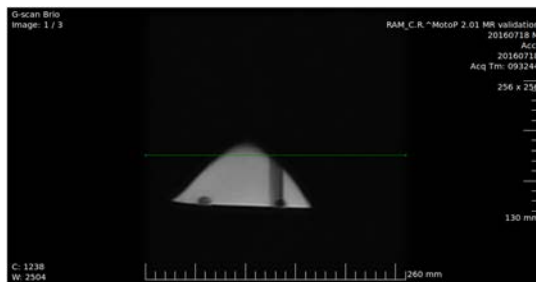
(b) Breast phantom (side view). The actuator is on the right side of the phantom (invisible to the MRI)
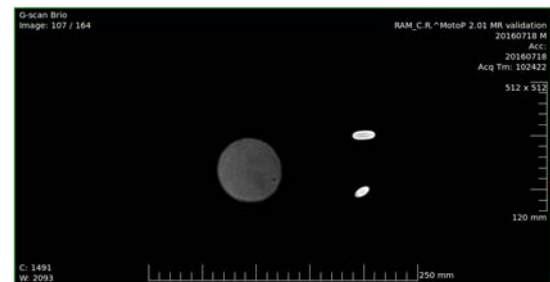
(c) Breast phantom on the left (top view). Markers attached on top of the actuator on the right.

Figure 5.2: MRI scan

MotoP 2.015 was designed to deliver $1Nm$ of torque at $0.5barG$ and its size is $134.2mm \, x \oslash 77mm$. Due to the above mentioned leakage, the barrels were de-pressurised resulting in significantly decreased performance as shown in Figure 5.4. Even when delivering roughly three times less torque than its predecessor (Zhi's actuator), the shift teeth failed due to the material's poor mechanical properties.

Figure 5.4 suggests that the dynamic behaviour of the actuator is non-linear. A peak in the dynamic torque is conspicuous around the frequency of $5.24rad/s$. Apparently, the rotor's mass stores momentum while it travels from one extreme position to another. This, introduces dynamics to the system. The static torque was greater than $269.5mNm$

Unfortunately, it was not possible to evaluate this prototype according to the specifications list given during the detailed design phase, since its performance diverges from the theoretical values due to the excess air leakage. In theory, it should be possible to outperform Zhi's actuator in terms of delivered torque with a MotoP 2 comparable in size. When the leakage issue is solved, a functional prototype should be made and checked along the specifications list.
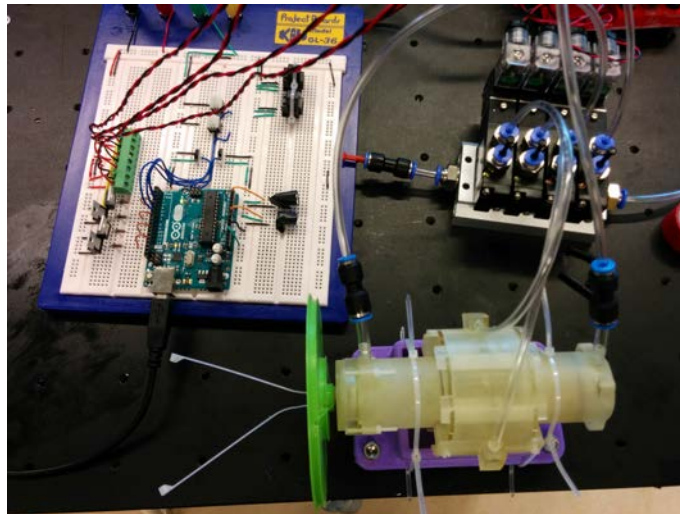
Figure 5.3: Characterisation set-up. Left: Demonstrative platform. Right-Top: Actuation valves. Right-Bottom: MotoP 2.015
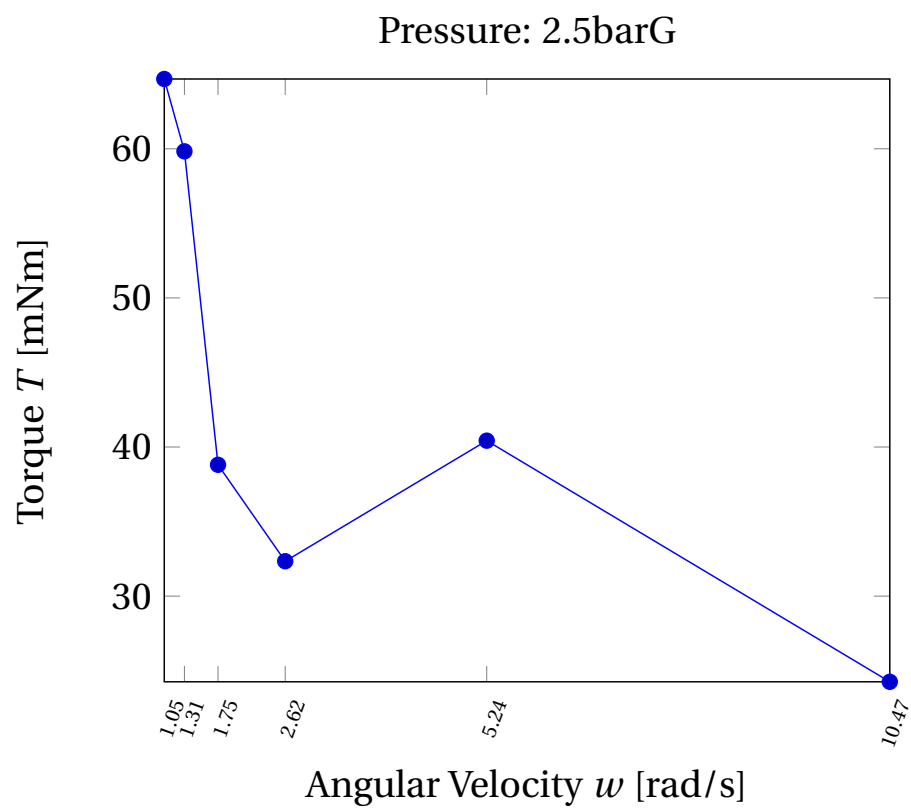
Figure 5.4: Dynamic torque of MotoP 2.015 at pressure P = 2.5 barG with zero length hose.

6 Conclusion

During this project, a multi-modality compatible (MRI & CT) actuator has been designed and prototyped. Several issues have been confronted, mostly related to the restricting nature of the MR environment, as well as the medical nature of the application fields. After a thorough exploration of the design space, the shape of the actuator that respects all the requirements, including but not confined to adjustable back-drivability stiffness, compactness, modularity, has been finalised. The resulting actuator is a rotational, pneumatic, stepper motor solely made out of plastic, glass and rubber.

A detailed design face yielded the mathematical model which allows for customisability. The process follows the "indirect design" concept, where an automated script produces the CAD models according to the mathematical model, given a minimal set of performance specifications, in this case the desired torque, resolution and the working pressure.

The actuator has been prototyped in-house with an Objet Eden printer, out of the FullCure720 resin. The mechanical properties of this material turned out to be insufficient for the proposed design, since it was too fragile. The final (5th) prototype presented excess air leakage, resulting in poor performance.

Along with the actuator, a multi-modality compatible fibre-optic quadrature position sensor was designed and prototyped as a module to be attached on the actuator. The sensor is produced by the same script, that creates the actuator, respecting the necessary criteria such that it properly functions when attached on it. The prototype housing and encoder disk were made out of ABS and FullCure 720 respectively, while for the signal transmission, COTS fibre optic audio cables were used. The prototype functions satisfactorily.

The actuator is supposed to be supplied by the air outlet through a long pneumatic tube of at least $5m$. In order to examine how it affects the dynamics of the system, a pneumatic model was derived in order to relate the output pressure with the diameter, the length and the input pressure of the tube. The resulting model presents extraordinary results, explaining experimental data for different diameters, lengths and input pressures.

Finally, in order to make the design independent of the air hose dynamic behaviour and allow for any combination of pressure/speed, i.e. delivered power, an MR compatible valve was designed and prototyped. The plastic pneumatic valve is pneumatically activated and it acts as a relay, amplifying the pressure supplied to the actuator.

Combining all the above mentioned modules, it is possible to set-up a complete multi-modality compatible actuation system to be used as a COTS on mechanisms to be used in such environments for tele-operated minimally invasive interventions.

6.1 Future work

As far as MotoP is concerned, more work has to be done before it is ready to be used on a mechanical structure. It became apparent earlier that better sealing is needed in order to achieve the desired pressure in the barrels and therefore the desired forces. Even if this is the case though, the currently used material is so fragile, that the shift teeth will fail instantly. Two actions have to be taken in order to avoid this. Firstly, the mass of the rotor must be reduced, decreasing the stored momentum and thus the applied forces. Secondly, a material with better mechanical properties must be used. If it turns out impossible to make the shift teeth robust enough, there is still a fall-back solution. The design could be revised such that the actuator is not back-drivable itself. In this case, the shift teeth do not have to be split (see Figure 3.9), therefore they would be much stronger. Then, the back-drivability could be provided by a modular clutch
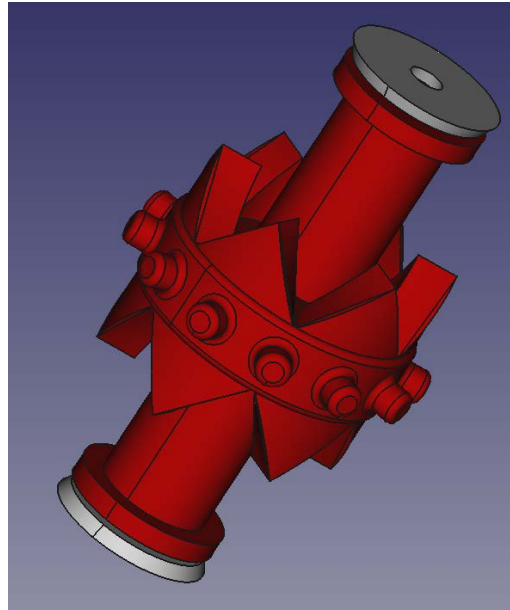
Figure 6.1: Proposed shape of MotoP 2.016 rotor.

mechanism. Finally, proper retraction springs must be used according to the necessary retraction forces in each case.

Figure 6.1 shows the proposed concept for MotoP 2.016 rotor. The rotation teeth are moved on the rotor connecting rim utilising the already existing free space. This not only increases the supplied torque, since the rotation teeth radius is increased, but it also frees the piston ends from the rotation teeth. Then, a sealer may be glued on the flat surface on the pistons allowing both the inner and outer gaps to be sealed. Finally, the piston column's radius is reduced as much as the material's strength allows, in an attempt to reduce the rotor's mass. A piston head is then necessary to accommodate the necessary piston area that allows for the desired forces to be applied. ValveP on the other hand is functionally competent. Still, the material properties do not allow for a robust prototype. Therefore, the design may be structurally changed in order to improve its strength. The sealing issue is existing in the valve as well.

Finally, the encoder is working properly. Further steps should include choosing proper fibre optic cables with low attenuation and integrating those for distances of about $5m$.

6.2   Towards a commercial product

MR environments is not the only field that MotoP can be useful in. It is possible to use such an actuator wherever magnets or electronics are prohibited. Radioactive environments such as nuclear reactors or in space could take advantage of an electronic free actuator. Moreover, underwater vehicles could benefit since no waterproofing would be necessary.

Nevertheless, MotoP was developed for MR environments, and as such it should follow the applicable safety standards. Once the design and its fabrication procedure is finalised, a functional prototype should be produced. Then, the compliance of the design to the applicable safety standards must be validated and MR compatibility tests must be conducted in order to get an "MR-Conditional" certification.

Solely non-magnetic, non-metallic materials are allowed to be used for MotoP. Sajima et al. (2012) used polyacetal (polyoxymethylene) for their housing, and Poly-Ether Ether Ketone (PEEK) for the shaft, reporting satisfactory performance. Nylon could also be a candidate for the shaft as well as the screws. The springs could be either laser-cut out of packaging foam sheets or produced out of glass.

A Proofs

Lemma A.0.1. *An increment over a bigger radius yields a bigger increment of a disk area than the same increment over a smaller radius.*

Proof. Taking two circular disks of different diameters, their initial areas are given by $A_{10} = \pi R^2$ and $A_{20} = \pi r^2$ respectively, where $r < R$. Then an infinitesimal change in either one's radius would yield a change in their area according to:

$$dA_1 = A_1 - A_{10} = \pi((R+dr)^2 - R^2) = \pi(2Rdr + dr^2)$$

Similarly:

$$dA_2 = A_2 - A_{20} = \pi(2rdr + dr^2)$$

Since $r < R$,

$$dA_1 - dA_2 = 2\pi Rdr - 2\pi rdr > 0$$

Therefore $dA_1 > dA_2$ □

Proposition A.0.2. *A rotor/stator pair composed of interlocking teeth can not comprise bi-directional motion with equal speeds and periods for both directions, unless the rotor's and stator's teeth are symmetric as seen from both directions of motion.*

Proof. Take a cylindrical stator, composed of n identical teeth arranged in a circular motion. Then, the sum of the arcs of the teeth is equal to the circumference of the stator's outer circle:

$$\sum_{i=1..n} S_i = nS_t = S_c$$

Assuming that:

- a rotation period is composed of k strokes and

- each tooth accommodates for an increment of S_{tr} to the right (S_{tl} to the left)

Then, the rotor moves by an arc of $S_r = k * S_{tr}$ when it moves k steps to the anti-clockwise direction and by $S_l = k * S_{tl}$ to the clockwise direction respectively.

If:
$u = \frac{S_c}{T}$ is the speed of the actuator

T the period of rotation

$u_r = \frac{S_r}{T_r}$ the anti-clockwise speed

T_r the period of anti-clockwise rotation

$u_l = \frac{S_r}{T_r}$ the clockwise speed

T_l the period of clockwise rotation

Then:

$$u_r = u_l \Rightarrow \frac{S_r}{T_r} = \frac{S_l}{T_l}$$

Since, by assumption $T_r = T_l$ then:

$$S_r = S_l \Rightarrow k * S_{tr} = k * S_{tl} \Rightarrow S_{tr} = S_{tl} =: S_{ht}$$

Of course:

$$S_l + S_r = S_c \Rightarrow S_{ht} = S_{tr} = S_{tl} = \frac{S_c}{2}$$

which means that $k = 2 * n$ strokes are required to complete a full rotation in either direction.

$\square$

Lemma A.0.3. *The arc corresponding to a segment of length l of a circle with radius r is equal to:* $S = 2r \arcsin \frac{l}{2r}$

Proof.
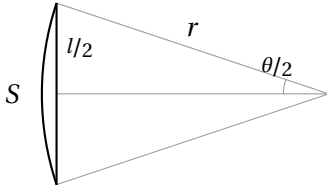
$$\sin \frac{\theta}{2} = \frac{l/2}{r}$$
$$\theta = 2 \arcsin \frac{l}{2r}$$
$$S = \theta r$$
$$S = 2r \arcsin \frac{l}{2r}$$

(A.1)

$\square$

Proposition A.0.4. *The roots of* $\quad C_\theta^2 - S_\theta^2 - 2\mu S_\theta C_\theta = 0 \quad$ *are given by* $\quad \hat{\theta} = \arccos\left\{\pm\sqrt{\frac{1\pm\sqrt{1-1/a}}{2}}\right\}$

Proof.

$$(C_\theta^2 - S_\theta^2 - 2\mu S_\theta C_\theta) = 0$$
$$C_\theta^2 - \sqrt{1 - C_\theta^2}^2 - 2\mu\sqrt{1 - C_\theta^2}C_\theta = 0$$
$$\frac{2C_\theta^2 - 1}{2\mu C_\theta} = \sqrt{1 - C_\theta^2}$$
$$\frac{4C_\theta^4 - 4C_\theta^2 + 1}{4\mu^2 C_\theta^2} = 1 - C_\theta^2$$
$$4C_\theta^4 + 4\mu^2 C_\theta^4 - 4C_\theta^2 - 4\mu^2 C_\theta^2 + 1 = 0$$
$$(1 + \mu^2)C_\theta^4 - (1 + \mu^2)C_\theta^2 + \frac{1}{4} = 0$$

(A.2)

Defining:

$$x := C_\theta^2$$
$$a := 1 + \mu^2$$

(A.3)

yields:

$$0 = ax^2 - ax + \frac{1}{4}$$

$$0 = hx^2 - x + \frac{1}{4a}$$

$$\Rightarrow x = \frac{1 \pm \sqrt{1 - 1/a}}{2}$$

$$\Rightarrow C_\theta = \pm\sqrt{\frac{1 \pm \sqrt{1 - 1/a}}{2}}$$

$$\Rightarrow \hat{\theta} = \arccos\left\{ \pm\sqrt{\frac{1 \pm \sqrt{1 - 1/a}}{2}} \right\}$$

(A.4)

$\square$

B Experimental results

B.1 Pneumatic tube step response
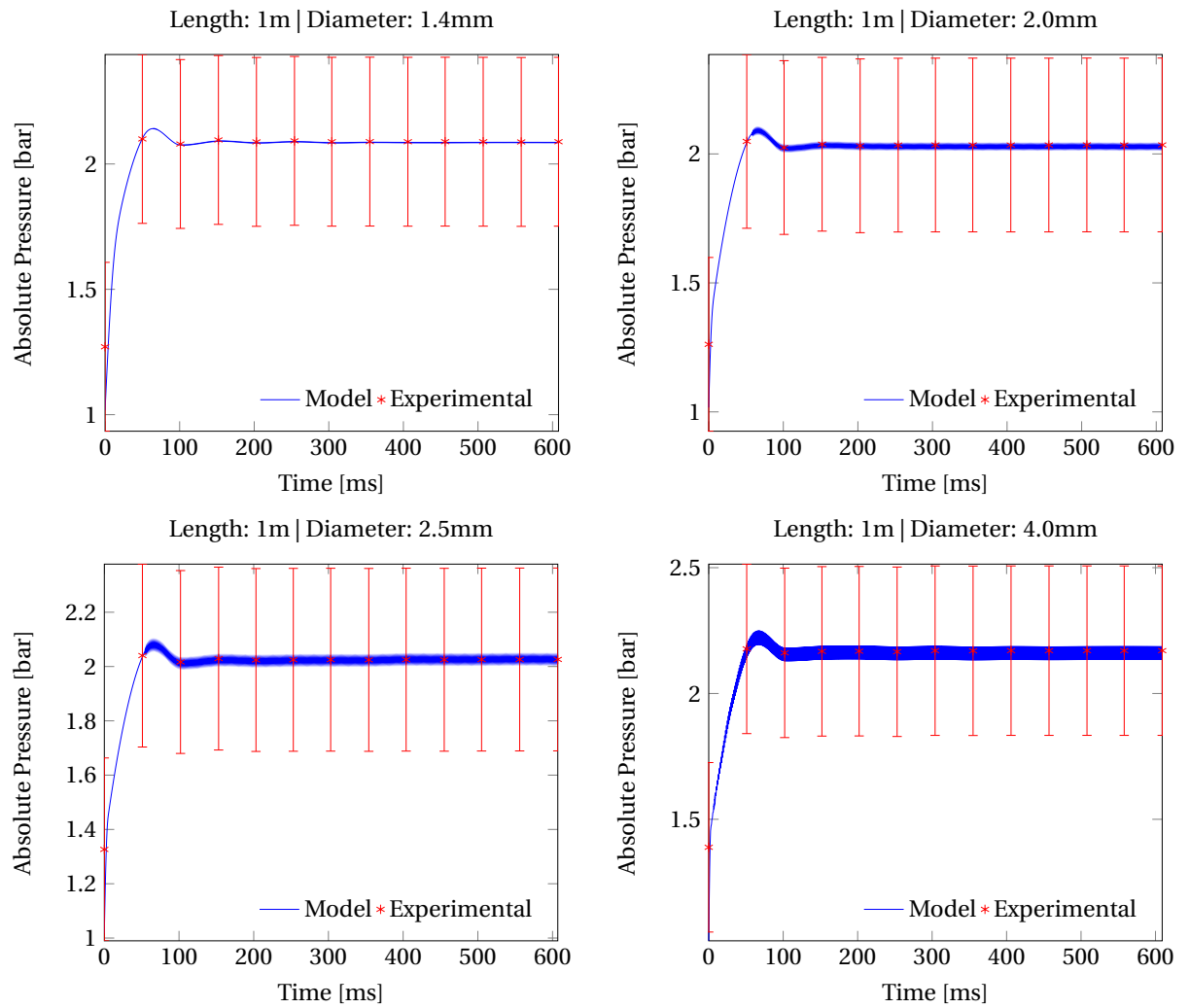
Figure B.1: Diameter sweep with 2 bar source pressure and 1 meter long tube
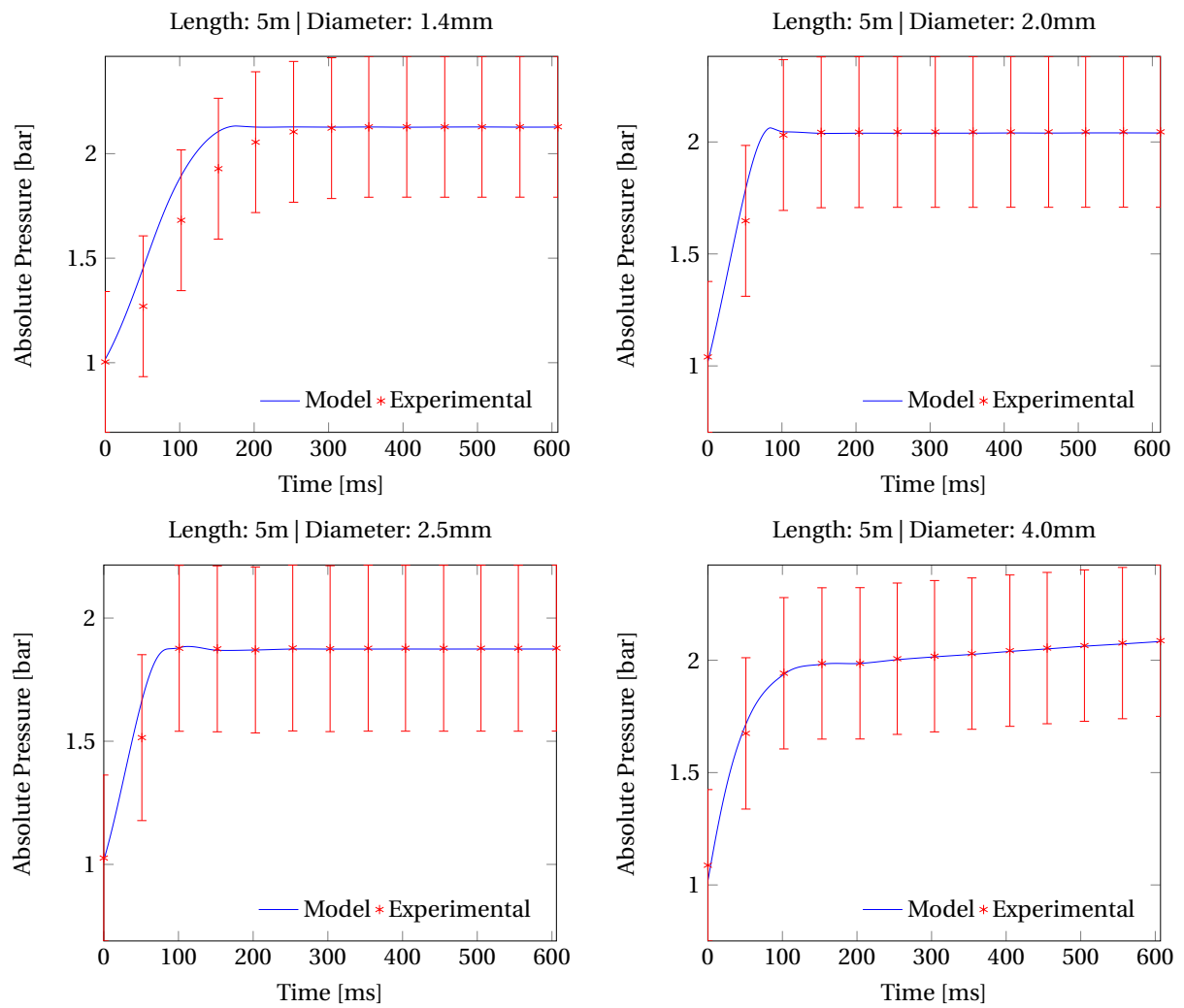
Figure B.2: Diameter sweep with 2 bar source pressure and 5 meter long tube
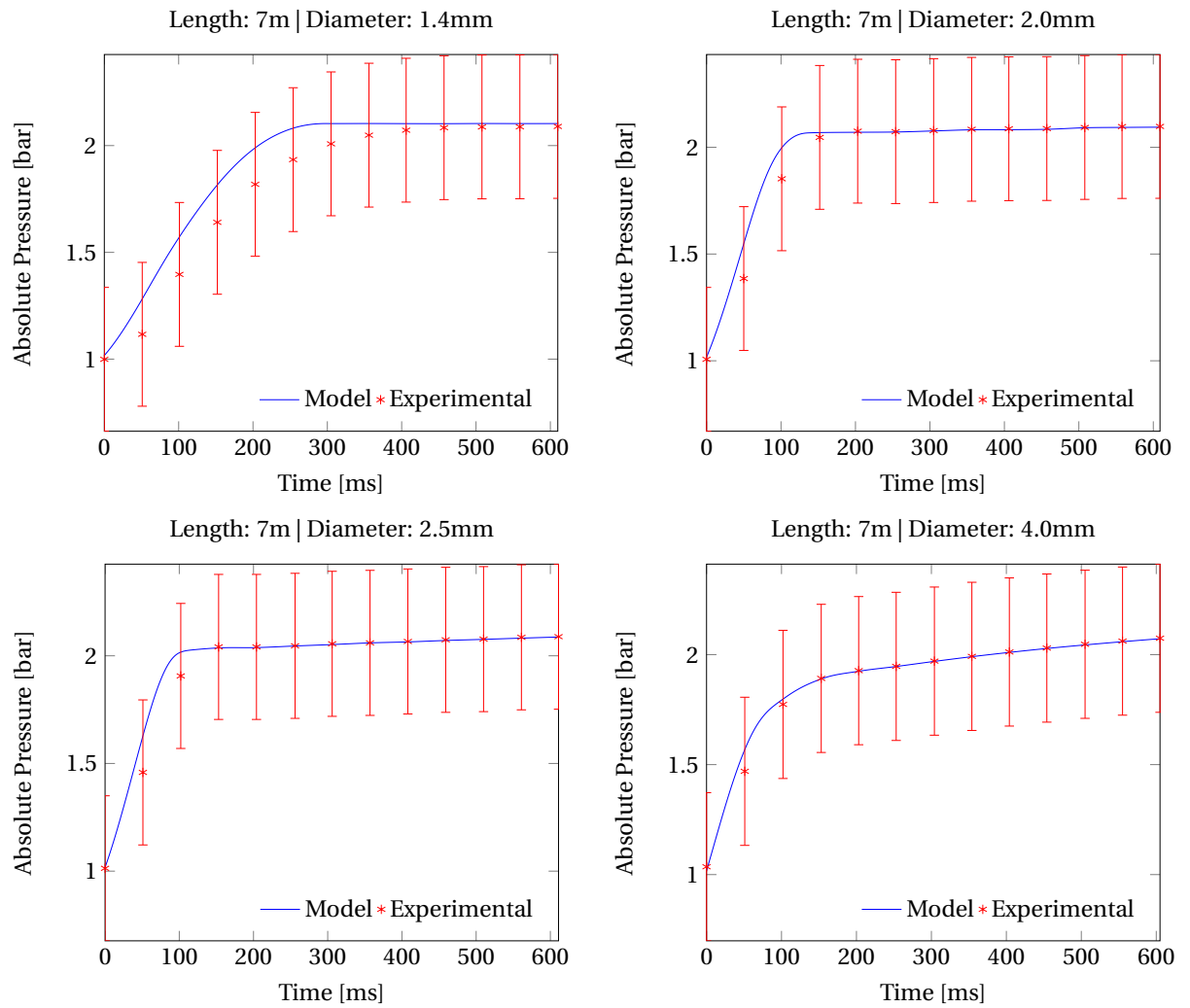
Figure B.3: Diameter sweep with 2 bar source pressure and 7 meter long tube
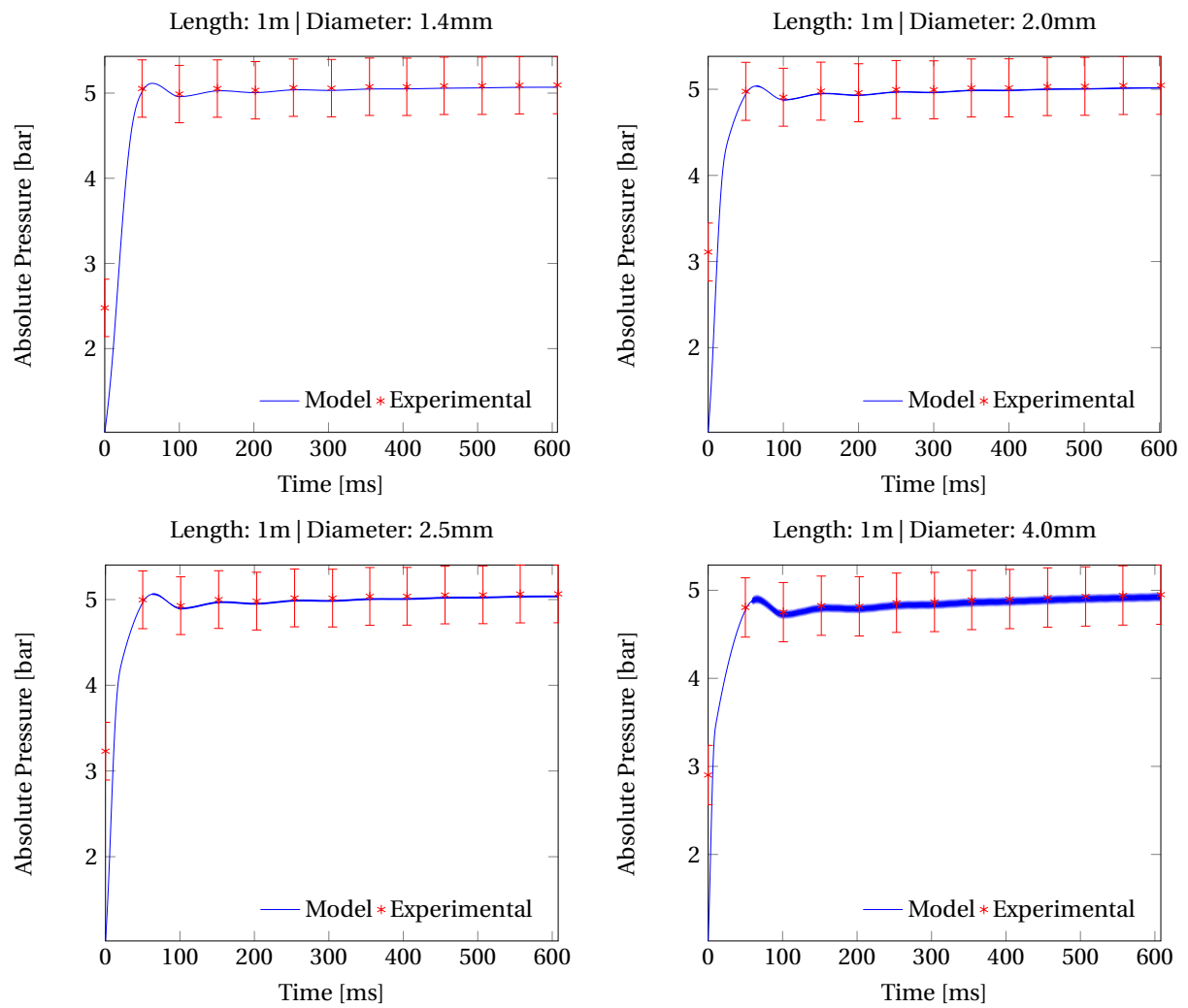
Figure B.4: Diameter sweep with 5 bar source pressure and 1 meter long tube
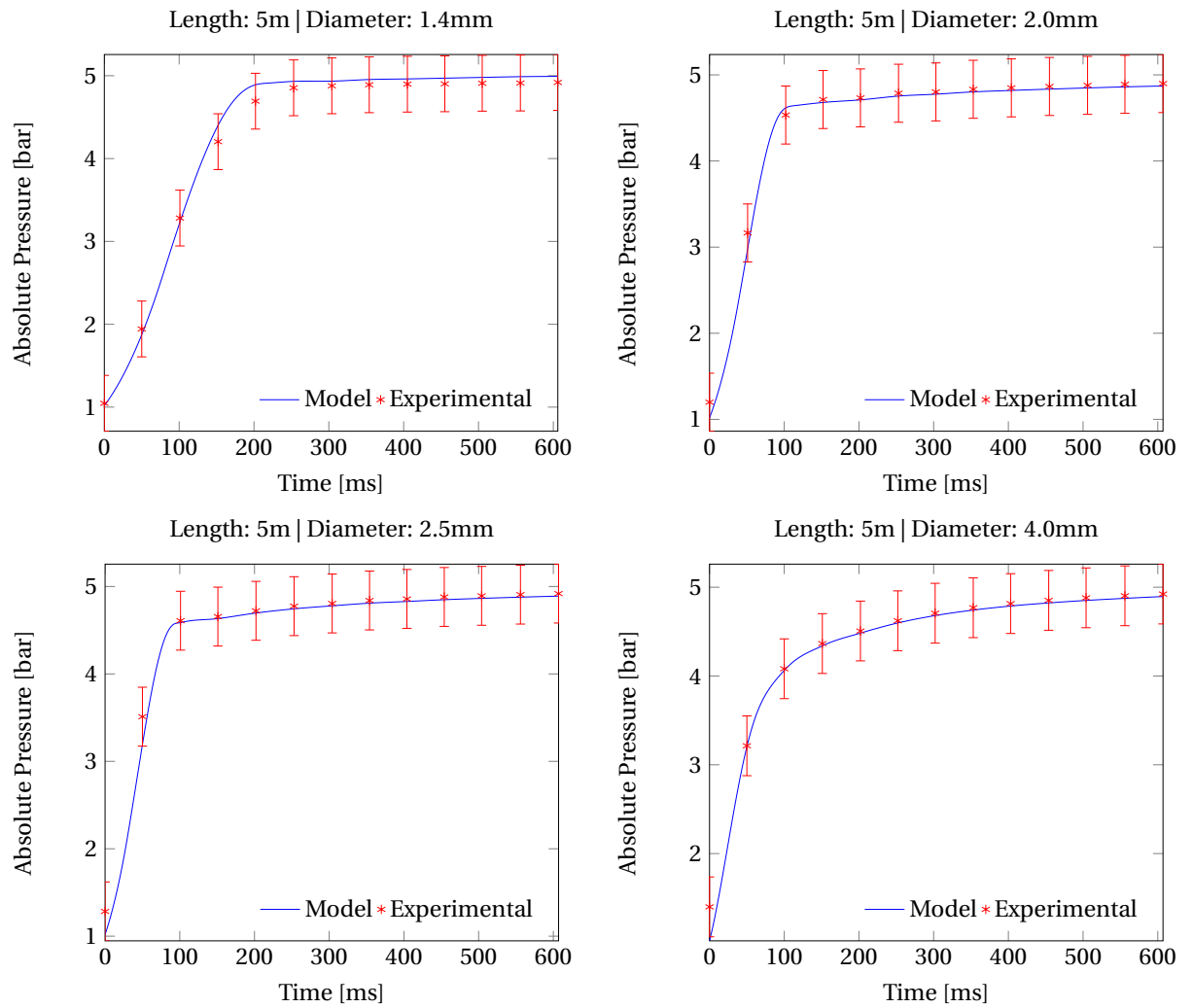
Figure B.5: Diameter sweep with 5 bar source pressure and 5 meter long tube
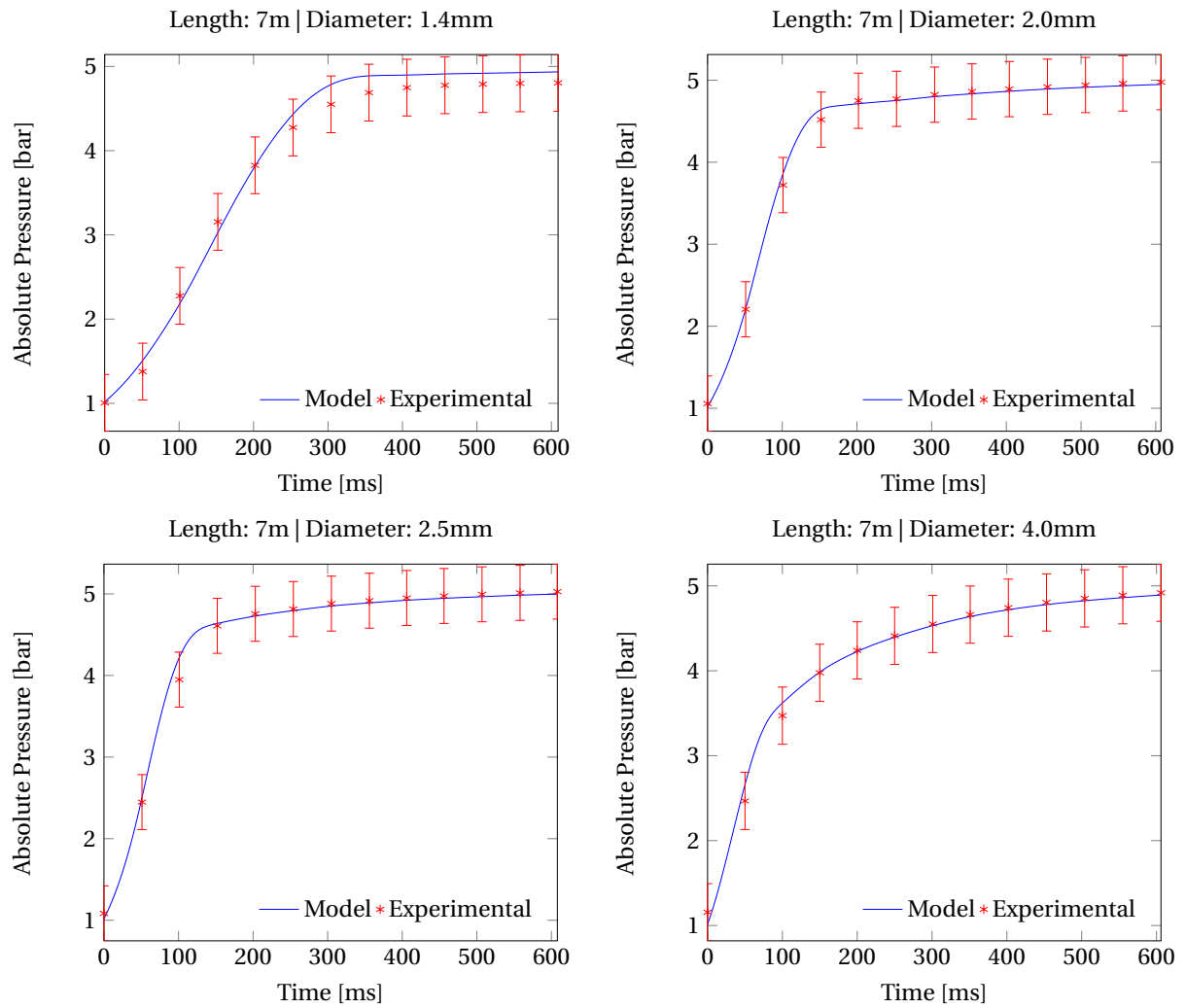
Figure B.6: Diameter sweep with 5 bar source pressure and 7 meter long tube
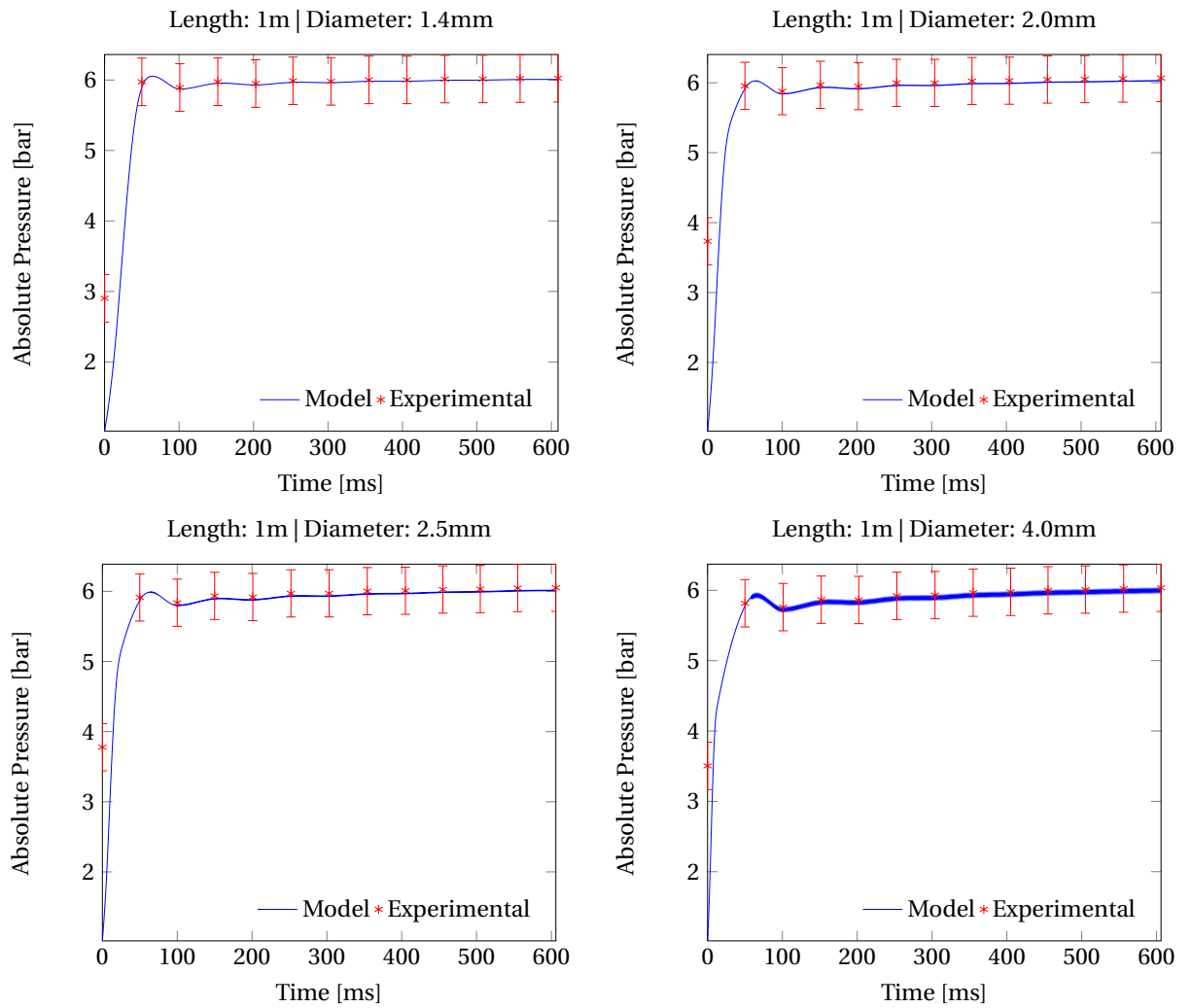
Figure B.7: Diameter sweep with 6 bar source pressure and 1 meter long tube
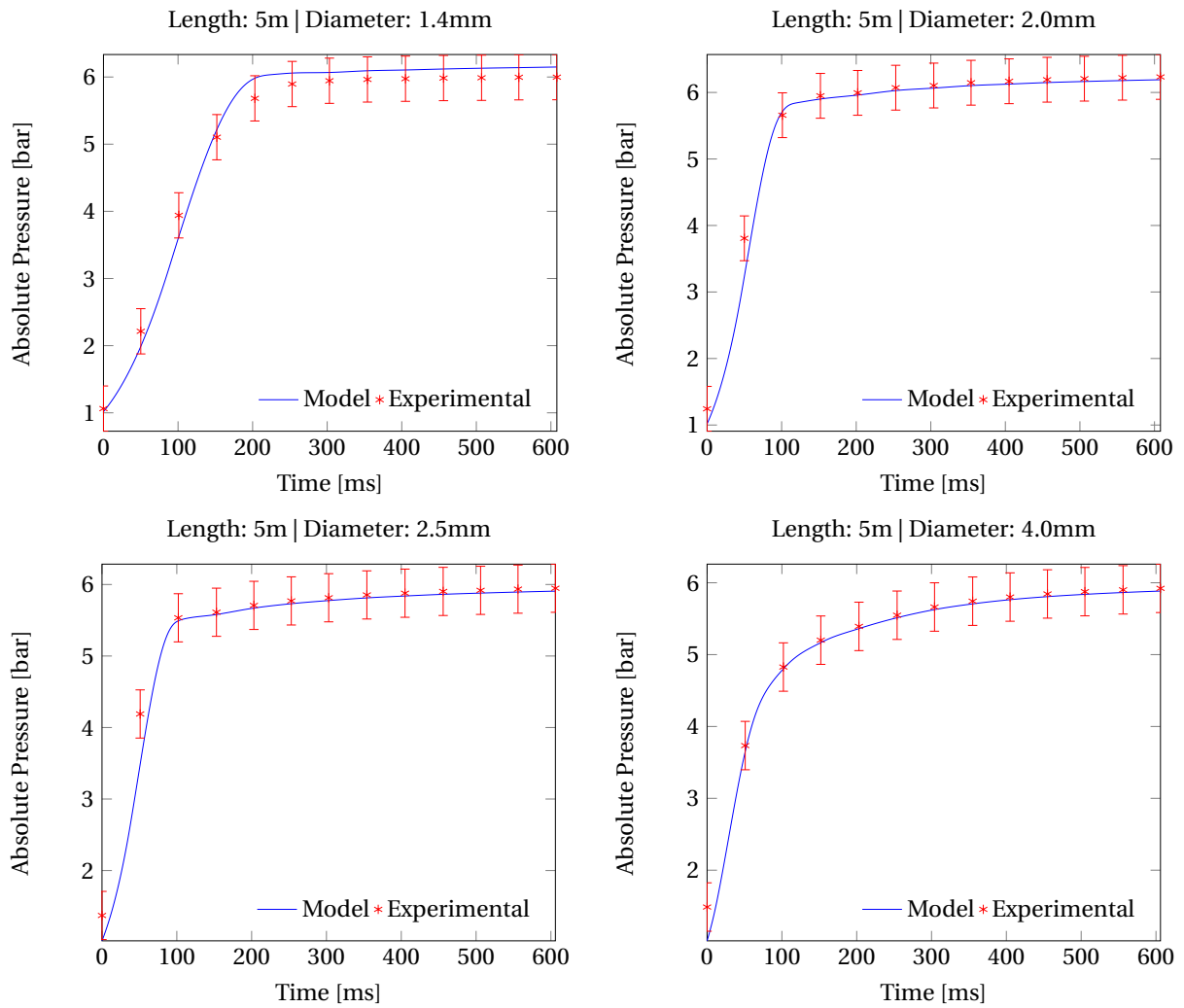
Figure B.8: Diameter sweep with 6 bar source pressure and 5 meter long tube
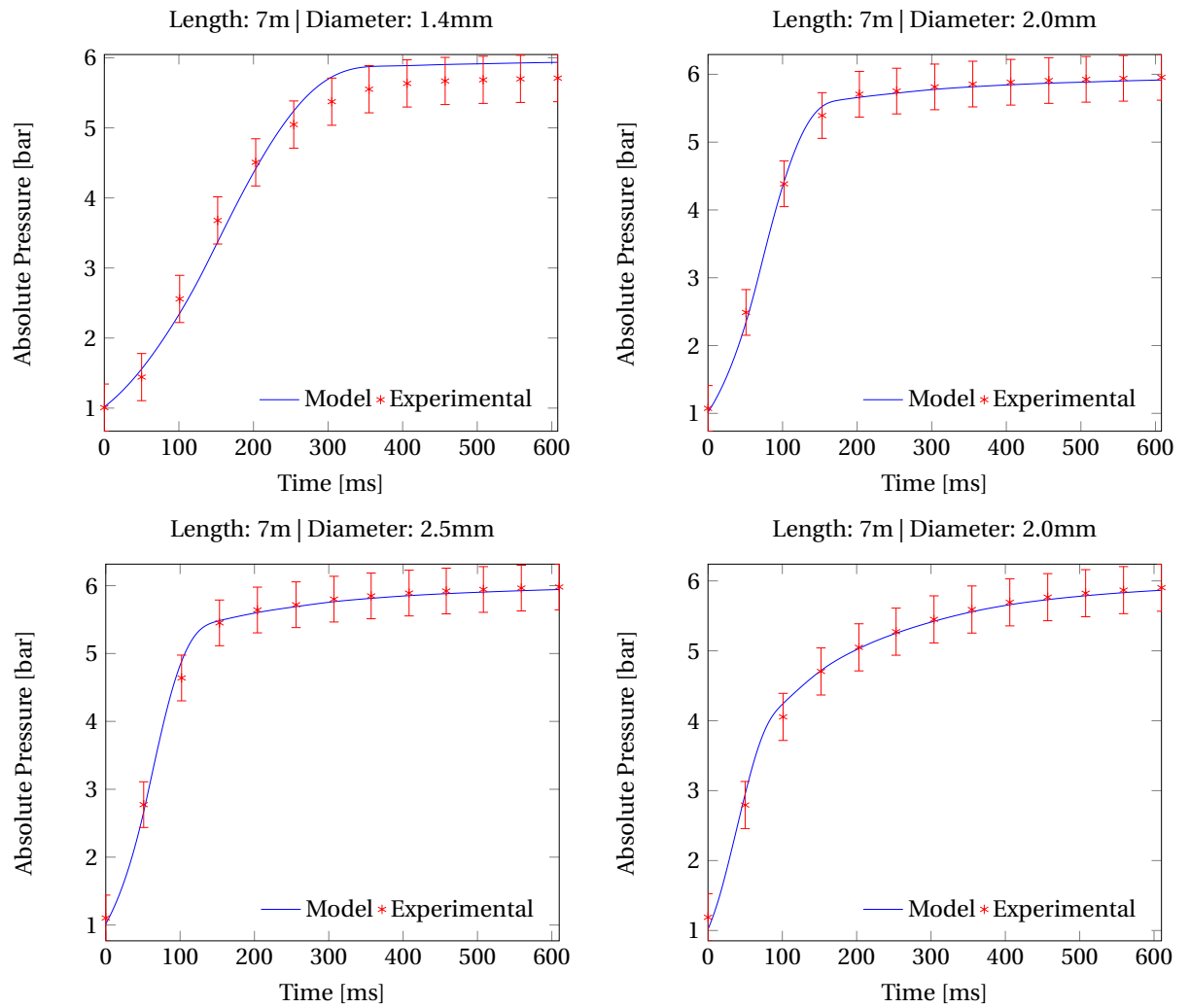
Figure B.9: Diameter sweep with 6 bar source pressure and 7 meter long tube

Bibliography

(2016a), Arduino Uno, online; accessed on Monday 22nd August, 2016.
https://www.arduino.cc/en/Main/ArduinoBoardUno

(2016b), FreeCAD, online; accessed on Monday 22nd August, 2016.
http://www.freecadweb.org/

(2016c), Objet Eden 250 3D printer, online; accessed on Monday 22nd August, 2016.
http://www.smg3d.co.uk/objet_eden250

(2016d), Pneumatiek Voordeel valves, online; accessed on Monday 22nd August, 2016.
https://www.arduino.cc/en/Main/ArduinoBoardUno

(2016e), Python scripting for FreeCAD, online; accessed on Monday 22nd August, 2016.
http://www.freecadweb.org/wiki/index.php?title=Python_
scripting_tutorial

(2016f), SciLab, online; accessed on Monday 22nd August, 2016.
http://www.scilab.org/

(2016g), Trotec Speedy 300 laser cutter, online; accessed on Monday 22nd August, 2016.
http://www.troteclaser.com/en-US/Laser-Machines/Pages/
laser-engraving-machines-speedy.aspx

(2016h), Ultimaker 3D printer, online; accessed on Monday 22nd August, 2016.
https://ultimaker.com/en/products

ASTM International (2001), *ASTM F2119 Test Method for Evaluation of MR Image Artifacts from Passive Implants*, American Society for Testing and Materials (ASTM), West Conshohocken, PA.

ASTM International (2005), *ASTM F2503-05 Standard Practice for Marking Medical Devices and Other Items for Safety in the Magnetic Resonance Environment*, American Society for Testing and Materials (ASTM), West Conshohocken, PA.

Chen, Y., K. . Kwok and Z. T. H. Tse (2014a), An MR-conditional high-torque pneumatic stepper motor for MRI-guided and robot-assisted intervention, *Annals of Biomedical Engineering*, **vol. 42-9**, pp. 1823–1833.

Chen, Y., C. D. Mershon and Z. T. H. Tse (2014b), A 10-mm MR-conditional unidirectional pneumatic stepper motor, *IEEE/ASME Transactions on Mechatronics*, **vol. 20-2**, pp. 782–788.

Fisher, T., A. Hamed, P. Vartholomeos, K. Masamune, G. Tang, H. Ren and Z. T. H. Tse (2014), Intraoperative magnetic resonance imaging-conditional robotic devices for therapy and diagnosis, *Proceedings of the Institution of Mechanical Engineers, Part H: Journal of Engineering in Medicine*, **vol. 228-3**, pp. 303–318.

Gassert, R., A. Yamamoto, D. Chapuis, L. Dovat, H. Bleuler and E. Burdet (2006), Actuation methods for applications in MR environments, *Concepts in Magnetic Resonance Part B: Magnetic Resonance Engineering*, **vol. 29-4**, pp. 191–209.

Groenhuis, V. and S. Stramigioli (2016), Laser-cutting Pneumatics, *IEEE/ASME Transactions on Mechatronics*, **vol. PP-99**, pp. 1–1, ISSN 1083-4435, doi:10.1109/TMECH.2015.2508100.

Huettel, S., A. Song and G. McCarthy (2009), *Functional Magnetic Resonance Imaging*, Freeman, ISBN 9780878932863.

Magnetic Resonance Safety Testing Services (2016), MR-Conditional test factors and result parameters, online; accessed on Monday 22nd August, 2016.
http://www.magneticresonancesafetytesting.com/genpg.asp?pgname=
Terminology

Renn, J. . and C. . Liao (2004), A study on the speed control performance of a servo-pneumatic motor and the application to pneumatic tools, *International Journal of Advanced Manufacturing Technology*, **vol. 23-7,8**, pp. 572–576.

Sajima, H., H. Kamiuchi, K. Kuwana, T. Dohi and K. Masamune (2012), MR-safe pneumatic rotation stepping actuator, *Journal of Robotics and Mechatronics*, **vol. 24-5**, pp. 820–826.

Sajima, H., I. Sato, H. Yamashita, T. Dohi and K. Masamune (2010), Two-DOF non-metal manipulator with pneumatic stepping actuators for needle puncturing inside open-type MRI, in *2010 World Automation Congress, WAC 2010*.

Secoli, R., M. Robinson, M. Brugnoli and F. Rodriguez y Baena (2015), A low-cost, high-field-strength magnetic resonance imaging-compatible actuator, *Proceedings of the Institution of Mechanical Engineers, Part H: Journal of Engineering in Medicine*, **vol. 229-3**, pp. 215–224.

Soemers, H. (2011), *Design Principles: For Precision Mechanisms*, Herman Soemers, ISBN 978903653103.

Stoianovici, D. (2005), Multi-imager compatible actuation principles in surgical robotics., *The international journal of medical robotics and computer assisted surgery : MRCAS*, **vol. 1-2**, pp. 86–100.

Stoianovici, D., A. Patriciu, D. Petrisor, D. Mazilu and L. Kavoussi (2007), A new type of motor: Pneumatic step motor, *IEEE/ASME Transactions on Mechatronics*, **vol. 12-1**, pp. 98–106.

Suzumori, K., T. Hashimoto, K. Uzuka and I. Enomoto (2002), Pneumatic direct-drive stepping motor for robots, in *IEEE International Conference on Intelligent Robots and Systems*, volume 2, pp. 2031–2036.

Uzuka, K., I. Enomoto and K. Suzumori (2009), Comparative Assessment of Several Nutation Motor Types, *IEEE/ASME Transactions on Mechatronics*, **vol. 14-1**, pp. 82–92, ISSN 1083-4435, doi:10.1109/TMECH.2008.2004035.

Zhi, X. (2015), *Design and Prototyping of McRobot Version 3.1: Multi-modality Compatible Robot for Image Guided Minimally Invasive Intervention and Therapy (MSc Thesis)*, Prentice Hall International.